SIGNAL RECONSTRUCTION FROM NONUNIFORM SAMPLES USING PROLATE SPHEROIDAL WAVE FUNCTIONS: THEORY AND APPLICATION

by

Seda Senay

B.Sc in Electrical and Electronics Eng., Yeditepe University, 2001

M.Sc in Electrical and Electronics Eng., Yeditepe University, 2005

Submitted to the Graduate Faculty of

the Swanson School of Engineering in partial fulfillment

of the requirements for the degree of

Doctor of Philosophy

University of Pittsburgh

2011

UNIVERSITY OF PITTSBURGH

SWANSON SCHOOL OF ENGINEERING

This dissertation was presented

by

Seda Senay

It was defended on

April 7, 2011

and approved by

Luis F. Chaparro, Associate Professor, Department of Electrical and Computer Engineering

Robert J. Sclabassi, Professor Emeritus, Department of Neurosurgery

Mingui Sun, Professor, Department of Bioengineering, Electrical and Computer Engineering, Department of Neurosurgery

Juan Manfredi, Professor, Department of Mathematics

Patrick Loughlin, Professor, Department of Bioengineering

Zhi-Hong Mao, Assistant Professor, Department of Bioengineering, Electrical and Computer Engineering

Dissertation Director: Luis F. Chaparro, Associate Professor, Department of Electrical and Computer Engineering

SIGNAL RECONSTRUCTION FROM NONUNIFORM SAMPLES USING PROLATE SPHEROIDAL WAVE FUNCTIONS: THEORY AND APPLICATION

Seda Senay, PhD

University of Pittsburgh, 2011

Nonuniform sampling occurs in many applications due to imperfect sensors, mismatched clocks or event-triggered phenomena. Indeed, natural images, biomedical responses and sensor network transmission have bursty structure so in order to obtain samples that correspond to the information content of the signal, one needs to collect more samples when the signal changes fast and fewer samples otherwise which creates nonuniformly distibuted samples. On the other hand, with the advancements in the integrated circuit technology, small scale and ultra low-power devices are available for several applications ranging from invasive biomedical implants to environmental monitoring. However the advancements in the device technologies also require data acquisition methods to be changed from the uniform (clock based, synchronous) to nonuniform (clockless, asynchronous) processing. An important advancement is in the data reconstruction theorems from sub-Nyquist rate samples which was recently introduced as compressive sensing and that redefines the uncertainty principle. In this dissertation, we considered the problem of signal reconstruction from nonuniform samples. Our method is based on the Prolate Spheroidal Wave Functions (PSWF) which can be used in the reconstruction of time-limited and essentially band-limited signals from missing samples, in event-driven sampling and in the case of asynchronous sigma delta modulation.

We provide an implementable, general reconstruction framework for the issues related to reduction in the number of samples and estimation of nonuniform sample times. We also provide a reconstruction method for level crossing sampling with regularization. Another

way is to use projection onto convex sets (POCS) method. In this method we combine a time-frequency approach with the POCS iterative method and use PSWF for the reconstruction when there are missing samples. Additionally, we realize time decoding modulation for an asynchronous sigma delta modulator which has potential applications in low-power biomedical implants.

TABLE OF CONTENTS

LIST OF FIGURES

PREFACE

First of all I would like to express my gratitude to my advisor Professor Luis F. Chaparro, without his guidance this dissertation would not have been possible. I would like to thank Professor Sclabassi, Professor Manfredi, Professor Sun, Professor Loughlin and Professor Mao for being in my committee and for all their support during my Ph.D. at the University of Pittsburgh. I especially appreciate the support of Professor Sclabassi and Professor Sun. Finally, I would like to thank Professor Jinsung Oh, it was a pleasure to work with him.

(I dedicate my dissertation to my family– especially to my dear mother **Güleser Şenay**)

1.0 INTRODUCTION

In many practical areas, such as medical imaging, geophysics, astronomy and communication systems, it is often not appropriate to assume uniformly spaced samples. Nonuniform sampling occurs in many applications, due to imperfect sensors, mismatched clocks or event-triggered phenomena [1, 2]. Indeed, natural images, biomedical responses and sensor network transmission have bursty structure so in order to obtain samples that correspond to the structure (information content) of the sampled signals, one needs to collect more samples when the signal changes fast and fewer samples otherwise which creates nonuniformly distributed samples. Nonuniform sampling is also desirable for data compression since during nonuniform sampling, higher instantaneous bandwidth/precision is obtained and resolution is improved without increasing the bit rate. In the case of data compression, level-crossing (LC) or event-based sampling is quite efficient [3]. LC sampling is a threshold based nonuniform sampling method which creates samples whenever the signal crosses the predefined thresholds providing reduction in the amount of data to be transmitted especially in wireless sensor networks.

On the other hand, with the advancements in the integrated circuit technology, small scale and ultra low-power devices are available to be used for several applications ranging from invasive biomedical implants to environmental monitoring. However the advancements in the device technologies also require data acquisition methods to be changed from the uniform (clock based, synchronous) to nonuniform (clockless, asynchronous) processing. Synchronous data gathering and continuous transmission create constrains when attempting to limit size and energy consumption of the sensors. One most recent advancement in the data acquisition methods in connection with the developments in integrated circuit technology is called continuous time digital signal processing [4]. Another important advancement is in the

data reconstruction theorems from sub-Nyquist rate samples which redefines the uncertainty principle. These new kind of reconstruction methods are known as compressive sensing (CS) [6]. In CS, random measurements allow perfect reconstruction for ideal sparse signals when there is no measurement noise. For other signal and noise distributions CS method loses its efficiency and becomes less useful for practical applications.

In this dissertation, we considered the problem of signal reconstruction from nonuniform samples in connection with the CS method such that a signal dependent nonuniform sampling method takes the place of random measurements and eliminates the restriction of the signal being sparse. In that case we can process all kind of signals. However, a question remains: can we still obtain a perfect reconstruction? Our method is based on the Prolate Spheroidal Wave Functions (PSWF), also known as Slepian functions, that can be modified for use in the realization of signal reconstruction from missing samples, in event-driven (signal dependent) sampling and in the case of asynchronous sigma delta modulation [7, 16, 3].

We provide an implementable, general reconstruction framework for the issues related to reduction in the number of samples and estimation of nonuniform sample times. We also provide a reconstruction method for level crossing sampling with regularization. Another way is to use projection onto convex sets (POCS) method. In this method we combine a time-frequency approach with the POCS iterative method and use PSWF for the reconstruction where there are missing samples. Additionally, we realize reconstruction from time codes for an asynchronous sigma delta modulator which has potential applications in low power biomedical implants. Our future work is to make PSWF based reconstruction more applicable for event-based sampling in low-power applications such as health monitoring and wireless sensor networks.

1.1 DISSERTATION OUTLINE

As a background, in Chapter 2, we explain the theory of nonuniform sampling and prolate spheroidal wave functions (PSWF). In this dissertation, we consider reconstructing a time-limited and nearly bandlimited signal from its nonuniformly spaced samples using the discrete

form of PSWF [7]. The PSWF are the natural basis of the space of simultaneously band-limited and time-limited functions. No functions can be completely band-limited and time-limited simultaneously, but the prolates are the closest functions to fit this description. This is why they are of such interest in information theory, signal processing and optics. In Chapter 3, we show our approach for nonuniform sampling problem together with the necessary derivations, analysis and results. Although, there are some difficulties associated with nonuniform sampling and its applications in the signal recovery, the advantages of the nonuniform sampling are many. First of all, it is possible to obtain signal dependent nonuniform sampling scheme by using a level crosser (LC) sampler [3, 8]. The LC sampling is not a new method but it is known as being the most efficient way of sampling due to its economical sampling which is akin to compressive sampling [8, 3, 6]. The conventional LC sampling is threshold based where the samples are taken in the time domain when the signal crosses any of the predefined uniformly separated levels. The efficiency of LC sampling is due to its being signal-driven.

In LC sampling the data collection depends on the signal: more samples are taken when the signal is bursty and fewer otherwise. Chapter 4 is about LC sampling and reconstruction where we compare the compressive sensing to PSWF based reconstruction. Chapter 5 is about a time-frequency approach and iterative reconstruction for nonuniform reconstruction problem. In this chapter we explain a time-frequency method which is called Discrete Evolutionary Transform (DET) [11, 12] and use it for the reconstruction using a Projection Onto Convex Sets (POCS) method [14, 15] based on PSWF.

In Chapter 6, we explain asynchronous sigma delta modulators (ASDMs) and accompanying time encoding modulation [16, 17, 4] and show how our reconstruction method can be used. Likewise we present an orthogonal frequency division multiplexing communication method applicable to a group of sensors that are using ASDMs. Chapter 7 is an overview of future work that we want to continue exploring.

1.2 CONTRIBUTIONS AND RELATED PUBLICATIONS

In this dissertation, we would like to present our following contributions:

- We provide a general reconstruction framework for nonuniformly sampled time-limited and essentially band-limited signals. In this framework, we calculate the minimum dimension of the signal to be sampled in a transform domain and estimate the nonuniform sample times. We use properties of the prolate spheroidal wave functions (PSWF) and provide an efficient way of signal reconstruction.
- In the case of level-crossing sampling, there may be large gaps between samples depending on the signal structure and the number of levels. We exploit regularization approach for the PSWF-based reconstruction and compare our results with compressive sensing based reconstruction.
- It is also possible to use an iteration method for reconstruction such as projection onto convex sets (POCS) when there are missing data. In this case we can also exploit a time-frequency approach to create a PSWF-based iterative method.
- Finally, we focus on asynchronous sigma delta modulation and provide a time decoding method for the time codes as the nonuniform samples of a signal to obtain a reconstruction.

Some of the related publications are:

1. S. Senay, L. F. Chaparro, M. Sun, R. J. Sclabassi, and A. Akan,"Asynchronous signal processing for brain computer interfaces," *Turkish J. Elec. Eng & Comp Sci*, Vol.19, No. 2, 2011, Published by The Scientific and Technological Research Council of Turkey, (TUBITAK) doi:10.3906/elk-1001-382.
2. J. Oh, S. Senay and L. F. Chaparro,"Signal reconstruction from nonuniformly spaced samples using evolutionary Slepian Transform–based POCS," *Eurasip Journal on Advances in Signal Processing*, special issue on Applications of Time-Frequency Signal Processing in Wireless Communications and Bioengineering, vol. 2010, Article ID 367317, 12 pages. doi:10.1155/2010/3673172010.

3. S. Senay, L. F. Chaparro, and L. Durak, "Reconstruction of nonuniformly sampled time-limited signals using Prolate Spheroidal Wave Functions," *Signal Processing, Elsevier*, Vol. 89, pp. 2585-2595, 2009.
4. S. Senay, L.F. Chaparro, M. Sun, R. J. Sclabassi, "Time encoding and reconstruction of multichannel data by brain implants using asynchronous sigma delta modulators," *31st Intl. Conf. of the IEEE Engineering in Medicine and Biology Society* (EMBC), Minneapolis, Minnesota, USA, Sept., 2009.
5. S. Senay, L.F. Chaparro, M. Sun, R. J. Sclabassi, "Time-frequency multiplexing for time encoded signals from brain computer interfaces," pp.1186-1189, *17th European Signal Processing Conference* (EUSIPCO), Scotland, Aug. 2009.
6. S. Senay, L.F. Chaparro, M. Sun, R. J. Sclabassi, "Asynchronous sigma delta modulators based subdural neural implants for epilepsy patients," *35th IEEE Northeast Bio-Engineering Conf.*, (NEBEC), April 3-5, 2009.
7. S. Senay, A. Akan, and L. F. Chaparro, "Sampling and reconstruction of non-bandlimited signals using Slepian functions," *16th European Signal Processing Conference*, (EUSIPCO), Switzerland, Aug. 2008.
8. S. Senay, L. F. Chaparro, M. Sun, and R. J. Sclabassi, "Compressive sensing and random filtering of EEG signals using Slepian basis," *16th European Signal Processing Conference* (EUSIPCO), Switzerland, Aug. 2008.

2.0 BACKGROUND

2.1 NONUNIFORM SAMPLING

Over the past 60 years, a great deal of research has been done to improve Shannon's sampling theory [18]. Some of the extensions of the theory have been about sampling of band-pass signals [19], nonuniform sampling [23], and application of joint time-frequency methods for dealing with sampling of non-stationary signals [25]. A recent approach applies wavelet structures [27] to develop new sampling and reconstruction techniques. In signal recovery problems with missing data, sparsity and bandlimiting, the important work [28] about the generalized uncertainty principle provides useful concepts. In this chapter, we consider the basics of nonuniform sampling theory and describe some of the problems associated with them for which we would like to find solutions. A number of applications that use nonuniform sampling either inherently or by choice are:

1. ***Medical applications***: Health monitoring can benefit from nonuniform sampling since nonuniform sampling allows economical data acquisition which is the aim in most of the developing device technologies that are to be used in invasive biomedical implants [4, 16, 80].
2. ***Sensor networks***: Event-based sampling or send-on-delta method are some of the ways of efficient nonuniform sampling for sensors providing reduction in the number of samples to be transmitted [5].
3. ***Radar***: Many radar applications result in nonuniform data on a two-dimensional grid [29]. In one-dimensional radar measurements, (e.g., long range radars or pulse radars) frequency estimation is used to detect movements by Doppler effects. Usually, that

frequency is much larger than the possible Nyquist frequency, so different nonuniform sampling techniques can be used to increase performance. Also, in military applications the use of nonuniform sampling makes detection and jamming of the radar harder.

4. ***Automotive applications***: In today's vehicles there exist many sensors for different purposes. For example, toothed wheels with sensors registering when teeth pass the sensor give a nonuniformly sampled signal, effected by the wheel speed [1].
5. ***Astronomical time series***: Due to weather conditions and equipment failures, the collected astronomical data are nonuniformly spaced. One special application is in stellar physics such that luminosity of variable stars are recorded to describe their frequency contents [30]. For example, detection of periods in both the number of sunspots and observed properties of other stars is an important task for astronomers. These data are often nonuniformly sampled as well as sparse and noisy.
6. ***Packet data traffic***: In routers, some data flow controlling algorithms are based on packet data arrivals. It is clear that data packets will arrive totally at random, therefore several of the network calculations have to deal with nonuniform sampling. At these arrival instants these algorithms are assumed to collect measurements, calculate decision variables and perform a suitable action [1].

Nonuniform sampling may appear due to imperfections in the hardware, as well. For instance, interleaved analog to digital (A/D) converters are used to increase sampling rates [31]. If N A/D converters are used to sample a signal, the n^{th} A/D converter samples at times

$$t_{k,n} = (kN + n)T \tag{2.1}$$

to get an overall inter-sampling time T for $n = 1, \cdots, N$ and k an integer. The results from the individual A/D converters are multiplexed to get the sampled sequence $y(kT)$. Individual A/D converters suffer from time errors, δ_n, due to the internal clocks, and the sampling clock also suffers from noise, which gives rise to jitter, $\tau_{k,n}$. The actual sampling time for the n^{th} A/D converter is therefore,

$$t_{k,n} = (kN + n)T + \delta_n + \tau_{k,n}. \tag{2.2}$$

Here δ_n is constant for individual A/D converters and $\tau_{k,n}$ is random. The resulting sequence $t_{1,1}, t_{1,2}, ..., t_{1,N}, t_{2,1}, ..., t_{2,N}, ...$ is clearly nonuniform. Nonuniform sampling can occur in different forms and if the probability distribution for the sampling times t_m, is represented as $p_m(t)$, depending on the type of sampling, $p_m(t)$ can be deduced from the probability density function (pdf), $p_\tau(t)$, of the sampling noise, τ_m. Basic models for nonuniform sampling times are as follows [1]:

- **Additive random (AR) sampling**: the sampling times are constructed by adding the sampling noise to the previous sampling time,

$$t_m = t_{m-1} + \tau_m = \sum_{k=1}^{m} \tau_k, \quad t_0 = 0 \tag{2.3}$$

  where $\tau_m \in (0, \infty)$ and $E[\tau_m] = T$. This means that $E[t_m] = mT$, while the variance increases with m. The pdf is given as a convolution of the sampling noise pdf m times. For example, the exponential distribution gives a Poisson sampling process. The central limit theorem gives that $p_m(t)$ will approach a Gaussian distribution when m goes to infinity, since it is the pdf of a sum of m independent identically distributed variable.

- **Stochastic jitter (SJ) sampling**: the sampling noise is added to the expected sampling time,

$$t_m = mT + \tau_m, \tag{2.4}$$

  with $\tau_m \in (-T/2, T/2)$ and $E[\tau_m] = 0$. In this case the variance is constant over time and the pdf of t_m is given directly by the pdf of τ_m. One natural distribution is the uniform distribution, $p_\tau(t) = 1/T$, $-T/2 < t < T/2$, but it is also possible to imagine a truncated Gaussian distribution or other bounded distributions.

- **Missing data (MD) sampling**: the underlying sampling procedure is uniform but sometimes samples are missed. This can, for example, be described with a discrete sampling noise,

$$t_m = t_{m-1} + \tau_m, \tag{2.5}$$

  and $\tau_m \in T, 2T, ...$ which is a special case of AR sampling, with a discrete pdf for the sampling noise.

2.1.1 Nonuniform Reconstruction Methods

In order to know (i) how a function f can be stably reconstructed from its nonuniform samples and (ii) the conditions under which f can be uniquely defined by its samples, many theories for nonuniform sampling have been derived [32, 34, 36, 37]. The following section is an overview of some algorithms to reconstruct signals from their nonuniform samples.

2.1.1.1 Iterative Reconstruction An iterative reconstruction algorithm is an alternating mapping method using the information from the nonuniform sample values and the spectral support of a signal f. A two-step iterative algorithm is typical and it works as follows:

1. Using and approximation operator A, an auxiliary signal Af is constructed from the given sampling values of f.
2. The signal Af, which is generally not bandlimited, is projected onto the space of Ω bandlimited signals by an orthogonal projection P. This projection smoothes Af and eliminates its discontinuities.

The projection of f, Pf can be interpreted as convolution of f with a sinc-type function if P is described as a low pass filter, such that

$$Pf = sinc * f$$

The approximated signal, f_a after implementing the above steps is $f_a = Af * sinc$. The next iteration creates a new auxiliary signal $Af^{(1)}$, denoting the difference $f - Af * sinc$ by $f^{(1)}$, we have to add $f^{(1)}$ to the filtered $Af^{(1)}$ to obtain $f^{(2)}$, giving the following formula for $(n+1)_{th}$ iteration:

$$\begin{aligned} f^{(n+1)} &= f^{(n)} + A(f - f^{(n)}) * sinc \\ &= f^{(n)} - Af^{(n)} * sinc + Af * sinc \end{aligned} \tag{2.6}$$

More information on the choice of the approximation operator, numerical implementation and convergence of the iteration issues, can be found in [23].

2.1.1.2 The Frame Approach A set of functions $\{f_i\}_{i\in I}$ is a frame in a Hilbert space H, if for two constants $0 < A \leq B$,

$$A||f||^2 \leq \sum_{i\in I} | < f, f_i > |^2 \leq B \parallel f \parallel^2,$$

for all $f \in H$. The frame operator S is invertible and

$$Sf = \sum_i < f, f_i > f_i$$

which gives $f = S^{-1}(Sf) = S(S^{-1}f)$ for $f \in B^2_\Omega$. where B^2_Ω is the space of Ω bandlimited functions. Since the Sf can be obtained from $\{f(x_i)\}_{i=1}^p$ and the knowledge of the spectral support Ω, it is possible to reconstruct$f$ from sampling values. Frames are associated with oversampling and redundancy. We meet frames in nonuniform sampling methods when it is difficult to sample at exactly the right rate. If the sampling rate is exactly right, the interpolating functions $\text{sinc}(t - t_n)$ are a basis for the bandlimited space and they are a frame when we oversample.

If the uniformly taken samples satisfy the Nyquist criteria, the set of shifted sinc functions becomes a frame which is also a tight frame. There are some sufficient conditions that must be satisfied for the set of shifted sinc functions to be a frame [33]:

1. Kadec 1/4 theorem: If $\{x_i\}_{i\in Z}$ satisfy $|2x_i\Omega - i| \leq L < \frac{1}{4}$, then shifted sinc functions form an exact frame and there exists a biorthonormal sequence $\{g_i\}$ such that $f(x) = \sum_i f(x_i)g_i(x)$. This theorem only allows a maximal deviation of 1/4 of the distance between two sampling points of the uniform set.
2. Duffin-Schafer theorem: Given a sequence $\{x_i\}$, if there exist constants $\alpha, D > 0$ on $0 < \Omega < \gamma$ such that

$$\begin{aligned} |x_i - x_j| &\geq \alpha > 0 \quad \forall i \neq j \\ |x_i - \frac{i}{j}| &\geq D \quad \forall i \end{aligned}$$

   then shifted sinc functions form a frame which are linearly dependent. This linear dependency is useful for good reconstruction of f, if some samples are missing or not exact due to round off error or noise. In this case, the inexact frames are preferable to exact frames and orthogonal bases.

2.1.1.3 Pseudo-inverse Matrix Reconstruction Method Pseudo-inverse methods consider the nonuniform sampling problem from an algebraic point of view based on the solution of systems of linear equation. Pseudo-inverse methods work efficiently when the number of sampling points and the size of the spectrum are small [2]. One can prefer using iterative methods, if only a small percentage of sampling points are missing and the gaps between sampling points are not too large. However, if these conditions are not met, pseudo-inverse methods become an alternative to recover signals from nonuniform samples.

- Let M be a matrix with p row vectors of length n which can be shifted versions of some function $g \in L^2$, in particular g is the sinc function. If the rows of M are linearly independent, the orthogonal projection of a given function $f \in B_\Omega^2$ onto the linear span of M can be described by

$$P_M f = f M^T (M M^T)^{-1} M$$

  There is a unique series representation of f by $f = \sum_{i=1}^{p} \lambda_i g_i(. - i)$, where λ_i are the coefficients. If M is not of full rank p, the λ_i are not unique, then pseudo inverse $M^\dagger$ approach is needed which allows to determine the minimal norm least squares solution $\wedge = \{\lambda_i\}_{i=1}^{p}$ of $f = \sum_{i=1}^{p} \lambda_i g_i(. - i)$ using $\wedge = f M^\dagger$. That way one can obtain an approximation f_a for f for which $||f_a - f||_2$ is minimal. The problem with this approach is calculation of $\wedge$ requires the whole f, however we only have some samples of f. Using the following formulas, one can obtain $\wedge$ without the use of whole signal f:

$$M^\dagger = (M M^T) M = M^T (M M^T)^\dagger$$

  so that $\wedge = f M^T (M M^T)^\dagger$ where $f M^T = \langle f, g(. - x_i) \rangle_{i=1}^{p} = f(x_i)_{i=1}^{p}$ [9]. One can find a connection between frame approach and the method described above: Frame expansion $f = \sum_{n=1}^{p} \langle f, S^{-1} f_n \rangle f_n$ and for $\lambda_n := \langle , S_{-1} f_n \rangle$ the sequence $(\lambda)_{n=1}^{p}$ is a minimal norm solution.

- The other way is to consider linear mapping from the space of Fourier coefficients to the space of sampling sets (described by matrix M) such that the following equation is obtained

$$\hat{f}(\Omega) M = (f(x_i))_{i=1}^{p}$$

and multiplying $M^{\dagger}$ by $(f(x_i))_{i=1}^{p}$ results in minimal norm sequence of k Fourier coefficients of the approximation signal $\hat{f}_a$. The computation time depends mostly on the size of M and if the number of sampling points and the spectrum are small, the algorithm works efficiently.

2.1.1.4 POCS Method Projection onto convex sets (POCS) method is a recursive algorithm for finding a point in the intersection of closed convex sets [14]. The theory of POCS method was developed in 1967 and first applied to images in 1982. Considering a Hilbert space L^2 with norm $||.||$ of all square integrable functions and a convex set $C \subset L^2(R)$, for any $f \in L^2(R)$, the projection Pf of f onto C is by definition the nearest neighbor to f in C such that if C is closed and convex, Pf exists and is uniquely determined by f and C as

$$||f - Pf|| = min_{g \in C}||f - g||$$

Nearly most data of an unknown signal $f \in L^2(R)$ can be interpreted as a constraint that restricts f to lie in a closed convex set $C_i, i = 1, ..., p$. In such a case there are p closed convex sets for p unknown properties and f must lie in the intersection

$$C_0 := \bigcap_{i=1}^{p} C_i$$

Then a point in C_0 must be found given the sets C_i and projection operators P_i projecting onto C_i for $p = 1, ..., p$. The convergence properties of the sequence $(f^{(k)})$ are based on the theorems given by [14] such as

$$f^{(k+1)} = P_p P_{p-1} ... P_1 f^{(k)}, \quad k = 0, 1, ...$$

An important example for C is the set of all square integrable functions. In other words C_i is the set of band-limited functions whose values at the sampling point x_i coincides with the value of the sampled function. There are basically two different methods to reconstruct a signal by POCS: 1. Iterative algorithm, 2. One step method.

1. Iterative algorithm: The information of the sampling values is used step by step as a correction term and each step a certain multiple of the shifted sinc function is added to the approximation such that

$$f^{(k+1)} = P_p P_{p-1} ... P_1 f^{(k)} \tag{2.7}$$

$$f^{(0)}(x) := h(x) \tag{2.8}$$

where $h(x)$ is the initial estimate. The algorithm converges to a point in the set $C_0 := \bigcap_{i=1}^{p} C_i$, which is in general the original signal f.

2. One step method: The aim of the one step method is to project directly onto the intersection set C_0 which can be defined as $C_0 = g|g \in B_{\Omega|^2}$ for $g(x_i) = f(x_i)$, $i = 1, ..., p$. The $g(x_i) = \alpha \Longleftrightarrow \langle g, sinc(. - x_i)\rangle$, hence the projection of f onto C_0 is $P_0 = (f(x_i))A^{-1}M$ where M is composed of shifted sinc functions and $A := MM^T$.

Additionally there are other methods such as the ones that use polyphase filter banks for efficient reconstruction of nonuniformly decimated bandlimited signals [38] or by means of time-varying discrete-time FIR filters [39]. In the case of signal reconstruction from sparse samples, compressive sensing [6] is the most attractive method for both signal processing and mathematics communities. Compressive sensing is also a form of nonuniform sampling together with reconstruction, therefore in the following part we will explain it.

2.1.1.5 Compressive Sensing Compressive sampling (CS), also known as sparse sampling, is basically the process of creating an underdetermined system of equations where there are far fewer equations than unknowns and finding sparse solutions to this system utilizing the prior knowledge that the signal is sparse or compressible [55, 65]. Given a basis $\{\psi_i\}_{i=1}^{N}$, a signal $\mathbf{x} \in \Re^N$ can be represented in terms of N coefficients $\{s_i\}_{i=1}^{N}$ as

$$\mathbf{x} = \sum_{i=1}^{N} s_i \psi_i, \tag{2.9}$$

which can also be written as $\mathbf{x} = \mathbf{\Psi s}$ where $\mathbf{\Psi}$ is $N \times N$ and has ψ_i as its columns. In CS the signal $\mathbf{x}$ is not acquired directly, but rather $M < N$ linear measurements

$$\mathbf{y} = \mathbf{\Phi x} = \mathbf{\Phi \Psi s} = \mathbf{\Theta s} \tag{2.10}$$

are taken using $M \times N$ measurement matrix $\mathbf{\Phi}$. If the signal is K sparse then $K << N$ entries are nonzero and M is preferred to be as close as possible to K. In order to recover a good estimate of $\mathbf{x}$, the measurement matrix must satisfy the restricted isometry property (RIP) [6]. According to RIP at least $M = K\log(N/K)$ measurements are needed. For K-sparse signals, since $M < N$ there are infinitely many solutions $\tilde{\mathbf{s}}$ that satisfy $\mathbf{\Theta}\tilde{\mathbf{s}} = \mathbf{y}$. This is because if $\mathbf{\Theta}\mathbf{s} = \mathbf{y}$ then $\mathbf{\Theta}(\mathbf{s} + \mathbf{r}) = \mathbf{y}$ for any vector $\mathbf{r}$ in the null space of $\mathbf{\Theta}$. The signal reconstruction algorithm aims to find the signal's sparse coefficient vector $\hat{\mathbf{s}}$ in the $N - M$ dimensional null space. Using ℓ_1 optimization approach, the recovery is given as

$$\hat{\mathbf{s}} = \arg\min||\tilde{\mathbf{s}}||_1 \quad \text{such that} \quad \mathbf{\Theta}\tilde{\mathbf{s}} = \mathbf{y} \tag{2.11}$$

Some other recovery algorithms are orthogonal matching pursuit [56] and StOMP [57].

2.2 PROLATE SPHEROIDAL WAVE FUNCTIONS

In this dissertation, our contributions emerge from using some properties of the *prolate spheroidal wave functions* (PSWF) which are also known as Slepian functions. The question *to what extent are functions which are confined to a finite bandwidth also concentrated in the time domain?* that was posed by Claude E. Shannon raised the interests of researchers in the late 1950's. In the 1960's David Slepian and others published papers defining the dimensionality of time-frequency region and showed that the PSWF are the set of functions that simultaneously optimized energy concentration in time and in frequency when either or both has a finite interval. However, the initial work of Slepian and others were valid for continuous time and frequency. Later, in 1978 Slepian published his prominent work where he defined the *discrete prolate spheroidal sequences* (DPSS).

In our work, we aim to provide PSWF- based reconstruction solutions for nonuniformly sampled signals that are not necessarily bandlimited. Our motivation is to find a stable reconstruction method for the signals from their nonuniform samples using a basis other than sinc function such that we can obtain a finite dimensional solution without making the reconstruction problem ill posed. We will see that practical problems of the classical sampling

theory under the assumption of band-limitedness and the use of a sinc interpolation kernel can be dealt successfully when PSWF are used as the basis of interpolation. The following section will explain the theory and properties of PSWF and of DPSS that have inspired us to choose them as the tool for the realization of the work in this dissertation.

2.2.1 Notation and Properties

The notation for the PSWF used in this dissertation is $\varphi_n(t)$. Indeed, the PSWF are dependent on a total of four parameters:

- t : the continuous time parameter
- n : the order of the function
- τ: the interval on which the function is known
- γ : the bandwidth parameter

where $\gamma = \tau\sigma$ and σ is the finite bandwidth or cutoff frequency of $\varphi_n(t)$ of a given order n.

Spheroidal Wave Functions (SWF) are solutions of the Laplace equation that are found by writing the equation in spheroidal coordinates and applying the technique of separation of variables, just like the use of spherical coordinates lead to spherical harmonics. They are called oblate spheroidal wave functions or oblate harmonics if oblate spheroidal coordinates are used and prolate spheroidal wave functions or prolate harmonics if prolate spheroidal coordinates are used [20]. Prolate spheroidal coordinates are a three-dimensional orthogonal coordinate system that result from rotating a spheroid around its major axis, i.e., the axis on which the foci are located. Rotation about the other axis produces the oblate spheroidal coordinates. Prolate spheroidal coordinates can be used to solve various partial differential equations in which the boundary conditions match its symmetry and shape, such as solving for a field produced by two centers, which are taken as the foci on the z-axis. One example is solving for the wave function of an electron moving in the electromagnetic field of two positively charged nuclei. Considering the spheroidal differential equation [20, 98],

$$\frac{d}{dx}((1-x^2)\frac{dw}{dx}) + (\lambda + \gamma^2(1-x^2) - \frac{\mu^2}{1-x^2})w = 0, \tag{2.12}$$

with real parameters λ, γ^2 and μ for $\mu = 0, 1, 2, \ldots$, the PSWF are solutions of (2.12) that are bounded on (-1,1). The properties of PSWF $\{\varphi_n(t)\}$ can be itemized as follows:

- They exist for special values of λ which are eigenvalues and for $\gamma = 0$, they are the associated Legendre functions [96]. In the case of $\mu = 0$ with $\gamma^2 > 0$, the SWF are called the PSWF which can be fully symbolized as $\{\varphi_{n,\sigma,\tau}(t)\}$ where $\gamma = \tau\sigma$ and $\tau, \sigma > 0$.
- The most interesting property that $\varphi_{n,\sigma,\tau}(t)$ satisfy is the double orthogonality relations

$$\int_{-\tau}^{\tau} \varphi_{n,\sigma,\tau}(t)\varphi_{m,\sigma,\tau}(t)dt = \lambda_n \delta_{m,n} \tag{2.13}$$

$$\int_{-\infty}^{\infty} \varphi_{n,\sigma,\tau}(t)\varphi_{m,\sigma,\tau}(t)dt = \delta_{m,n} \tag{2.14}$$

- The PSWF are also the eigenfunctions of the two integral equations

$$\int_{-\tau}^{\tau} \varphi_{n,\sigma,\tau}(x)\frac{\sin\sigma(t-x)}{\pi(t-x)}dx = \lambda_{n,\sigma,\tau}\varphi_{n,\sigma,\tau}(t) \tag{2.15}$$

$$\int_{-\tau}^{\tau} \varphi_{n,\sigma,\tau}(t)e^{-j\sigma\omega/\tau}dt = \gamma_{n,\sigma,\tau}\varphi_{n,\sigma,\tau}(\omega) \tag{2.16}$$

and since they are bandlimited in $(-\sigma, \sigma)$,

$$\int_{-\tau}^{\tau} \varphi_{n,\sigma,\tau}(x)\frac{\sin\sigma(t-x)}{\pi(t-x)}dx = \varphi_{n,\sigma,\tau}(t) \tag{2.17}$$

From (2.17),

$$\frac{\sin\sigma(t-x)}{\pi(t-x)} = \sum_{n=0}^{\infty} \varphi_{n,\sigma,\tau}(t)\varphi_{n,\sigma,\tau}(x) \tag{2.18}$$

and the discrete orthogonality relation is obtained

$$\sum_{n=0}^{\infty} \varphi_{n,\sigma,\tau}(k\pi/\sigma)\varphi_{n,\sigma,\tau}(m\pi/\sigma) = \delta_{k,m} \tag{2.19}$$

- The Fourier transform of the PSWF satisfy the following relations,

$$\int_{-\infty}^{\infty} e^{-jt\omega}\varphi_{n,\sigma,\tau}(t)dt = (-j)^n\sqrt{2\pi\tau/(\sigma\lambda_n)}\varphi_{n,\sigma,\tau}(\tau\omega/\sigma)\chi_\sigma(\omega) \quad (2.20)$$

$$\int_{-\tau}^{\tau} e^{-jt\omega}\varphi_{n,\sigma,\tau}(t)dt = (j)^n\sqrt{2\pi\tau\lambda_n/\sigma}\varphi_{n,\sigma,\tau}(\tau\omega/\sigma) \quad (2.21)$$

where $\chi_\sigma(\omega)$ is the characteristic function of $(-\sigma,\sigma)$. We can normalize the PSWF by setting $\tau = 1$ and hence $\gamma = \sigma$ so that they are orthonormal on $(-1,1)$ where $\varphi_{n,\sigma,1}$ can be shown as φ_n which gives,

$$\int_1^1 e^{-jt\sigma\omega}\varphi_n(t) = \gamma_n\varphi_n(\omega)$$

where $\gamma_n = (j)^n\sqrt{2\pi\tau\lambda_n/\sigma}$ and after rearranging

$$e^{-jt\sigma\omega} = \sum_n \gamma_n\varphi_n(\omega)\varphi_n(t) \quad (2.22)$$

for $t,\omega \in [-1,1]$.

- As can be measured from the value of $\lambda_n(\gamma)$, the energy of PSWF becomes less concentrated as the order n increases in the interval $[-1,1]$ for fixed values of γ. This property makes the summation of eigenvalues a finite value [22].

$$\sum_{n=0}^{\infty}\lambda_n(\gamma) = \frac{2\gamma}{\pi} \quad (2.23)$$

The first $\lceil(2\gamma)/\pi\rceil$ eigenvalues are close to 1 and for n beyond $\lceil(2\gamma)/\pi\rceil$, the eigenvalues become close to 0.

- The oscillation frequency of PSWF increases as γ increases. The various orders of PSWF are aperiodic which poses an alternative for the study of cyclic behavior of any type of motion since cyclic patterns are by nature aperiodic.

2.2.2 Discrete Prolate Spheroidal Sequences

The computational and derivational complexity have been the main reasons for the unpopularity of PSWF in engineering and scientific areas for many years. The hardness in their computation is not an obstacle anymore, thanks to the speed of the today's computers and the developed algorithms [20, 21, 22]. Although generation of the function set for studying them can be dealt successfully with today's computer speeds, it is still difficult to implement the algorithm that generates the function set for higher orders of n and high bandwidth values of γ [26]. The algorithms that have been proposed so far can be analyzed in terms of their advantages and disadvantages. As for the generation of function sets with higher orders of n and γ, one approach is to follow the expansion:

$$\varphi_{n,\sigma,\tau}(t) = \sum_{k=0}^{\infty} \beta_k^n P_k(t) \tag{2.24}$$

where $P_k(t)$ is the normalized Legendre polynomial of order k. The coefficients β_k^n can be calculated from a recurrence relation [22].

In his work Slepian claimed that $\varphi_{n,\sigma,\tau}(t)$ were simply normalized versions of the SWF of order zero. In order to find the eigenvalues, he used the radial solution in spheroidal wave coordinates of the Helmholtz wave equation of first type

$$\lambda_{n,\sigma,\tau} = \frac{2\gamma}{\pi}[R_{0n}(\gamma, 1)^2] \tag{2.25}$$

and for the $\varphi_{n,\sigma,\tau}(t)$, the angular solution of the Helmholtz wave equation of the first type

$$\lambda_{n,\sigma,\tau} = \frac{\sqrt{\lambda_n(\gamma)/\tau}}{\mu_n(\gamma)} S_{0n}(\gamma, \frac{t}{\tau}) \tag{2.26}$$

where

$$\mu_n(\gamma) = \sqrt{\int_{-1}^{1} (S_{0n}(\gamma, t))^2 dt} \tag{2.27}$$

The solution to $S_{0n}(\gamma, t)$ is found using the following expansion:

$$S_{mn}(\gamma, t) = \sum_{r=0,1}^{\infty} d_r^{mn}(\gamma) P_{m+r}^m(t) \tag{2.28}$$

where $P_{m+r}^{m}(t)$ is the Legendre polynomial and $d_r^{mn}(\gamma)$ is the expansion coefficient. The coefficient can be obtained in an iterative way as shown in [20]. This approach to generate $\varphi_{n,\sigma,\tau}(t)$ is only valid for the time interval $[-1, 1]$. Outside this interval the following equation can be applied [41]:

$$\varphi_{n,\sigma\tau}(t) = (\frac{\lambda_n(\gamma)}{\tau N_n})^{1/2}\kappa \sum_{r=0,1}^{M(n)} (-1)^{(r-n)/2} d_r^{0n}(\gamma) j_r(\frac{\gamma t}{\tau}) \tag{2.29}$$

where j_r are spherical Bessel functions. The recovery of one-dimensional discrete functions from uniformly separated samples using PSWF has been explored by [22, 47, 52]. In practical applications, PSWF is converted into the discrete prolate spheroidal sequences (DPSS) which can be defined as $\varphi_{n,\sigma,\tau}[kT]$, where T is the sampling period for k being an integer. When using DPSS for signal recovery, the number of DPSS coefficients and the frequency parameter γ should be decided. This is a special property that makes the DPSS analysis different than the Fourier series analysis. The function to be analyzed can be represented with DPSS basis with regard to a truncation based on the energy concentration of the eigenvalues. The free parameter γ can be decided based on the desired accuracy of the representation.

The DPSS are also closely related to the eigenfunctions of the harmonic oscillator in quantum mechanics which describe the location probability of a particle trapped in a parabolic potential well. The solution to this kind of concentration problem is similar to the solutions of maximally concentrating orthogonal functions in time. The difference is that the DPSS are maximally concentrated between the times $-T/2$ and $T/2$, whereas the harmonic oscillator eigenfunctions extend to $\pm\infty$ although they are exponentially damped. The oscillator eigenfunctions are products of Hermite polynomials with symmetric Gaussian functions. The harmonic oscillator eigenfunctions are their own Fourier transforms with appropriate scale changes. The same holds true for their time-sampled forms: the DPSS and their discrete Fourier transforms are identical except for appropriate scale factors (asymptotically the DPSS become Hermite functions). Figure 1 shows an example of a DPSS where $N = 100$ is the length in time, $NW = 2$ is the time bandwidth product and $K = 8$ for the MATLAB function *dpss* which is used as: [E,V] = DPSS(N,NW,K). Here dpss function creates K most band-limited discrete prolate spheroidal sequences and their corresponding concentrations (in vector V). In order to get eigenvalues, first the eigenvalues of a tridiagonal matrix are

found. It then uses inverse iteration using the exact eigenvalues on a starting vector with approximate shape, to get the eigenvectors required. It then computes the eigenvalues V of the Toeplitz sinc matrix using a fast autocorrelation technique [79].

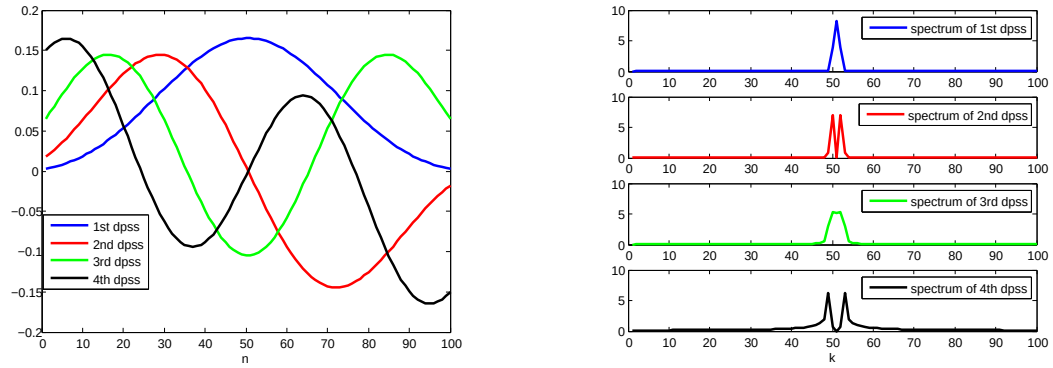

Figure 1: Left: The first 4 most band-limited DPSS (N=100, NW=2), Right: Corresponding spectra.

2.2.3 Discrete Prolate Spheroidal Sequences and Sampling Theory

When a function needs to be interpolated, integrated and differentiated, it is assumed to be approximated by a polynomial of certain order. However, the polynomial is almost never constructed explicitly. It is possible to assume that the function to be interpolated is bandlimited and use PSWF as a tool of numerical analysis for interpolation, quadrature and differentiation formulas for bandlimited functions [22]. The PSWF have already been used for the recovery of signals from *uniformly* spaced samples. In one of the approaches, the recovery of infinite length signals was proposed [47]. According to this approach when the discrete set of samples are concentrated on the interval $[-t_0, t_0]$, then the function $f(t)$ can be recovered as

$$f(t) \simeq \sum_{k=-\tau}^{\tau} y[k]\{\sum_{n=0}^{2\tau} \varphi_n[k]\varphi_n(t)\}\chi_\tau(t) \tag{2.30}$$

where the characteristic function χ compensates for the truncation to a finite discrete set of $y[k]$. The other approach is to find the roots or quadrature nodes of the PSWF set [22] such that a function can be interpolated as

$$f(t) = \rho_1\varphi_1(t) + \rho_2\varphi_2(t) + \cdots + \rho_n\varphi_n(t) \tag{2.31}$$

However, this method is limited to the functions of which zero crossings coincide to the zero crossings of a given PSWF. Indeed, the classical space in which to study all aspects of sampling is the space of finite energy signals ($Paley - WienerSpace : PW_\Omega$), bandlimited to $[-\Omega/2, \Omega/2]$ and leads to the expansion:

$$f(t) = \sum_n f(n/\Omega)\frac{\sin\pi(\Omega t - n)}{\pi(\Omega t - n)}. \tag{2.32}$$

The Paley-Wiener provides a good model for reconstruction of bandlimited signals. However, since bandlimited signals are analytic no such signal can be compactly supported [63]. We can suppose the values of $f \in PW_\Omega$ are negligible outside an interval $[-T/2, T/2]$, then in the sampling results only $f(n/\Omega)$ contribute to the reconstruction sum and for small error the the sum may be truncated to

$$f(t) = \sum_{[-T\Omega/2]}^{[T\Omega/2]} f(n/\Omega)\frac{\sin\pi(\Omega t - n)}{\pi(\Omega t - n)} \tag{2.33}$$

and it can be deduced that the functions bandlimited to $[-\Omega/2, \Omega/2]$ and approximately time-limited to $[-T/2, T/2]$ have dimension $2[T\Omega/2] + 1 \approx T\Omega$. This result comes from the work of Landau, Slepian and Pollak [34, 7] the so called *Bell Labs* theory, concerning time and bandlimiting. Although Bell Labs theory addressed several aspects of time-frequency localization, it did not address potentially useful connections between time-frequency localization and sampling [63]. Some of the examples of such connections are [98, 47]. Loosely speaking a function is time-frequency (T, Ω) localized if it is a sum of eigenfunctions of $P_\Omega Q_T$ having eigenvalues close to one where Q_Ω and P_T are the bandlimiting and time limiting operators, respectively [63]. In the real applications the assumption of bandlimitedness is not always true and the serious drawback is that the above result can only be applied to *uniformly* sampled signals [10]. The simplest way is to treat a function as being essentially time

and bandlimited and to assume that the most of the signal energy is concentrated in a time-frequency rectangle. There is no joint eigenfunction for the eigenvalue $\lambda = 1$, since there are no simultaneously time and band limited functions. It can be said that $f(t)$ is *essentially time and bandlimited*, if $f(t)$ nearly lies in the span of those eigenfunctions for $\lambda \approx 1$. This fundamental result can be used in practical applications. If we again represent time limiting operator as Q_T and bandlimiting operator as P_Ω, the application of these operators on the (2.32) leads to

$$Q_T P_\Omega f(x) = \int_{-T}^{T} f(t) \frac{\sin \pi(\Omega x - t)}{\pi(\Omega x - t)} dt. \tag{2.34}$$

Since the kernel $K(x,t) = \Omega sinc\Omega(x-t)_{\chi[-T/2,T/2]}(t)$ satisfies $||K||^2_{L^2(\Re\times\Re)} = \Omega T < \infty$, $P_\Omega Q_T$ is a Hilbert-Schmidt operator and $||P_\Omega Q_T||^2_{HS} = ||K||^2_{L^2(\Re\times\Re)} = \Omega T$ such that $P_\Omega Q_T$ is compact on PW_Ω. The eigen values of that compact operator are all positive and arranged as $\lambda_0 \leq \lambda_1 \leq, \cdots$. The associated eigenfunctions may be chosen to be real and after normalization they set an orthonormal basis for PW_Ω. PSWF are eigenfunctions of $P_\Omega Q_T$. The eigenvalues can also be interpreted as the time concentration of bandlimited functions. On the other hand, computing the trace of $P_\Omega Q_T$ gives

$$tr(P_\Omega Q_T) = \sum_{j=0}^{\infty} \lambda_j = \int K(t,t)dt = \int_{-T/2}^{T/2} \Omega dt = \Omega T. \tag{2.35}$$

In the continuous domain for a function $f(t)$, the analysis equation using the PSWF:

$$a_n = \lambda_n^{-1} \int_{-t_0}^{t_0} f(t)\varphi_n(t)dt \tag{2.36}$$

where a_n represents the expansion coefficients. The synthesis equation is

$$f(t) = \sum_{n=0}^{\infty} a_n \varphi_n(t)dt \tag{2.37}$$

and for the discrete case, the analysis and synthesis equations are

$$a_n = \frac{t_0}{M\lambda_n} \sum_{k=-M}^{M} y[k]\varphi_n[k] \tag{2.38}$$

$$f(t) \simeq \sum_{n=0}^{N} a_n \varphi_n(t) \tag{2.39}$$

As a result, we obtain the function $f(t)$ as:

$$f(t) \simeq \frac{t_0}{M} \sum_{n=0}^{N} \frac{\varphi_n(t)}{\lambda_n} \{ \sum_{k=-M}^{M} y[k] \varphi_n[k] \} \tag{2.40}$$

Accuracy of approximation depends on truncation value N and cut off frequency of the M^{th} DPSS, which will be explained in the following chapter.

3.0 SIGNAL RECONSTRUCTION FROM NONUNIFORM SAMPLES USING PROLATE SPHEROIDAL WAVE FUNCTIONS

In this chapter, we show our approach for nonuniform sampling problem together with the necessary derivations, analysis and results. According to the classical uncertainty principle, if an analog signal $x(t)$ that is essentially zero outside an interval of length Δt has a Fourier transform $X(\Omega)$, that is also essentially zero outside an interval of length $\Delta\Omega$, the following relation holds

$$\Delta\Omega\Delta t \geq 1/4\pi, \tag{3.1}$$

indicating that $x(t)$ and $X(\Omega)$ cannot both be highly concentrated. The authors in [28] propose a more general principle that does not require the signal and its Fourier transform to be concentrated on intervals. According to this new uncertainty principle, it is rather the number of non-zero terms — the signal "sparseness"— in either domain that is important. Thus, if $x(t)$ is practically zero outside a set $\mathcal{T}$, of measure $|\mathcal{T}|$, and $X(\Omega)$ is practically zero outside a set $\mathcal{W}$, of measure $|\mathcal{W}|$, then

$$|\mathcal{T}||\mathcal{W}| \geq 1 - \delta,$$

where δ is a small number related to the definition of "practically zero".

The generalized uncertainty principle shows that something unexpected is possible such as the recovery of a signal or image even if a significant amount of data are missing [32]. This new uncertainty principle has important consequences in the sampling and reconstruction of signals and has led to the new theories of compressive sensing [60, 64] and of random filtering [13] that exploit the sparseness of the signals in some basis for the reconstruction to use fewer

samples than the Nyquist sampling rate would require. According to Shannon's sampling theory, if a finite energy signal $x(t)$ has a Fourier transform $X(\Omega)$ that is bandlimited

$$x(t) \in B = \{x(t) \in \mathcal{L}^2(R) : X(\Omega) = 0, |\Omega| > \Omega_{max}\},$$

then $x(t)$ can be reconstructed from its uniform samples $\{x(kT_s)\}$:

$$x(t) = \sum_k x(kT_s)S(t - kT_s) \tag{3.2}$$

where $T_s < \pi/\Omega_{max}$ is the sampling period and $S(t)$ represents the sinc function.

Dimensionality reduction in the reconstruction of signals is an important issue in practical implementations. Considering that the time-frequency dimension is typically overestimated in the case of non-stationary signals where the frequency changes with time, a signal representation method called the Fractional Fourier Transform (FrFT) allows us to obtain optimum time-frequency dimensions. The assumption of band-limitedness for a signal makes sense in applications where the bandwidth of the signal is known *a priori*. However, bandwidth is not an exact measure of the frequency content of a signal but a mathematical idealization. Practically, it is time-limited signals that are being sampled, but such signals are not well represented by the sinc interpolation, since the sinc function spreads its energy over a wide time range. Attempting to approximate the infinite interpolation by a finite one, the signal reconstruction problem becomes *ill-posed* [2].

In the following section, we consider the general problems associated with the solution of linear equations that also provides a background for the nonuniform signal reconstruction problem. Next, we consider the problems caused by truncating Shannon's sinc interpolation in time. Later on, we present the PSWF interpolation of time-limited signals that are essentially bandlimited. This is followed by the nonuniform sampling and reconstruction. We discuss how to estimate the nonuniform sampling times as well as the minimal dimension of a signal, with a special consideration given to non-stationary signals considering the Landau-Pollak-Slepian dimensionality theorem [7, 62] which says that a discrete signal with a bandwidth β and N samples in a finite interval, has at most $N\beta$ degrees of freedom.

3.1 ANALYSIS OF SOLUTION FOR LINEAR SYSTEM OF EQUATIONS

The numerical processing of data (signals and images) require discrete form of data by means of sampling. In that case, instead of the signal or image f, only it's sampled values $f(x_i)$ are stored. One wants to recover the original data from these samples. However, this is an ill-posed problem since the subspace of functions f with $f(x_i) = y_i$ are infinite dimension. In practical applications it is assumed that $\{f\}$ are bandlimited. Indeed, images and signals are not arbitrary functions, they have some smoothness and decay properties [23].

3.1.1 Problems with ill-conditioned matrices

The numerical solution for the very ill-conditioned linear system of equations is more complicated than the treatment of well-conditioned systems because of the following reasons [46]:

- The kind of ill conditioning must be known: *rank deficiency* or *ill posed*? Is it possible to include additional information to stabilize the solution i.e., to regularize? what additional information is available and is it suitable for stabilization purposes?
- The type of numerical regularization method must be known in order to treat the problem efficiently and reliably on a computer. Are both the analysis and solution sections important? Should one prefer a direct or an iterative method? How much stabilization should be added?

In other words, it is not possible to deal satisfactorily with ill-conditioned problems without both theoretical and numerical analysis. Any discussion of ill-conditioned matrices requires the knowledge of the SVD of matrix A. There are two important classes of problems to consider and many practical problems belong to one of these two classes [46]:

- *rank-deficient problems* are characterized by the matrix A having a cluster of small singular values and there is a well-defined gap between large and small singular values. This implies that one or more rows and columns of A are nearly linear combinations of some or all of the remaining rows and columns. Therefore the matrix A contains almost redundant information and the key to the numerical treatment of such problems is to

extract the linearly independent information in A, to arrive at another problem with a well conditioned matrix.

- *discrete ill-posed problems* arise from the discretization of ill-posed problems such as Fredholm integral equations of the first kind. Here all the singular values of A, as well as the SVD components of the solution, on the average decay gradually to zero such that a discrete Picard condition is satisfied. Since there is no gap in the singular value spectrum, there is no notion of a numerical rank for these matrices. For discrete ill-posed problems, the goal is to find a balance between the residual norm and the size of the solution that matches the errors in the data as well as one's expectations to the computed solution where the size can be measured by a norm, a seminorm, or a Sobolev norm.

Due to the large condition number of A, both classes of problems are effectively underdetermined such that many of the regularization methods can be used for both classes of problems. Moreover, in both cases there is a strong relation between the amount of extracted linearly independent information, the norm of the solution and the corresponding residual. The difference between the two problem classes is the gap in singular value spectrum versus an overall decay. If the matrix is ill conditioned and the problem does not belong to either of the two classes, the regularization can not produce a suitable solution which can be dealt with iterative refinement or extended precision software [46].

3.1.2 The singular value decomposition analysis

The singular value decomposition (SVD) reveals all the difficulties associated with the ill-conditioning of the matrix A. Let A$\in R^{m\times n}$ be a rectangular or square matrix and assuming $m \geq n$. The SVD of A is a decomposition of the form [46]:

$$A = U\Sigma V^T = \sum_{i=1}^{n} u_i \sigma_i {v_i}^T \tag{3.3}$$

where $U = (u_1, ..., u_n) \in R^{m\times n}$ and $V = (v_1, ..., v_n) \in R^{n\times n}$ are matrices with orthonormal columns, $U^TU = V^TV = I_n$, and the matrix $\Sigma = diag(\sigma_1, ..., \sigma_n)$. The singular values are always well conditioned with respect to perturbations: if A is perturbed by a matrix E, then $||E||_2$ is an upper bound for the absolute perturbation of each singular value. The

singular values σ_i can also be defined as stationary values of $||Ax||_2/||x||_2$. From the relations $A^TA = V\Sigma^2V^T$ and $AA^T = U\Sigma^2U^T$, it is seen that the SVD of A is strongly linked to the eigenvalue decompositions of the symmetric semi-definite matrices A^TA and AA^T. This shows that the SVD is unique for the given matrix A, up to a sign change in the pair (u_i, v_i) except for singular vectors associated with multiple singular values where only the spaces spanned by the vectors are unique. In the discrete ill-posed problems, the features of the SVD [46]:

- The singular values σ_i decay gradually to zero with no particular gap in the spectrum, an increase of the dimensions of A will increase the number of small singular values.
- The left and right singular vectors u_i and v_i tend to have more sign changes in their elements as the index i increases as σ_i decreases.

Another use of SVD is in connection with least squares problems, possibly rank deficient. If A is invertible, then its inverse is given by $A^{-1} = \sum_{i=1}^{n} v_i\sigma_i^{-1}{u_i}^T$. The solution to $Ax = b$ is $x = \sum_{i=1}^{n} {\sigma^{-1}}_i({u^T}_i b)v_i$. Otherwise, the pseudoinverse or Moore-Penrose generalized inverse $A^\dagger$ is given by

$$A^\dagger \equiv \sum_{i=1}^{rank(A)} v_i\sigma_i^{-1}{u_i}^T \tag{3.4}$$

and the least squares solution x_{LS} to the least squares problem $||Ax - b||_2$ with minimum 2-norm, if $rank(A) < n$ is given by

$$x_{LS} = A^\dagger b = \sum_{i=1}^{rank(A)} \frac{{u^T}_i b}{\sigma_i} v_i \tag{3.5}$$

The sensitivity of the solutions vector x and x_{LS} to perturbations of A and b can be measured by the 2-norm condition number of A. Condition number of A is defined by:

$$cond(A) \equiv ||A||_2||A^\dagger||_2 = \sigma_1/\sigma_{rank(A)} \tag{3.6}$$

3.2 ANALYSIS FOR TRUNCATED SINC INTERPOLATION

In this section, we will analyze numerical problems in the reconstruction of signals if the kernel is the sinc function. Let us consider the case of π-bandlimited signals, i.e., $\Omega_{max} = \pi$, and define the corresponding sinc function as

$$S(t) = \frac{\sin \pi t}{\pi t} \qquad -\infty < t < \infty.$$

If the set of time-shifted sinc functions $\{S(t - t_k)_{k\in\mathcal{Z}}\}$ is a frame for the bandlimited signals, then a bandlimited signal $x(t)$ is uniquely represented by [2]

$$x(t) = \sum_{k\in\mathcal{Z}} c_k \; S(t - t_k). \tag{3.7}$$

Here the entries $\{c_k\}$ of an infinite vector $\mathbf{c}$ are the solution of the Grammian matrix equation

$$\mathbf{Rc} = \mathbf{b} \tag{3.8}$$

where $\mathbf{R}$ is a matrix with entries $\{R_{mn} = S(t_m - t_n)\}$ and $\mathbf{b}$ a vector with entries $\{x(t_k)\}$, both of infinite dimension. Thus according to equation (3.7), the reconstruction of $x(t)$ is obtained from its samples $\mathbf{c} = \mathbf{R}^{\dagger}\mathbf{b}$, where $\mathbf{R}^{\dagger}$ is the pseudo-inverse of $\mathbf{R}$.

When the shifted sinc functions form a frame which are linearly dependent, this linear dependency is useful for good reconstruction of f, if some samples are missing or not exact due to round off error or noise. Hence, inexact frames are preferable to exact frames and orthogonal bases. However, frame approach can lead to fast and stable numerical methods only when the finite dimensional model is carefully designed. In practice, the reconstruction as indicated above cannot be implemented since it requires the solution of an infinite-dimensional equation.

To compute a finite-dimensional approximation to $\{c_j\}_{j\in\mathcal{Z}}$ the sum in equation (3.7) is truncated to a finite support $-M \leq k \leq M$. Although this resolves the dimensionality problem, numerically the reconstruction problem becomes ill-posed [2]. If the sinc is a non exact frame, we have the following situation: Considering a bandlimited signal and letting the sampling points be $t_k = \frac{k}{m}$ indicating the uniform oversampling, where $k \in Z$ and $m < 1$. In this case, the signal is oversampled m times the Nyquist rate and the reconstruction is

trivial since the sinc constitutes a tight frame where m is the frame bounds. According to Shannon's theorem, the numerical approximation is obtained by truncating the summation in (3.7) as:

$$x(t) = \sum_{k=-M}^{M} c_k \; S(t - t_k). \tag{3.9}$$

where $c_k = \frac{x(t_k)}{m}$. The truncated frame approach makes $\mathbf{R}$ a Toeplitz matrix which can be represented by $\mathbf{R}_M$ with entries

$$R_{k,n} = \frac{\sin \frac{\pi}{m}(k-n)}{\frac{\pi}{m}(k-n)}, \;\; k, n \in Z. \tag{3.10}$$

It is known that this matrix has the singular values clustered around 0 and 1, with $logM$ singular values in the transition region [7, 35] and since the singular values of R_M decay exponentially to 0, the finite dimensional problem becomes ill posed [94].

In the case of nonuniform sampling the situation is not any better. It can be concluded that for infinite dimensional approach the singular values of $\mathbf{R}$ are bounded away from zero, however the smallest singular values of $\mathbf{R}_M$ will approach to zero as $M \to \infty$ [35]. This is a well known problem in regularization theory [94]. A standard technique to compute a stable solution is to use truncated singular value decomposition which requires to compute a regularized pseudo inverse. However, the optimal truncation level depends on the dimension M, the sampling geometry and the noise level. The truncation level is not known a priori hence must be calculated for each M independently [2]. Conjugate gradient method is another approach to solve (3.9) which can be at the same time used as a regularization method [24] but for large scale reconstruction problems this method is not appropriate [2]. In the next section, we will propose a method for finite dimensional reconstruction which keeps the original simplicity and structural properties of the Shannon's sampling theory.

3.3 PSWF PROJECTION APPROACH

We are interested in the representation of time-limited signals, which by the conventional uncertainty principle are non-bandlimited. Our assumption is that the signals are essentially

bandlimited, i.e., most of the signal energy is concentrated in a bandwidth B, with a frequency $W(rad/sec)$ corresponding to a high percentage of the signal energy. Assuming that the signal $x(t)$ is sampled using Nyquist sampling rate F_s and its time support is $\tau = N_n T_s$, then its time-frequency dimension [7, 62]

$$D_{TF}\{x(t)\} \quad = \quad [\tau][W/\pi] \tag{3.11}$$

which for the case of bandlimited signals, replacing τ and W we get that it is less than or equal to N_n, thus hinting to the possibility of representing these signal with less than N_n samples. The question is how can we obtain such a representation and how can we reconstruct the signal from it? We will show next that it is possible by using the PSWF.

The problems with the sinc interpolation are in part due to the nature of the sinc function. The sinc function is not concentrated in time, although well concentrated in frequency, thus not well suited to represent time-limited signals. As such it is not the appropriate basis. A more appropriate basis should have high energy concentration both in time and in frequency. The PSWF have such a characteristic. Now we can review the properties of the PSWF $\{\varphi_n(t)\}$ that are of interest in our method:

- $\{\varphi_n(t)\}$ is a sequence of real-valued functions with finite time support resulting from maximizing their energy in a given bandwidth.
- $\{\varphi_n(t)\}$ are eigenfunctions of the integral operator

$$\begin{aligned} \varphi_n(t) &= \frac{1}{\lambda_n}\int_{-T}^{T} \varphi_n(x) S(t-x)dx \\ &= \int_{-\infty}^{\infty} \varphi_n(x) S(t-x)dx \end{aligned} \tag{3.12}$$

leading to a dual orthogonality in finite and infinite domains

$$\begin{aligned} \int_{-T}^{T} \varphi_n(t)\varphi_m(t)dt &= \lambda_n \delta_{nm} \\ \int_{-\infty}^{\infty} \varphi_n(t)\varphi_m(t)dt &= \delta_{nm} \end{aligned}$$

and as such they constitute an orthogonal basis of finite energy signal of finite support $\mathcal{L}^2(-T,T)$ and an orthonormal basis for the space of bandlimited functions [47].

Of special significance, the sinc function $S(t)$, which belongs to the space of bandlimited signals, can be expanded in terms of the basis $\{\varphi_n(t)\}$ [47] such that

$$S(t - kT_s) = \sum_{m=0}^{\infty} \varphi_m(kT_s)\varphi_m(t) \tag{3.13}$$

which allows us to write the sinc interpolation in Eq.(3.7) (for $\Omega_{max} = \pi$) as

$$\begin{aligned} x(t) &= \sum_{k=-\infty}^{\infty} x(kT_s) \sum_{m=0}^{\infty} \varphi_m(kT_s)\varphi_m(t) \\ &= \sum_{m=0}^{\infty} \left[\sum_{k=-\infty}^{\infty} x(kT_s)\varphi_m(kT_s) \right] \varphi_m(t) \\ &= \sum_{m=0}^{\infty} \gamma_m \varphi_m(t) \end{aligned} \tag{3.14}$$

which is an infinite dimensional interpolation of the continuous signal in terms of PSWF. Thus the result (Eqs. 3.7 and 3.8) is changed by using PSWF as the frames and a new Grammian equation

$$\mathbf{R}\gamma = \mathbf{b} \tag{3.15}$$

where $\mathbf{R}$ is now a matrix with entries $\{R_{mn} = \varphi_m(t_n)\}$ and $\mathbf{b}$ is a vector with entries $\{x(t_j)\}$, is obtained.

Like in the sinc case, the reconstruction of $x(t)$ is obtained using $\gamma = \mathbf{R}^{\dagger}\mathbf{b}$, where $\mathbf{R}^{\dagger}$ represents the pseudo-inverse of $\mathbf{R}$. In practice this reconstruction is not possible because of the infinite dimension of $\mathbf{R}$, thus we would like to explore if truncations in time and in frequency make the reconstruction possible. Figures 2 and 3 illustrate the effect of applying finite dimensional modeling to matrices composed of sinc and DPSS, respectively. In Fig. 2 we illustrate the case of oversampling in the truncated sinc interpolation [2], while Fig. 3 shows the case of the DPSS-based matrix. In the first case some of the eigenvalues of $\mathbf{R}_M$ become close to zero, giving very large values in the corresponding pseudo-inverse. The DPSS-based matrix does not show such a behavior!

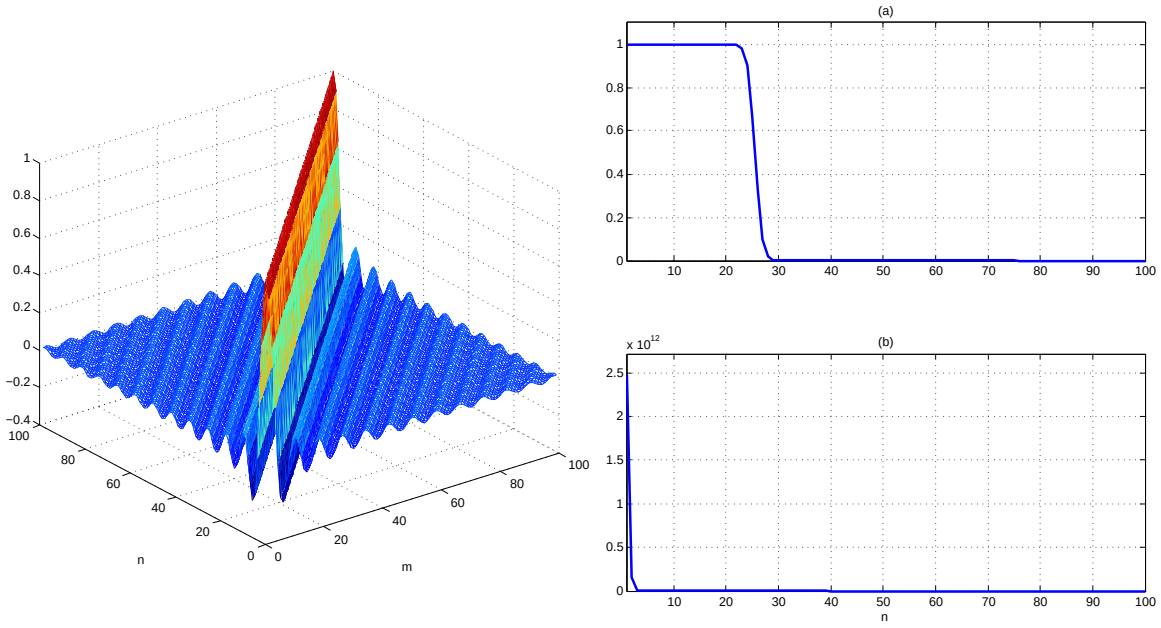

Figure 2: Left: $\mathbf{R}_M$ matrix, Right: (a) Singular values of $\mathbf{R}_M$ matrix, (b) Singular values of pseudoinverse of $\mathbf{R}_M$ matrix.

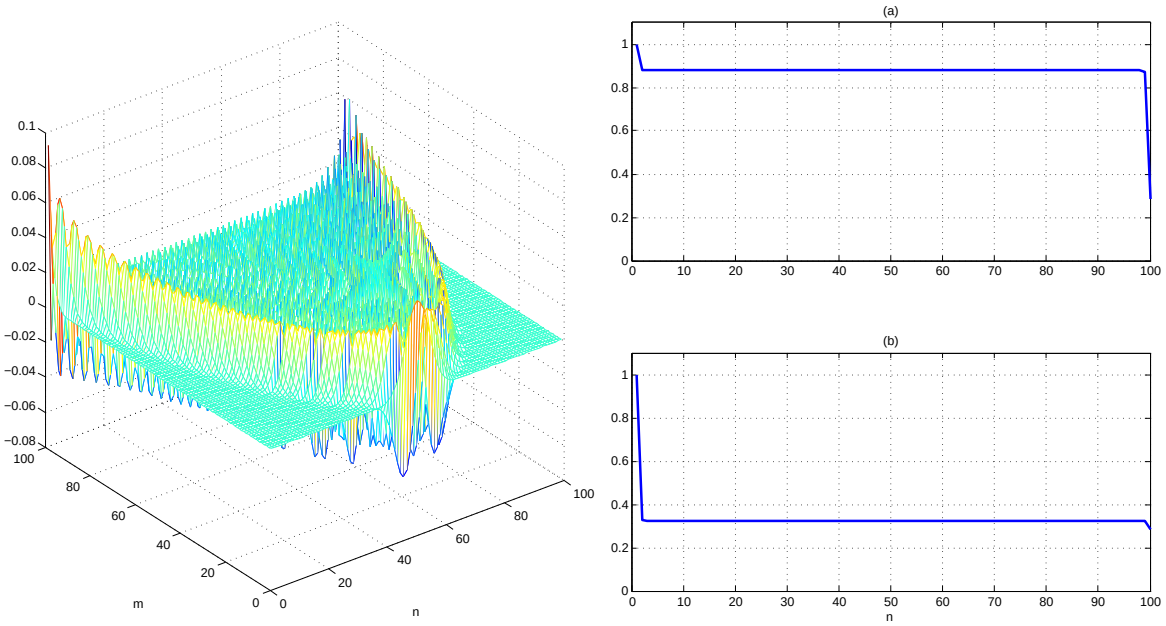

Figure 3: Left: DPSS matrix, (a) Singular values of DPSS matrix, (b) Singular values of pseudoinverse of DPSS matrix.

Considering a time-limited signal $x(t)$, $0 \leq t \leq (N-1)T_s$, for a sampling period T_s, that is essentially bandlimited to a frequency band $(-W, W)$ i.e., the normalized signal energy outside the given frequency band

$$\varepsilon = \frac{1}{2\pi||x||^2}\left[\int_W^{\infty} |X(\Omega)|^2 d\Omega + \int_{-\infty}^{-W} |X(\Omega)|^2 d\Omega\right] \tag{3.16}$$

is very small then an approximate of $x(t)$ is given by

$$x(t) \approx \hat{x}(t) = \sum_{m=0}^{M-1}\left[\sum_{k=0}^{N-1} x(kT_s)\varphi_m(kT_s)\right]\varphi_m(t) \tag{3.17}$$

where M depends on W. Accuracy of that approximation depends on how concentrated the energy is within the given frequency band. If we define the projection error to be

$$\varepsilon_p = \frac{||x - \hat{x}||^2}{||x||^2} \tag{3.18}$$

where $||.||$ is the Euclidean norm, it can be shown that the M value can be chosen as the largest integer [62] for which

$$\lambda_{M-1} \geq \frac{(1-\varepsilon) - \lambda_0(1-\varepsilon_p)}{\varepsilon_p} \tag{3.19}$$

where λ_{M-1} and λ_0 are eigenvalues of the DPSS. If we assume $\lambda_0 = 1$, we obtain an approximate relation between the projection error ε_p and the essential bandlimitedness error ε for a chosen M:

$$\frac{\varepsilon}{\varepsilon_p} \geq 1 - \lambda_{M-1} \tag{3.20}$$

It is clear that if we choose an M so that λ_{M-1} is very close to 0, the projection would have a small error ε_p which would then be the upper bound for ε. In the following section we consider how to choose an appropriate value for M and how it connects with W.

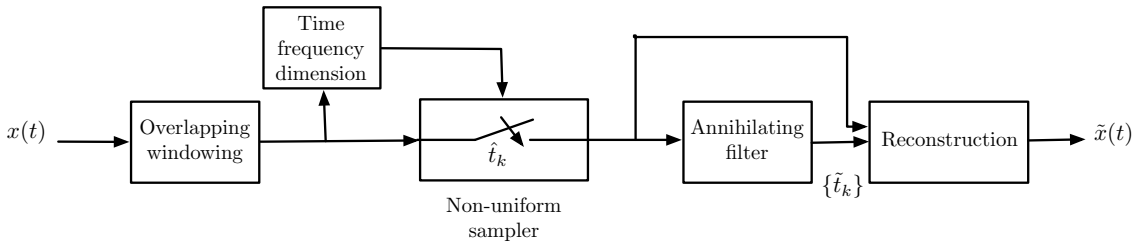

Figure 4: Overall sampling and reconstruction procedure.

3.4 NONUNIFORM SAMPLING AND PSWF RECONSTRUCTION

We would like to modify the conventional Nyquist-Shannon sampling and reconstruction procedure so as to

- consider time-limited and essentially bandlimited signals,
- decrease the sampling rate being characterized as nonuniform,
- reconstruct the original signal without aliasing effects.

Figure 4 displays the overall sampling and reconstruction procedure that we propose in this chapter. Suppose $x(t)$ has a finite support $0 \leq t \leq T$ and is essentially bandlimited to $W(rad/sec)$. If we used Nyquist sampling rate $F_s = 2W/2\pi$, then N_n samples (such that $N_n T_s = T$) are needed to reconstruct the signal. The projection for the uniform sampling times $t_k = kT_s$ would be

$$\hat{x}(t_k) \quad = \quad \sum_{m=0}^{M-1} \gamma_{M,m} \varphi_m(t_k) \tag{3.21}$$

where the coefficients are

$$\gamma_{M,m} = \sum_{k=0}^{N_n-1} x(kT_s)\varphi_m(kT_s).$$

The M value is chosen by matching the Nyquist frequency with the cut-off frequency of $\varphi_{M-1}(t)$ or

$$WT_s = \frac{2\pi(M-1)}{N_n} \leq \pi$$

so that $M \leq \frac{N_n}{2} + 1$. Equivalently, the M value can be obtained either by

- using the time-bandwidth dimension in equation (3.11) $M = D_{TF}/2 + 1$,
- finding W so that

$$||x||^2 \approx \sum_{n=0}^{M-1} \lambda_n |\gamma_n|^2$$

  or the eigenvalues $\{\lambda_n\}$ are approximately zero for $n \geq M$.

The matrix form of the projected signal at the uniform times $\{t_k = kT_s\}$ is

$$\hat{x}(t_k) = \Phi(t_k)\gamma_M \tag{3.22}$$

where $\hat{x}(t_k)$ is an N_n vector containing samples $\{x(kT_s)\}$, γ_M is the vector formed by the coefficients resulting from the projection with respect to the DPSS. The $N_n \times M$ matrix is given by

$$\Phi = \begin{bmatrix} \varphi_0(t_0) & \varphi_1(t_0) & \cdots & \varphi_{M-1}(t_0) \\ \varphi_0(t_1) & \varphi_1(t_1) & \cdots & \varphi_{M-1}(t_1) \\ \vdots & \vdots & \cdots & \vdots \\ \varphi_0(t_{N_n-2}) & \varphi_1(t_{N_n-2}) & \cdots & \varphi_{M-1}(t_{N_n-2}) \\ \varphi_0(t_{N_n-1}) & \varphi_1(t_{N_n-1}) & \cdots & \varphi_{M-1}(t_{N_n-1}) \end{bmatrix}$$

where $0 \leq k \leq N_n - 1$.

3.4.1 Nonuniform Sampling Scheme

The assumption in Nyquist-Shannon sampling theory that the samples are taken at uniform times kT_s is typically not realistic due to imperfect sensors, mismatched clocks, etc. There are many possible forms in which these sampling times can occur [1]. In our simulations we consider stochastic jitter sampling with uniform distribution, but it is also possible to use a truncated Gaussian distribution or any other bounded distribution. Thus we assume the samples are taken at times

$$\hat{t}_k = \frac{N_n}{M} kT_s + \Delta \qquad 0 \leq k \leq M - 1 \tag{3.23}$$

where Δ is a random variable uniformly distributed in

$$\left[-0.5\frac{N_n}{M}T_s,\ 0.5\frac{N_n}{M}T_s\right].$$

From the M-dimensional projection of $x(t)$, the nonuniform samples are measured as

$$\begin{bmatrix} \hat{x}(\hat{t}_0) \\ \hat{x}(\hat{t}_1) \\ \vdots \\ \hat{x}(\hat{t}_{M-2}) \\ \hat{x}(\hat{t}_{M-1}) \end{bmatrix} = \begin{bmatrix} \varphi_0(\hat{t}_0) & \cdots & \varphi_{M-1}(\hat{t}_0) \\ \varphi_0(\hat{t}_1) & \cdots & \varphi_{M-1}(\hat{t}_1) \\ \vdots & \cdots & \vdots \\ \varphi_0(\hat{t}_{M-2}) & \cdots & \varphi_{M-1}(\hat{t}_{M-2}) \\ \varphi_0(\hat{t}_{M-1}) & \cdots & \varphi_{M-1}(\hat{t}_{M-1}) \end{bmatrix} \begin{bmatrix} \gamma_0 \\ \gamma_1 \\ \vdots \\ \gamma_{M-2} \\ \gamma_{M-1} \end{bmatrix}$$

or in a matrix form as

$$\hat{x}(\hat{t}_k) = \Phi(\hat{t}_k)\gamma_M \tag{3.24}$$

the matrix $\Phi(\hat{t}_k)$ of dimension $M \times M$ is random, given the random nature of the sampling. As such, it is not always possible to expect that it is invertible. Assuming that the sampling times $\{\hat{t}_k\}$ are known, or estimated, we can find the coefficients of the projection using the pseudo-inverse as

$$\gamma_M = \left[\Phi(\hat{t}_k)\right]^\dagger \hat{x}(\hat{t}_k).$$

Then, according to (3.24) the reconstructed Nyquist samples are given by

$$\begin{aligned} x_r(t_k) &= \Phi(t_k)\left[\Phi(\hat{t}_k)\right]^\dagger \hat{x}(\hat{t}_k) \\ &= \Theta\ \hat{x}(\hat{t}_k). \end{aligned} \tag{3.25}$$

To obtain the analog form of the reconstructed signal these samples are then passed through an ideal low-pass filter, just like in the Nyquist reconstruction. According to the model described in Fig.4, we need to calculate the projection order and estimate the nonuniform sampling times. We will describe the necessary steps in the following section:

3.4.2 Estimation of Sampling Times

In general, the nonuniform sampling times are not known. This section is about the estimation of nonuniform sampling times. Let the signal

$$z(t) = \sum_{k=0}^{M-1} x(\hat{t}_k)\delta(t - \hat{t}_k) + \eta(t), \qquad 0 \le t \le T$$

be a stream of M delta functions with additive noise $\eta(t)$ resulting from the nonuniform sampling. We wish to estimate the sampling times $\{\hat{t}_k\}$. If we consider the periodic extension of the stream of delta functions, the signal

$$z(t) = \sum_{k=-\infty}^{\infty} X_k e^{jk\Omega_0 t} + \eta(t) \qquad \Omega_0 = 2\pi/T,$$

where the Fourier coefficients are given by

$$\begin{aligned} X_k &= \frac{1}{T}\int_T \sum_{m=0}^{M-1} x(\hat{t}_m)\delta(t - \hat{t}_m)e^{-jk\Omega_0 t}dt \qquad \Omega_0 = \frac{2\pi}{T} \\ &= \sum_{m=0}^{M-1} x(\hat{t}_m)e^{-jk\Omega_0 \hat{t}_m} \end{aligned} \tag{3.26}$$

Considering that the frequencies of the original signal are in the interval $[-(M-1)\Omega_0, (M-1)\Omega_0]$, $z(t)$ can be low-pass filtered to obtain noisy Fourier coefficients given by

$$\hat{X}_k = \sum_{m=0}^{M-1} \hat{x}(\hat{t}_m)u_m^k \qquad u_m = e^{-j\Omega_0 \hat{t}_m}, \quad -(M-1) \le k \le (M-1) \tag{3.27}$$

The problem is then to find the parameters $\{\hat{x}(\hat{t}_m), \hat{t}_m\}$ that match the $\{\hat{X}_k\}$ for $-(M-1) \le k \le (M-1)$ obtained from the noisy nonuniform sampling, in particular the time delays. This problem is connected with Prony's method [66, 67], and with the annihilating filter [61]. If

$$A(z) = \prod_{m=0}^{M-1}(1 - u_m z^{-1}) = \sum_{m=0}^{M-1} \alpha_m z^{-m}$$

is the transfer function of the annihilating filter. Filtering the two-sided sequence $\{\hat{X}_k\}$ with it we get the convolution sum

$$\begin{aligned}\sum_{m=0}^{M-1} \alpha_m \hat{X}_{k-m} &= \sum_{m=0}^{M-1}\sum_{n=0}^{M-1} \hat{x}(\hat{t}_n) u_n^{k-m} \alpha_m \\ &= \sum_{n=0}^{M-1} \hat{x}(\hat{t}_n) \left[\sum_{m=0}^{M-1} \alpha_m u_n^{-m}\right] u_n^k = 0\end{aligned}$$

where the last term is due to u_n being a root of $A(z)$. Solving the above equations for $\{\alpha_m\}$ we obtain $A(z)$ and finding its roots we can then find the delays. From the roots of $A(z)$, $u_m = e^{-j2\pi\hat{t}_m/T}$, estimates of the nonuniform sampling times are given by

$$\hat{t}_m = \frac{-T}{2\pi j} \log u_m \qquad m = 0, \cdots M-1$$

which can be used in the signal reconstruction together with associated sample values.

3.4.3 Estimation of the DPSS Projection Order

As indicated in (3.11), the number of necessary sampling points needed to reconstruct the signal depends on the time-frequency dimension of the continuous signal. The time-frequency support of a signal $x(t)$ is defined as

$$\frac{\left[\int (t-\eta_t)^2 \ |x(t)|^2 dt\right]^{1/2} \left[\int (f-\eta_f)^2 |X(f)|^2 df\right]^{1/2}}{\|x\|^2} \tag{3.28}$$

where $\int |x(t)|^2 dt$ and $\int |X(f)|^2 df$ are the energies of the signal in time and in frequency domains, respectively. In the above definition, the mean values in time and frequency, η_t and η_f are expressed as

$$\begin{aligned}\eta_t &= \left[\int t \ |x(t)|^2 dt\right] / \|x\|^2 \ , \\ \eta_f &= \left[\int f \ |X(f)|^2 df\right] / \|x\|^2 .\end{aligned}$$

The time-frequency support of non-stationary signals usually become smaller when considering their actual instantaneous bandwidth [69]. This redundancy in the time-frequency support, in the case of time-limited chirp signals sweeping a large frequency band, is shown by the signal and its Wigner distribution [69] in Fig. 5(a) and (b), respectively. To provide

a rotation-invariant measure of signal support on the time-frequency plane, a generalized time-bandwidth product is introduced in [70]. Here we define the minimum time-frequency dimension of a signal $x(t)$ among all fractional Fourier domains interpolating between time and frequency as

$$\min_{0\leq a<4} D_{TF}\{x_a(\cdot)\}$$

where $x_a(\cdot)$ is the a^{th}-order fractional Fourier transform (FrFT) of $x(t)$, which is given by [71, 72]

$$\begin{aligned} x_a(t) &\equiv \{F^a x\}(t) \\ &= \int B_a(t,t')x(t')dt' \ , \ 0 \leq a < 4, \end{aligned} \tag{3.29}$$

where

$$B_a(t,t') = \frac{e^{-j(\pi \ \mathrm{sgn}(a)/4+\phi/2)}}{|\sin\phi|^{1/2}} \ e^{j\pi(t^2\cot\phi - 2tt'\csc\phi + t'^2\cot\phi)} \tag{3.30}$$

is the transformation kernel, $\phi = a\frac{\pi}{2}$ and $\mathrm{sgn}(\cdot)$ is the sign function.

FrFT is a linear transformation and can be defined for all signals that have Fourier transform. The FrFT of order $a = a_0$ transforms a signal into the ${a_0}^{th}$-order fractional Fourier domain, which is oriented by $\phi_0 = a_0\pi/2$ with respect to the time axis in the counter-clockwise direction [73]. The fractional Fourier domains corresponding to $a = 0$ and $a = 1$ are the time and frequency domains, respectively. The a_{th}-order FrFT for $0 < a < 1$ interpolates between the function $x(t)$ and its Fourier transform $X(f)$. The continuous FrFT given by equation (3.29) can be computed from discrete samples of $x(t)$ by using the fast computation algorithm proposed in [74] with $O(N\log N)$ operations. The FrFT rotates the Wigner distribution (WD) of a signal in the clockwise direction [75]. The appropriate order of the FrFT rotates the WD in the clockwise direction so that the chirp signal in Fig. 5 (a) is transformed into a windowed sinusoidal signal as shown in Fig. 5 (c) with a corresponding WD in (d). As the minimum time-frequency dimension is achieved by searching on the FrFTs, sampling at the appropriate FrFT order will reduce the required number of non-uniform samples for nonstationary signals at the expense of transforming the signal back into the time domain.

3.5 SIMULATIONS

In this section, the performance of the proposed reconstruction algorithm is demonstrated by applying it to (i) a combination of sinusoids, (ii) a chirp signal embedded in noise, and (iii) subdural electroencephalogram (EEG) signals. First, we consider a combination of three sinusoids as a test of our algorithm. As shown in Fig. 6, the spectrum of the M^{th} DPSS (red) includes the most significant frequency components of the original signal (black), and of the DPSS projection (blue) indicating the chosen value of M is appropriate. The signal is reconstructed using a projection of order M using half of the samples used for the sinc interpolation reconstruction, with an error value of 2.1×10^{-3} (see Fig. 6). However, the error in Shannon's reconstruction, with ideal low-pass filters, is 5.3×10^{-3} as shown in Fig. 8. This is an important improvement considering the non-uniformity of the sampling process and the reduction on the sampling rate.

In the second simulation, we consider the application of our method in denoising a linear frequency modulated signal embedded in noise. The method takes advantage of the FrFT for determining the optimal time-frequency dimension. In the noiseless case the value found for M is used as the *a priori* information in the denoising. On the left side of Fig. 7(a), we display the normalized mean square error (NMSE) with respect to signal to noise ratio (SNR) values between 0 to 25 (dB) as a result of Monte Carlo trials at each SNR. Fig. 7(b) displays the denoising for an SNR of 0dB. In the third part of our simulations, we consider subdural raw EEG signals and their wavelet processed components which are called fast, slow and primary [87]. To make the signal satisfy the time-limited and the essentially bandlimited conditions we process the EEG signals with overlapping windows, adding up to unity. This also guarantees that the annihilating filter works, by allowing to find the roots of a low-order polynomial.

3.6 CONCLUSIONS

We have presented a complete model for sampling and reconstruction of time-limited analog signals by using projection on the space of DPSS. By projecting the signal onto a finite di-

mensional DPSS subspace, it is shown that this method can deal with non-uniform sampling and does not seem to be affected by aliasing. The dimension of that subspace depends on a time frequency product which is at most half the sampling rate that needed in the sinc function based reconstruction. However, our method requires the estimation of the nonuniform sampling times, for which we apply an annihilating filter, and the possible optimization of the time-frequency dimension in the case of non-stationary signals, for this we apply the FrFT.

The computational complexity of the proposed reconstruction lies in the implementation of the annihilating filter due to the root-finding required by it. Otherwise, the algorithm behaves as a modification of Shannon's sinc interpolation. For nonstationary signals, computation of the minimal time-frequency dimension requires additional computation due to the FrFT. Besides the sampling and reconstruction, we have shown that our method can be applied in denoising and its performance can be related to that of the compressive sensing method as we will show in the following chapter. We have shown the performance of the method for synthetic as well as actual signals.

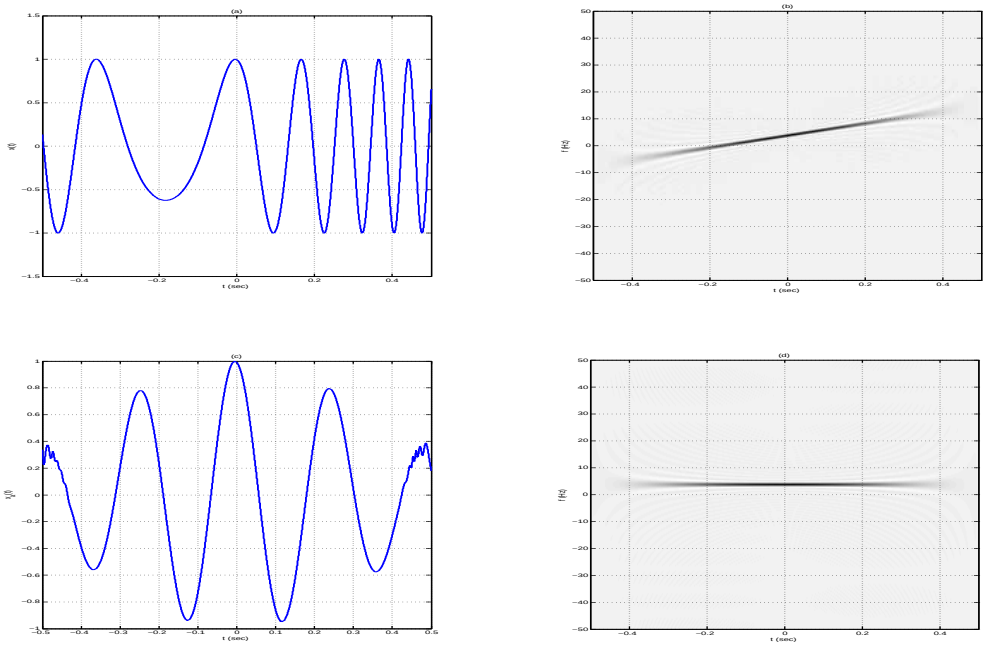

Figure 5: (a) Chirp signal, (b) its corresponding WD. (c) FrFT of the chirp and (d) its corresponding WD.

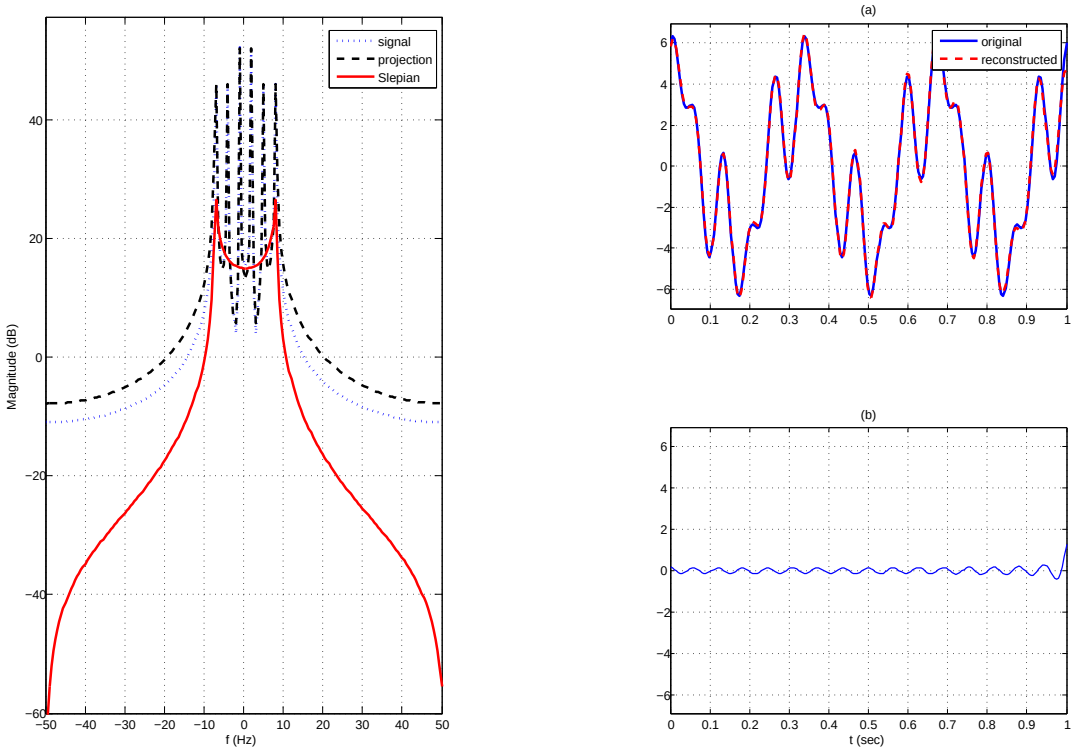

Figure 6: Left: Spectrum of signal, M^{th} DPSS and projected signal, Right: (a) reconstruction from nonuniform samples, (b) error.

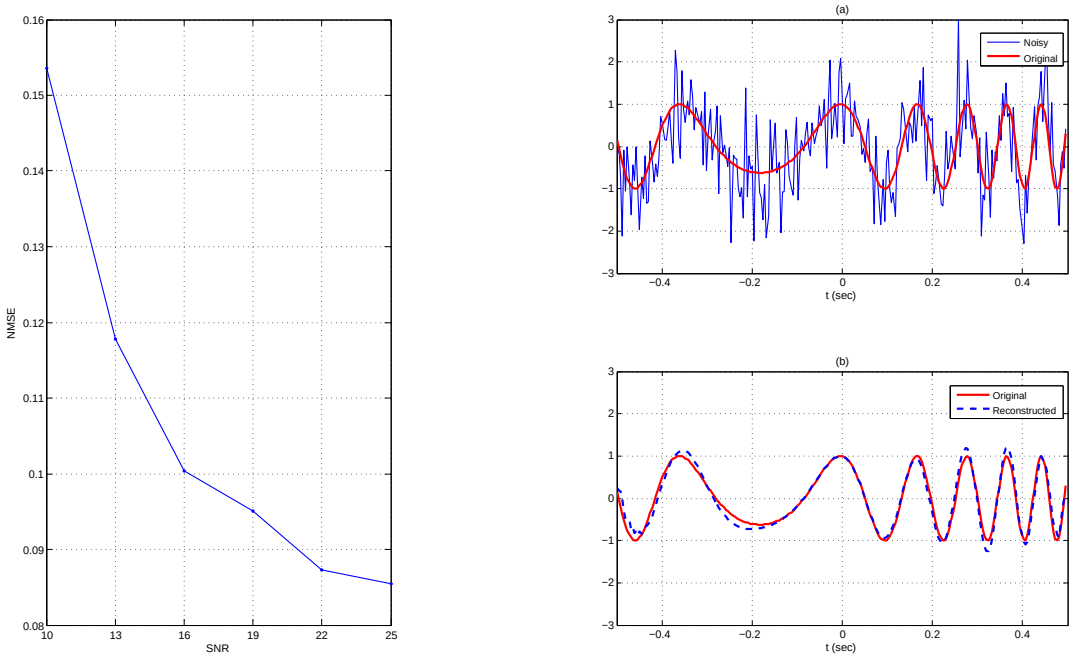

Figure 7: Left: Normalized Mean Square Error vs. SNR for noisy chirp, right: (a) original vs. noisy signal, (b) reconstructed vs. original signal.

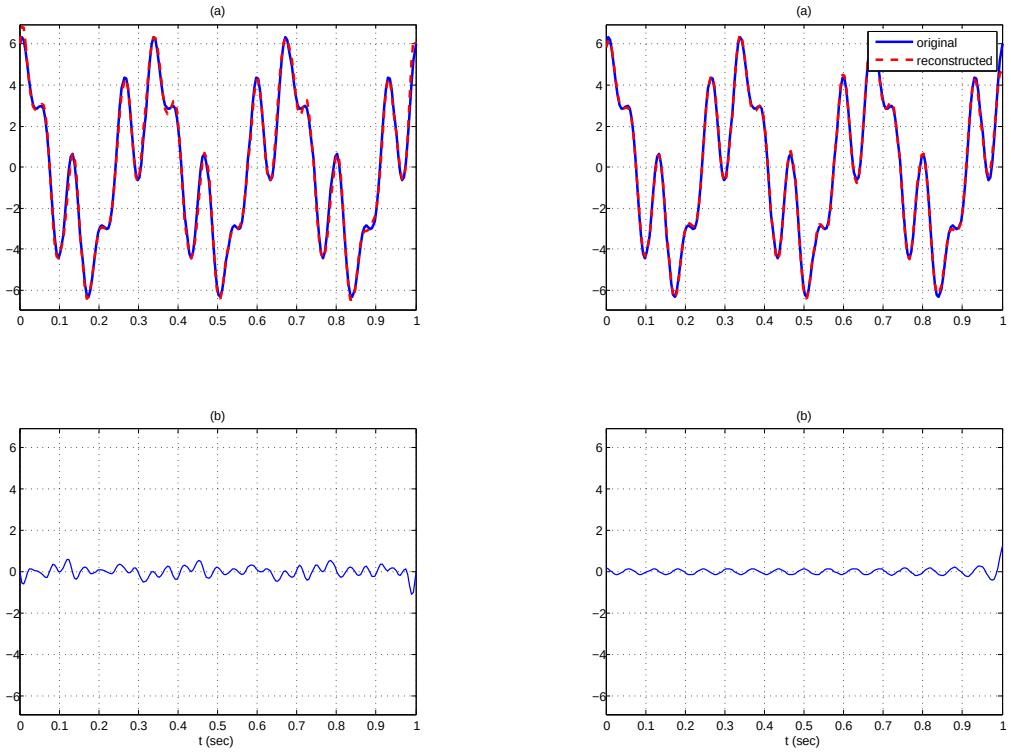

Figure 8: Nonuniform reconstruction, Left: sinc reconstruction, Right: PSWF reconstruction.

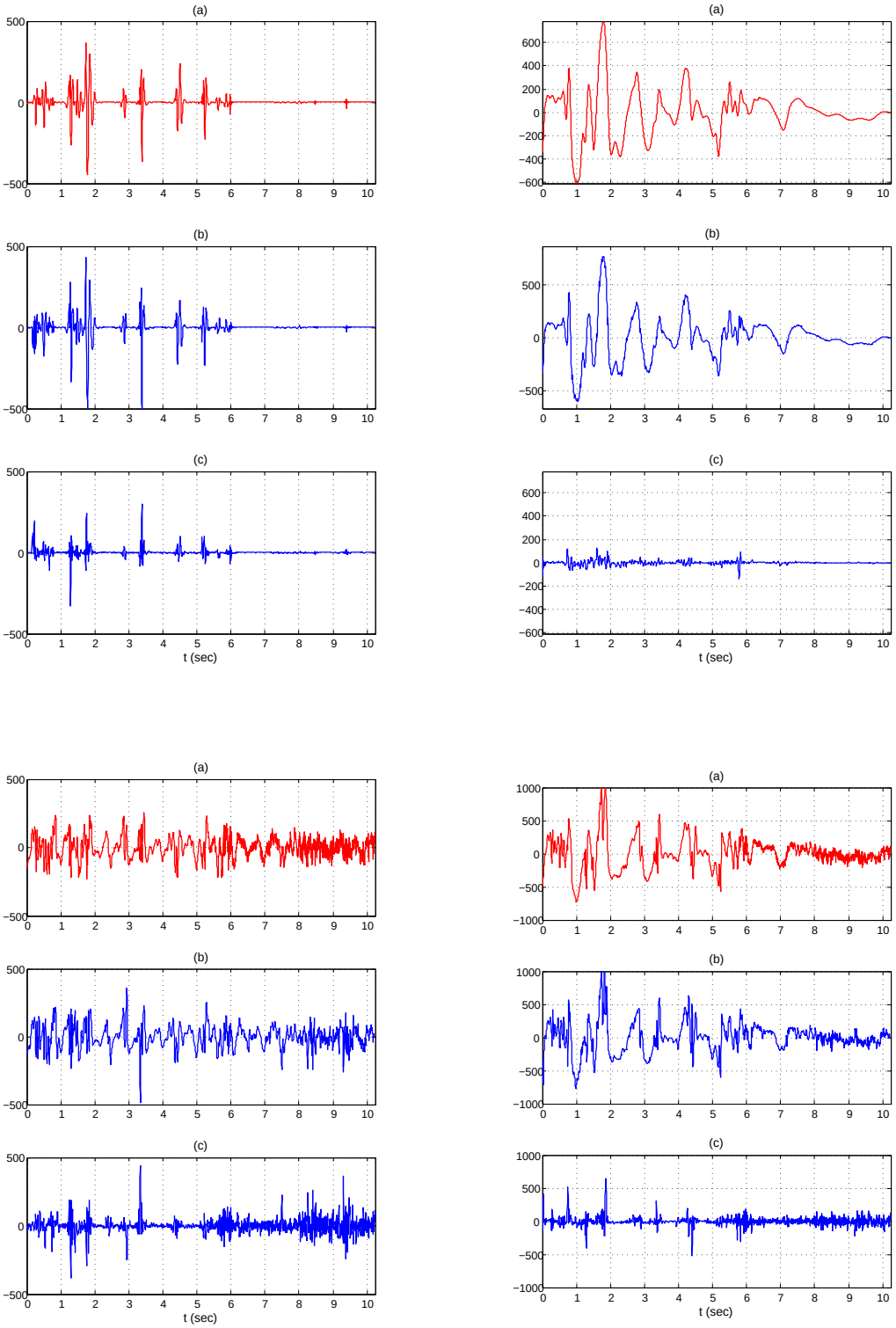

Figure 9: Top left: (a) Fast EEG, (b) reconstructed EEG, (c) error. Top right: (a) Slow EEG, (b) reconstructed EEG, (c) error. Bottom left: (a) Primary EEG, (b) reconstructed EEG, (c) error. Bottom right: (a) Raw EEG, (b) reconstructed EEG, (c) error.

4.0 REGULARIZED RECONSTRUCTION FROM LEVEL CROSSING SAMPLES

In this chapter, we provide a new method for reconstructing a signal from level crossing (LC) samples and in general from random samples under the assumption that the original signal is time-limited and essentially band-limited. Such a signal is well approximated in a low-dimensional subspace and the reconstruction can be achieved using the PSWFs projection. Since the LC samples are non-uniformly spaced in time and the sampling density depends on the local properties of the signal being sampled, we formulate estimation of the projection coefficients using the Tikhonov regularization [50]. The main objective of the regularization is to incorporate more information in order to get the desired solution. We demonstrate the effectiveness of the proposed method in terms of the reduction in the number of necessary samples for reconstruction, and in the case of noisy sampling by comparing our method with piecewise cubic interpolation and compressive sampling (CS) techniques [55]. The rest of the chapter is organized as follows. In section 4.1 we discuss level crossing sampling, compressive sampling and the nonuniform reconstruction problem. While in section 4.2, we consider the Tikhonov regularization procedure. In section 4.3, the reconstruction using PSWF and the use of the Tikhonov regularization in this problem are presented. Section 4.4 illustrates the application of our procedure and conclusions follow.

4.1 LEVEL CROSSING SAMPLING

Two efficient sampling procedures are the level-crossing sampling and compressive sampling [93, 8, 55, 65]. Level-crossing relates to the Lebesgue integral that approximates a signal with

a fixed set of amplitude values and with samples taken at non-uniform times depending on the signal. Compressive sampling uses the sparseness in the signal to decrease the number of samples needed to represent the signal. A signal is sparse if its support in some representation or basis is smaller than its actual support. Level crossing and compressive sensing are signal dependent methods that take advantage of the signal structure. Level crossing (LC) is an event-based nonuniform sampling that can be used efficiently for bursty or sparse signals [3, 93, 8, 95] and is known to be very useful especially for the processing of non-stationary signals [45].

In the LC sampling an analog signal $x(t)$ is compared with a set of reference levels located within the dynamic range of the signal, and only when the signal exceeds one of the reference levels the sample is taken in the time domain as shown in Figure 10. Thus, the signal determines when to take samples, and the result is a nonuniform sampling such that for a bursty signal more samples are taken during the burst and fewer otherwise. We propose an approach for the reconstruction of signals from their LC samples. Notice that different from

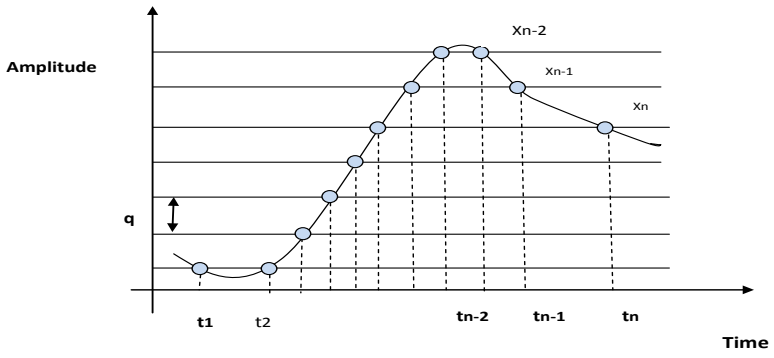

Figure 10: Level crossing sampling of a signal.

conventional sampling and quantization, LC provides a sample that is obtained by quantizing the signal amplitude. The resulting samples coincides exactly with the quantization levels, no quantization error, and the sampling does not require that the signal to be bandlimited. However, the reconstruction requires both sample levels and sampling times to be available.

4.2 TIKHONOV REGULARIZATION

Ill-posed problems arise in the form of inverse problems in many areas of science and engineering when the internal structure of a physical system is being determined from the measured behavior of system or in determining the unknown input that gives rise to a measured output signal. Some examples are acoustics, computerized tomography, continuation problems, electromagnetic scattering, geophysics, mathematical biology, optics, image restoration and remote sensing. Since the problem is not well-posed, it needs to be reformulated for numerical treatment by including additional assumptions, such as the smoothness of solution. This process is known as regularization and Tikhonov regularization is one of the most commonly used methods for regularization of linear ill-posed problems [50].

The linear least-squares approach is the standard one for the minimization of the residual

$$\|\mathbf{A}\mathbf{x} - \mathbf{b}\|^2$$

to solve an underdetermined system of linear equations $A\mathbf{x} = \mathbf{b}$ where $\|\cdot\|$ is the Euclidean norm. In order to obtain a particular solution with desirable properties, a regularization term is included in this minimization:

$$\|A\mathbf{x} - \mathbf{b}\|^2 + \|\mathbf{\Gamma}\mathbf{x}\|^2$$

for some suitably chosen Tikhonov matrix, $\mathbf{\Gamma}$. In many cases, this matrix is chosen as the identity matrix $\mathbf{\Gamma} = \mathbf{I}$ to give preference to solutions with smaller norms. An explicit solution, denoted by $\hat{\mathbf{x}}$, is given by:

$$\hat{\mathbf{x}} = (\mathbf{A}^T\mathbf{A} + \mathbf{\Gamma}^T\mathbf{\Gamma})^{-1}\mathbf{A}^T\mathbf{b} \tag{4.1}$$

The effect of regularization may be varied via a scale in the matrix $\mathbf{\Gamma}$. For $\mathbf{\Gamma} = \epsilon\mathbf{I}$, when $\epsilon = 0$ this reduces to the unregularized least squares solution where $(\mathbf{A}^T\mathbf{A})^{-1}\mathbf{A}^T$ is the pseudo-inverse provided that $(\mathbf{A}^T\mathbf{A})^{-1}$ exists.

The optimal value for regularization parameter ϵ is usually unknown and often in practical problems is determined by an ad-hoc method. Other methods include the discrepancy

principle, cross-validation, L-curve method, restricted maximum likelihood and unbiased predictive risk estimator [51]. Given the singular value decomposition

$$\mathbf{A} = \mathbf{U}\mathbf{\Sigma}\mathbf{V}^T$$

with singular values σ_i, the Tikhonov regularized solution can be expressed as $\hat{\mathbf{x}} = \mathbf{V}\mathbf{D}\mathbf{U}^T\mathbf{b}$ where $\mathbf{D}$ has diagonal values $D_{ii} = \sigma_i/(\sigma_i^2 + \epsilon^2)$ and is zero elsewhere demonstrating the effect of the Tikhonov parameter on the condition number of the regularized problem. As a general rule if the condition number $\kappa(A) = 10^k$, then k digits of accuracy are lost in addition to what would be lost due to loss of precision from arithmetic methods [49].

4.3 REGULARIZED PSWF RECONSTRUCTION FOR LEVEL CROSSING SAMPLING

In the level-crossing sampling scheme, samples are captured when the continuous time input signal crosses predefined levels as shown in Figure 10. The sampled signal can be represented by the pairs $\{t_k, x(t_k)\}$, where the values $\{x(t_k)\}$ belong to the set of those predefined levels. Although, the reconstruction of the non-uniformly sampled signal can be obtained by sinc-based reconstruction [2]

$$\hat{x}(t_k) = \sum_{n=-\infty}^{+\infty} C_n S(t_k - t_n) \tag{4.2}$$

where t_k is a time in nonuniform sampling and the interpolation coefficients C_n are assumed to be chosen such that $\hat{x}(t_k) = x(t_k)$, the sinc-based reconstruction is not appropriate since it requires an infinite number of samples.

Since as shown above, the sinc interpolation can be converted into a PSWF projection with finite dimension, an LC sampled signal $x(t_k)$ can be represented by the M-dimensional PSWF projection

$$x(t_k) = \sum_{m=0}^{M-1} \gamma_m \phi_m(t_k) \tag{4.3}$$

or in a matrix form as

$$\mathbf{x}(\mathbf{t_k}) = \mathbf{\Phi}(\mathbf{t_k})\gamma_M \tag{4.4}$$

such that

$$\begin{aligned}
\mathbf{x}(\mathbf{t_k}) &= [x(t_0)\ x(t_1)\ \cdots\ x(t_{N_{\ell c-2}})\ x(t_{N_{\ell c-1}})]^T \\
\gamma_{\mathbf{M}} &= [\gamma_0\ \gamma_1\ \cdots\ \gamma_{M-2}\ \gamma_{M-1}]^T \\
\mathbf{\Phi}(\mathbf{t_k}) &= \begin{bmatrix}
\phi_0(t_0) & \cdots & \phi_{M-1}(t_0) \\
\phi_0(t_1) & \cdots & \phi_{M-1}(t_1) \\
\vdots & \cdots & \vdots \\
\phi_0(t_{N_{\ell c-2}}) & \cdots & \phi_{M-1}(t_{N_{\ell c-2}}) \\
\phi_0(t_{N_{\ell c-1}}) & \cdots & \phi_{M-1}(t_{N_{\ell c-1}})
\end{bmatrix}
\end{aligned}$$

and $N_{\ell c}$ is the number of level-crossing samples.

The projection coefficients γ_M can be obtained by means of the pseudo-inverse. However, an inversion of the $N_{\ell c} \times M$ DPSS matrix ($\mathbf{\Phi}(\mathbf{t_k})$) is highly ill conditioned for the LC sampling. To overcome this ill-posed problem, using Tikhonov regularization the projection coefficients are obtained. In our approach, to obtain a regularized solution for $\mathbf{x}(\mathbf{t_k}) = \mathbf{\Phi}(\mathbf{t_k})\gamma_M$ in the least squares sense, we minimize the following expression:

$$\gamma_{M\epsilon} = \arg\ \min_{\gamma_M}\{\|\Phi(t_k)\gamma_M - \mathbf{x}(\mathbf{t_k})\|^2 + \epsilon\|\gamma_M\|^2\} \tag{4.5}$$

where the regularization parameter ϵ represents the tradeoff between losses and smoothness of the solution. As indicated in [59], the regularization term can deal with large sampling gaps, that is it allows these to be filled in a smooth way using the information from the surrounding samples. The regularized solution $\gamma_{M\epsilon}$ is given by

$$\gamma_{M\epsilon} = (\Phi(t_k)^T\Phi(t_k) + \epsilon\mathbf{I})^{-1}\Phi(t_k)^T\mathbf{x}(\mathbf{t_k}) \tag{4.6}$$

where $\mathbf{I}$ is the identity matrix. Note that $\lim_{\epsilon\to 0}\gamma_{M\epsilon} = [\Phi(t_k)]^\dagger\mathbf{x}(\mathbf{t_k})$ where $\dagger$ represents the pseudo inverse. The original signal $x(t_n)$ is then approximated as follows:

$$\mathbf{x}(\mathbf{t_n}) \approx \hat{\mathbf{x}}(\mathbf{t_n}) = \mathbf{\Phi}(\mathbf{t_n})\gamma_{M_\epsilon}. \tag{4.7}$$

In the next section, we simulate LC sampling for a chirp and a bursty signal and compare the regularized Slepian reconstruction to compressive sampling and piecewise cubic interpolation methods of which M values were determined as in Figure 11.

4.4 SIMULATIONS

In order to illustrate the efficiency of the proposed method we apply our reconstruction method to a LC sampled chirp and a bursty signal. The LC-sampling results are shown in Figure 12 and Figure 14. The LC-sampling results are shown in Figure 12 and Figure 14. We compare our reconstruction results with the reconstruction results obtained using compressive sampling technique and piecewise cubic interpolation, which is known to be well suited for the reconstruction from level-crossing samples. In Figure 12, we have $N_{\ell c}$=179 non-uniformly spaced samples as the result of level-crossing sampling. Figure 13 illustrates the comparison between original and reconstructed chirp signal and reconstruction error for the regularized Slepian reconstruction method. The reconstructed signals by using the proposed method show better performance when we compare our results with those from piecewise cubic interpolation and compressive sampling using approximate signal to noise ratios (SNRs) as shown in Figures 15 and 16. For our compressive sampling experiments, we used the MATLAB function $l1eq - pd.m$ from the ℓ_1-MAGIC toolbox [68].

In order to obtain similar results in compressive sampling, we needed to increase the number of measurements for the compressive sampling method, which requires $N_{cs} = 430$ measurements to reach the same SNR performance which is around 12dB for the chirp signal while our method is using $N_{\ell c} = 179$ level crossing samples.

In the bursty signal example we have $N_{\ell c} = 202$ non-uniformly spaced samples as the result of level-crossing sampling. In Figures 18 and 19, the bursty signal was reconstructed using piecewise cubic interpolation and compressive sampling approach, respectively. As shown in Figures 13 and 17, the reconstruction from the nonuniform samples can be possible with very small error after choosing the appropriate value of M. Figure 19 shows the reconstruction for the compressive sampling method, which requires $N_{cs} = 375$ measurements for the bursty signal while our method and piecewise cubic interpolation method are using 202 samples for an SNR around 17 dB. Finally, we demonstrate the reconstruction from noisy LC samples for the chirp by adding white Gaussian noise of SNR 30dB to the LC samples. For the chirp signal we have $N_{\ell c} = 186$ LC samples giving an SNR of 12.9 dB for the regularized Slepian reconstruction and 11.75 dB for the piecewise cubic interpolation.

In the CS reconstruction, we needed $N_{cs} = 409$ measurements to obtain an SNR of 11.2 dB as shown in Figures 20, 21, 22. In a general CS framework, the number of required samples, i.e., measurements for perfect recovery is known to depend on the sparsity of the given signal. However, our approach using level-crossing sampling and regularized Slepian reconstruction provides better results independent of the signal sparsity while using nearly half of the samples used in compressive sampling. Therefore our approach provides an alternative compression scheme based on level-crossing sampling and regularized PSWFs reconstruction. Since the above results demonstrate the ability of reconstruction in dealing with large sampling gaps, the proposed method is obviously also applicable to the case of random sampling.

4.5 CONCLUSIONS

In this chapter we proposed a new reconstruction method for non-uniformly spaced samples obtained from level-crossing sampling. By projection of signals on the space of PSWF and obtaining a regularized solution, we have shown that the proposed method can deal with reconstruction for level-crossing sampling. Simulation results present the effectiveness of the proposed method in terms of SNR and number of measurements. It was shown that in some cases the proposed reconstruction method can perform better than the piecewise cubic interpolation and compressive sampling reconstruction. As future work, we are investigating an estimation problem for the optimal value of M from non-uniformly spaced samples when the actual bandwidth of the signal is not available.

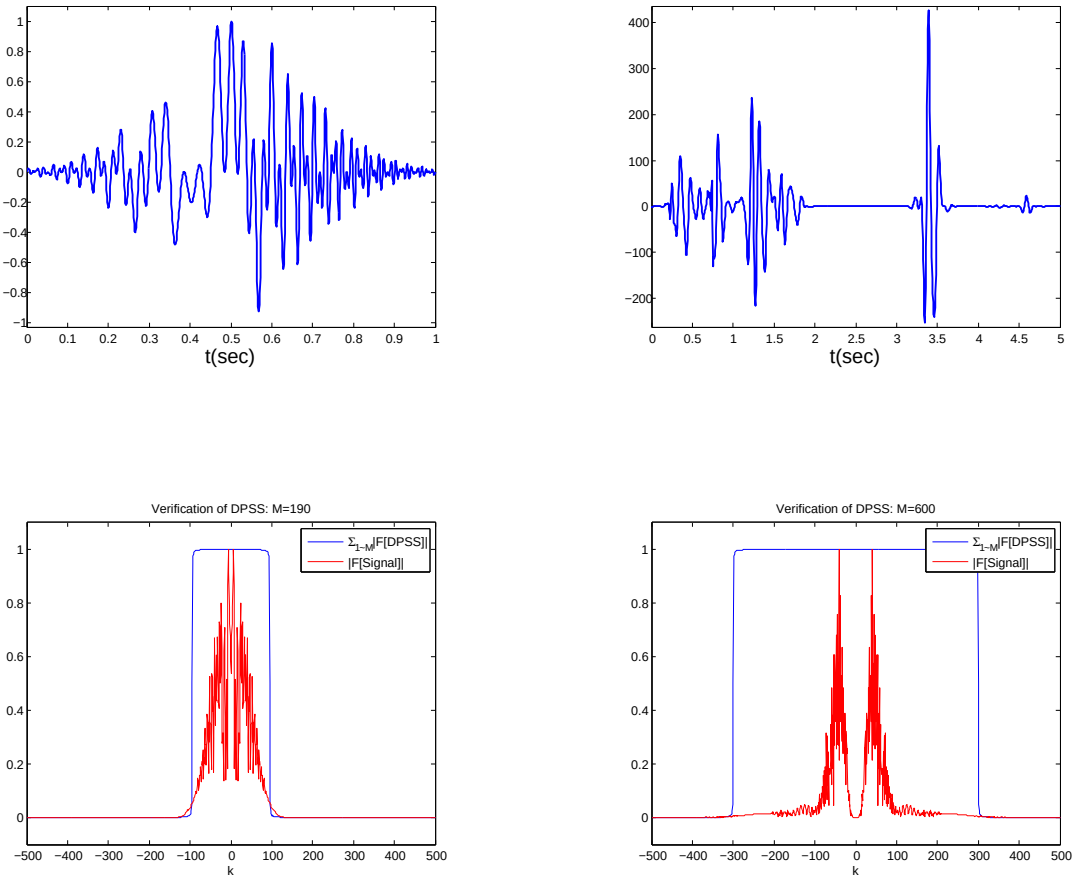

Figure 11: Determination of M using spectrum, Left: for chirp signal M=190, Right: for bursty signal M=600.

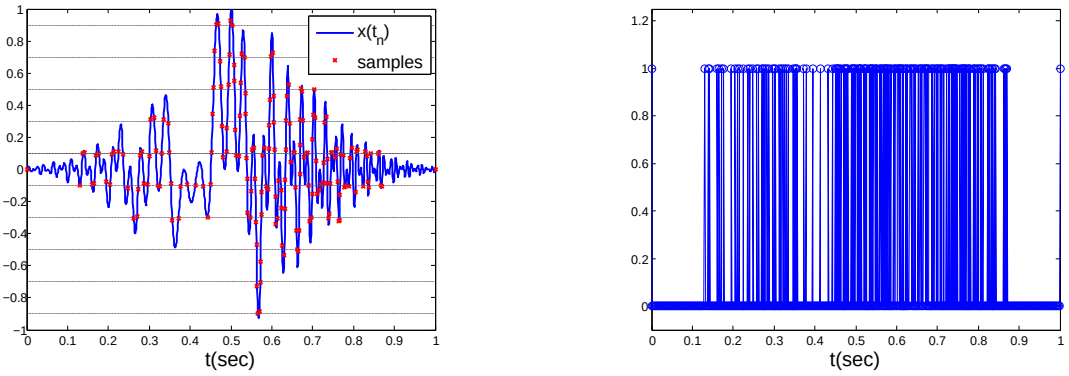

Figure 12: Left: level crossing sampling for chirp signal, Right: sample locations.

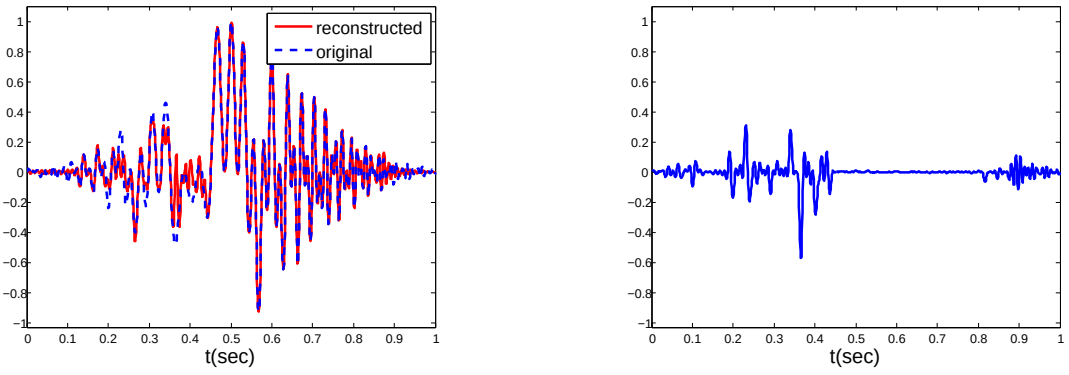

Figure 13: Left: regularized PSWF reconstruction, ($N_{\ell c}$=179, SNR=12.13dB), Right: reconstruction error.

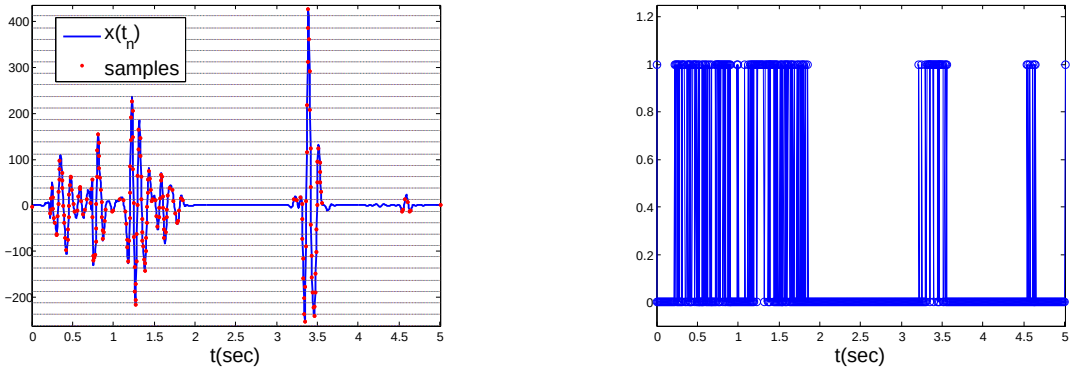

Figure 14: Left: level crossing sampling for bursty signal, Right: sample locations.

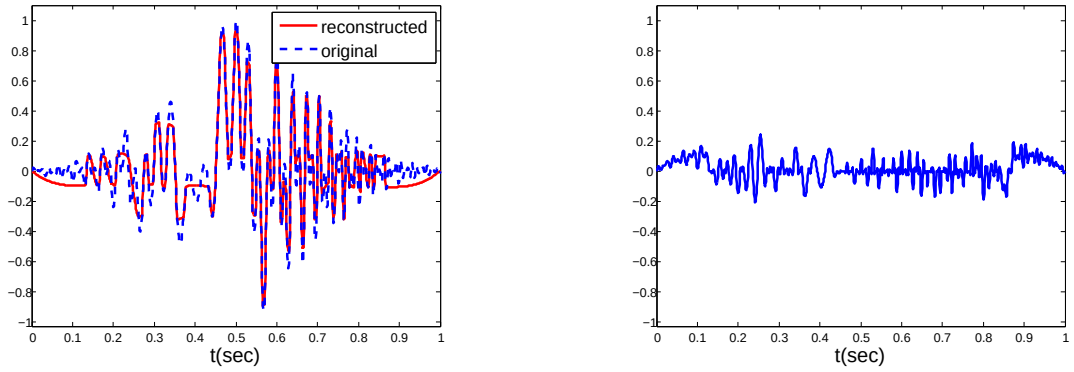

Figure 15: Left: piecewise cubic interpolation, ($N_{\ell c}$=179, SNR=11.03 dB), Right: reconstruction error.

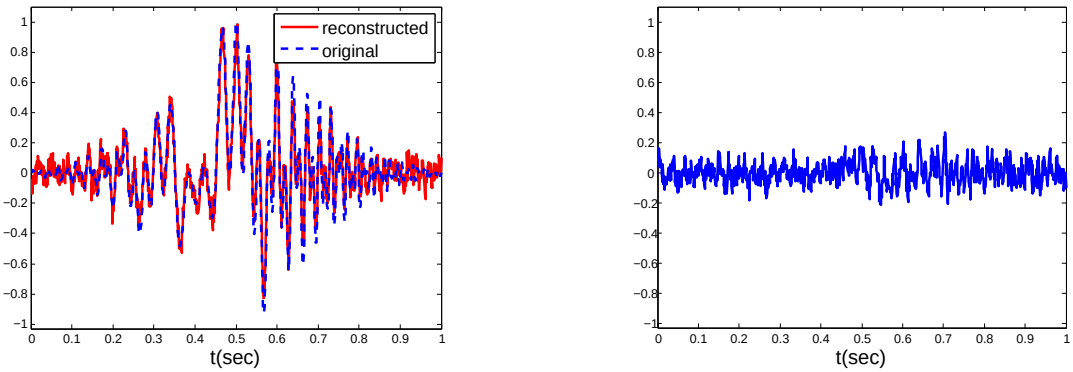

Figure 16: Left: compressive sampling reconstruction, (N_{cs}=430, SNR=11.30 dB), Right: reconstruction error.

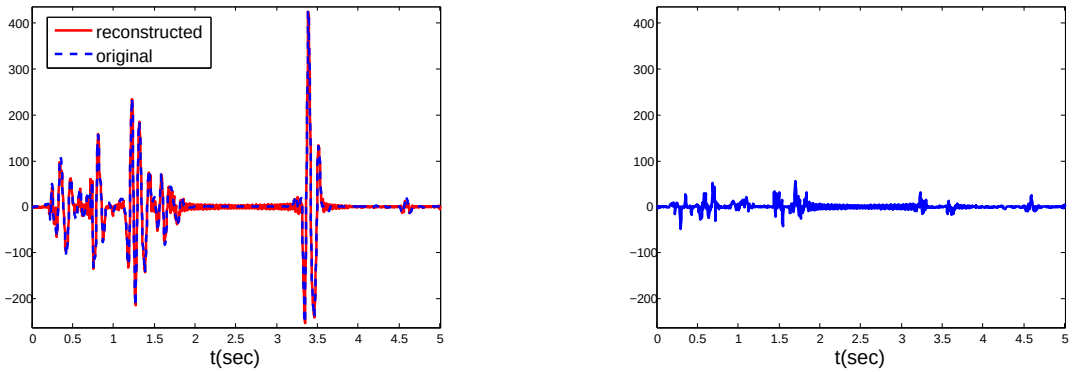

Figure 17: Left: regularized PSWF reconstruction, ($N_{\ell c}$=202, SNR=16.79 dB), Right: reconstruction error.

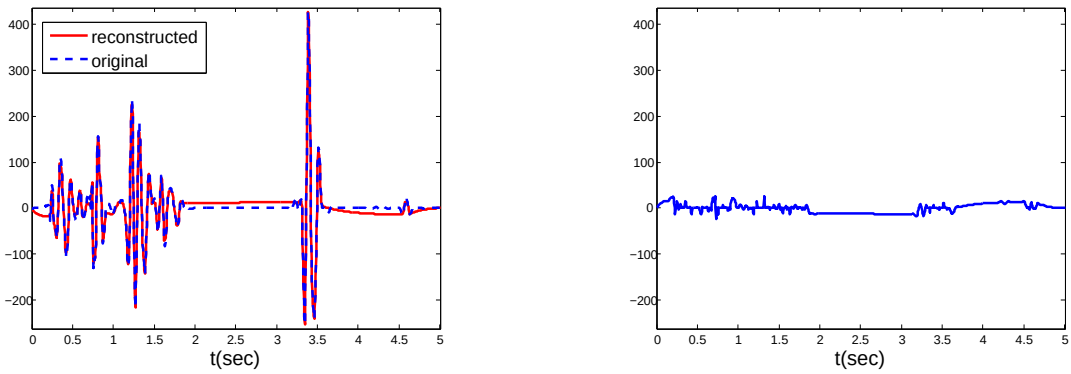

Figure 18: Left: piecewise cubic interpolation, ($N_{\ell c}$=202, SNR=15.47 dB), Right: reconstruction error.

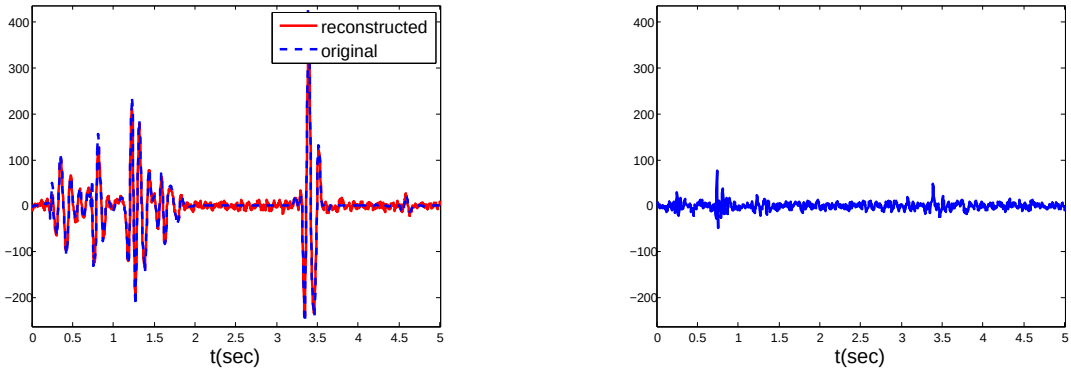

Figure 19: Left: compressive sampling reconstruction, (N_{cs}=375, SNR=16.67 dB), Right: reconstruction error.

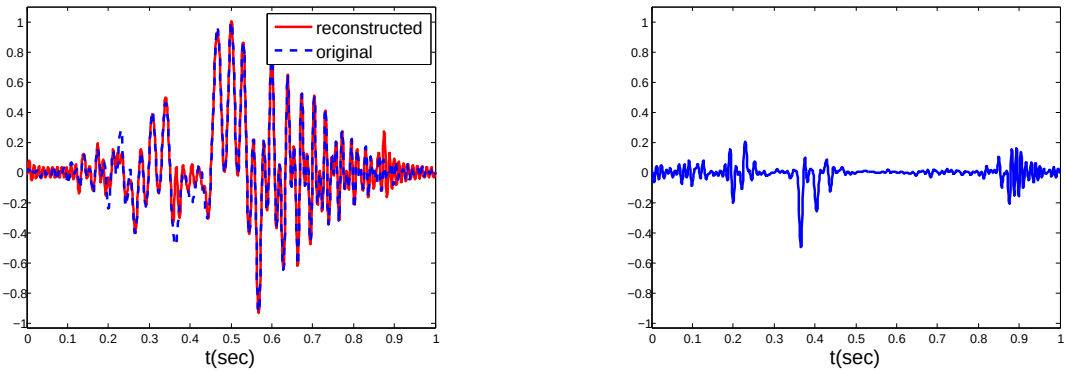

Figure 20: Left: Reconstruction from noisy LC samples, $N_{\ell c} = 186$ using regularized PSWF method Right: reconstruction error, SNR=12.89 dB.

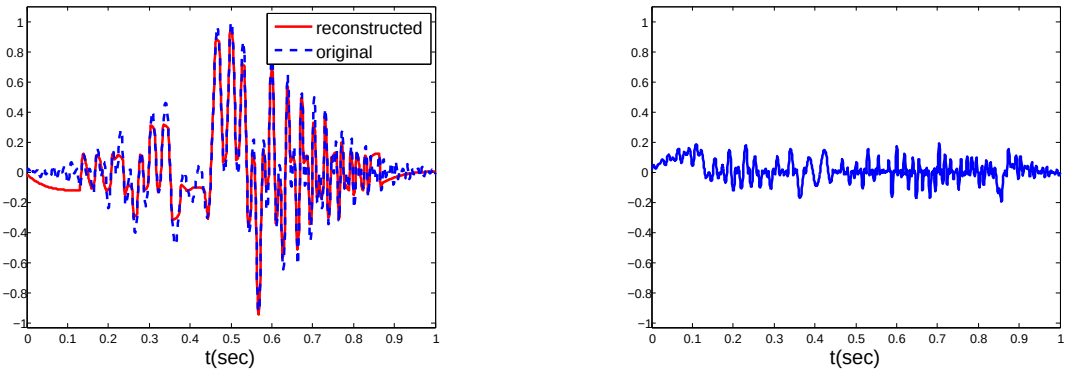

Figure 21: Left:Reconstruction from noisy LC samples, $N_{\ell c} = 186$ using piecewise cubic interpolation method, Right: reconstruction error, SNR=11.75 dB.

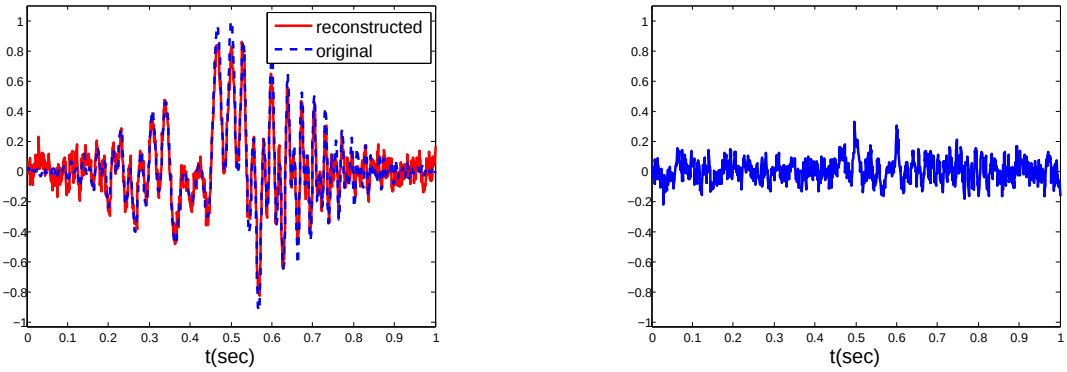

Figure 22: Left: Reconstruction from noisy measurements, $N_{cs} = 409$ using compressive sampling method, Right: reconstruction error, SNR=11.2 dB.

5.0 A TIME-FREQUENCY APPROACH AND PROJECTIONS ONTO CONVEX SETS

As explained in the previous chapters, the problem of signal reconstruction from nonuniformly spaced samples is central in many practical problems in image and signal processing [15, 86]. Nonuniform sampling is a common result of Nyquist-Shannon sampling caused by jittering in the sampler, but it is also the case when samples are missing, either according to some distribution or in segments. The reconstruction of finite energy signals can be viewed as an interpolation or an estimation problem in which projection of the observed signal minimizes an error criteria. Constraining the solution to satisfy time and frequency conditions iteratively, a close approximation to the signal, with the given samples, is obtained. This is the basic idea of the projection onto convex sets (POCS) method. This method was introduced by [15] and [14] as an iterative algorithm for signal restoration. Since then, the POCS method has been successfully used in many signal and image recovery problems [76, 86]. Time-frequency signal representations using short-time [84] and fractional Fourier transform [85, 86] have been recently used to implement this type of reconstruction.

In order to obtain the POCS iterative solution, we consider that the signals of interest have a finite time support and an approximately finite frequency support. As such, the PSWF or also called Slepian projection are used for this class of signals. To jointly consider time and frequency constraints, we develop a time-frequency representation from the Slepian projection. This can be done using the evolutionary spectral theory [12], where a signal can be represented in terms of a kernel which in turn can be obtained from the windowed signal. The magnitude square of the kernel is associated with the way the energy of the signal is distributed in time and frequency. It is also possible to obtain a similar representation, the discrete evolutionary transform (DET), for deterministic signals having components with

time-varying frequency components [11]. Imposing time and frequency limitations in the DET permits us to reconstruct the signal iteratively, i.e., the iterative projection generated by the time-frequency transformation converges into a close approximation to the original signal with the given nonuniform samples.

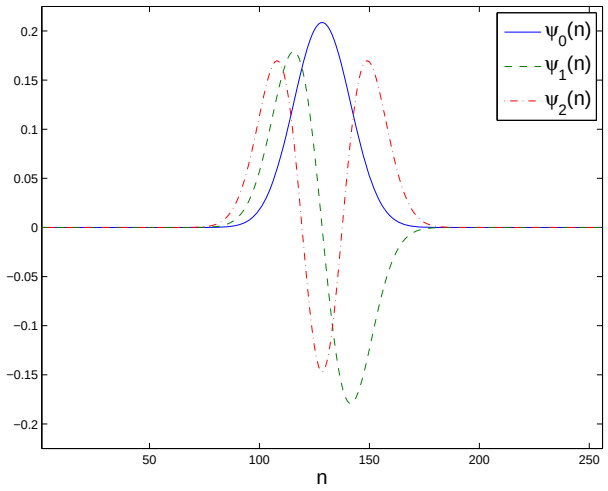

Figure 23: Baseband DPSS for $N = 256$, $W = \frac{1}{8}$ and $K = 64$ (Note that $K = \lfloor 2NW \rfloor$).

5.1 EVOLUTIONARY SPECTRAL REPRESENTATION

The spectral representation of a stationary signal consists of a superposition of sinusoids, of all possible frequencies, with randomly varying amplitudes and phases. To obtain a similar representation for non-stationary signals, one can consider the Wold-Cramer representation [12] characterizing a non-stationary signal as the output of a linear time-varying system with a stationary white noise as input. Thus, a discrete non-stationary signal $x(n)$ can be expressed as

$$x(n) = \sum_{k} X(n, \omega_k) e^{j\omega_k n} \tag{5.1}$$

where $X(n, \omega_k)$ is an evolutionary kernel. The evolutionary spectrum of $x(n)$ is given by $|X(n, \omega_k)|^2$.

In [11], it is shown that the above representation can be extended to deterministic signals. The discrete evolutionary transform (DET) obtained in there is a generalization of the short-time Fourier transform as the evolutionary kernel $X(n, \omega_k)$ is obtained in term of the signal windowed, but the window in the DET varies with time and frequency. Thus the kernel is

$$X(n, \omega_k) = \sum_{m=0}^{N-1} x(m) W_k(n, m) e^{-j\omega_k m} \tag{5.2}$$

where $W_k(n, m)$ is the window which can be expressed using non–orthogonal functions, such as Gabor's, or orthogonal functions such as Malvar's [11].

The POCS framework enables an iterative recovery algorithm incorporating time and frequency constraints. A desired signal $x(n)$ is assumed to lie in the region defined by the intersection of all the convex sets, i.e.,

$$x(n) \in C_0, \quad C_0 = \bigcap_i C_i$$

where C_i denotes the i-th closed convex set. Thus, the original signal can be restored by using the projection operators P_i onto each convex set C_i. The general form of the POCS reconstruction is

$$x_{(i+1)}(n) = P_i[x_{(i)}(n)] \tag{5.3}$$

where $x_{(i)}(n)$ is the reconstructed signal after i iterations. Assuming that the signal of interest is square summable and that the DET projects a signal into another square summable signal, under joint time-frequency constraints we develop an iterative POCS algorithm to recover the signal from partial information of it.

5.2 EVOLUTIONARY SLEPIAN TRANSFORM BASED POCS

A bandpass real-valued signal $x(t)$ can be also represented in terms of baseband signals as

$$x(t) = \mathcal{R}e\ [(a(t) + jb(t))e^{-j\Omega_0 t}] \tag{5.4}$$

where $a(t)$ and $b(t)$ are low-pass signals, and Ω_0 is the center frequency of the Fourier transform of $x(t)$, $X(\Omega)$. Assuming the $a(t)$ and $b(t)$ components have finite time support and are essentially band-limited, we can represent them using the DPSS projection presented above. In that case, the signal $x(t)$ can be expressed as

$$x(t) = \mathcal{R}e\ [\sum_{m=0}^{\infty}(\gamma_m + j\eta_m)\psi_m(t)e^{-j\Omega_0 t}] \tag{5.5}$$

i.e., in terms of modulated PSWF.

The bandpass DPSS [90, 91] which have the highest energy concentration in a given passband are defined by

$$\xi_k(n) = e^{-j2\pi W_c n}\psi_k(n) \tag{5.6}$$

where the passband is $[0 \leq W_c - W, W_c + W \leq \frac{1}{2}]$. When the signal energy outside the given frequency band is very small

$$\frac{1}{2\pi}\int_{\omega\notin[W_c-W,W_c+W]} |X(\omega)|^2 d\omega \approx 0 \tag{5.7}$$

the bandpass DPSS provide an efficient representation of passband signals and accurate channel estimation [90, 91]. The general representation for a complex signal $x(t)$ in terms of the PSWF is given by

$$x(t) = \sum_{m=0}^{\infty}\gamma_m\xi_m(t),\ \ \gamma_m = \sum_{k=0}^{\infty}x(kT_s)\xi_m(kT_s). \tag{5.8}$$

where $\{\xi_m(t)\}$ can be the band-pass or the base–band (when the center frequency is zero) Slepian functions. If the signal $x(t)$ is time–limited, and essentially in the frequency bands $\Omega_c \pm \Omega$ and $-\Omega_c \pm \Omega$, then we obtain

$$\begin{aligned} x(t) &= \sum_{m=0}^{M-1} \sum_{k=0}^{N-1} x(kT_s)\xi_m(kT_s)\xi_m(t) \\ &= \sum_{k=0}^{N-1} x(kT_s) \left[\sum_{m=0}^{M-1} \xi_m(kT_s)\xi_m(t) \right] \end{aligned} \tag{5.9}$$

where as indicated before M depends on the frequency–support and N on the time–support.

In [53], the reconstruction of the original signal from a given set of non-uniform samples is considered, while the effect of the distribution of the non-uniform samples in the reconstruction is studied in [89]. Assuming that q samples $x(k_iT_s)$, $i = 0, 1, \cdots, q-1$ are missing, then letting $\mathbf{u}$ be the q-dimensional vector of unknown samples and $t = k_iT_s$ we obtain from above $\mathbf{u} = \mathbf{\Lambda u} + \mathbf{g}$ where $\mathbf{\Lambda}$ is a matrix with a subset of the entries of the matrix generated by the terms in square brackets in (5.9) and

$$g(t) = \sum_{k \notin \mathbf{u}} x(kT_s) \left[\sum_{m=0}^{M-1} \xi_m(k_iT_s)\xi_m(t) \right]. \tag{5.10}$$

The missing samples are recovered if the above equation can be solved for $\mathbf{u}$, or if $\mathbf{I} - \mathbf{\Lambda}$ is invertible. Given the many possible ways the missing samples could be distributed this might not be possible. However, as indicated in [2, 89] there are cases where reconstruction is possible with the sinc interpolation, and we will show later that it is also the case when we are using the PSWF based POCS.

To apply joint time and frequency constraint in the POCS we develop a DET based on the Slepian representation of the signal. Suppose a discrete signal $x(n)$ can be represented in terms of some orthogonal basis $\{\phi_k(n)\}$,

$$\begin{aligned} x(n) &= \sum_{k=0}^{K-1} d_k\phi_k(n), \qquad 0 \le n \le N-1 \\ d_k &= \sum_{n=0}^{N-1} x(n)\phi_k^*(n), \qquad 0 \le k \le K-1 \end{aligned} \tag{5.11}$$

where $\{d_k\}$ are the expansion coefficients. Rewriting $x(n)$ as

$$x(n) = \sum_{k=0}^{K-1} \underbrace{[d_k \phi_k(n) e^{-j\omega_k n}]}_{=X(n,\omega_k)} e^{j\omega_k n} \tag{5.12}$$

where $\omega_k = 2\pi \frac{k}{N}$. The evolutionary kernel $X(n, \omega_k)$ can be expressed in terms of $x(n)$ by replacing the d_k coefficients:

$$\begin{aligned} X(n,\omega_k) &= d_k \phi_k(n) e^{-j\omega_k n} \\ &= \sum_{m=0}^{N-1} x(m) \underbrace{[\phi_k(n)\phi_k^*(m) e^{-j\omega_k(n-m)}]}_{=W_k(n,m)} e^{-j\omega_k m}. \end{aligned} \tag{5.13}$$

To obtain the evolutionary kernel, in particular the window $W_k(n, m)$, we consider the bandpass DPSS $\{\xi_k(n)\}$ as basis for the representation of baseband and passband signals. The window is then expressed as

$$W_k(n,m) = \xi_k(n)\xi_k^*(m) e^{-j\omega_k(n-m)}. \tag{5.14}$$

It is important to understand that when the signal under consideration is modulated, i.e. $x(n) = g(n)e^{-j\pi W_c n}$, and we use the bandpass Slepian functions, we can obtain the spectrum of $g(n)$ or $|G(n, \omega_k)|^2$. For a signal with bandpass characteristics, the signal can be represented by a small number of bandpass DPSS coefficients and then restored by small number of projection iteration compared to baseband DPSS based DET, which will be shown in next section.

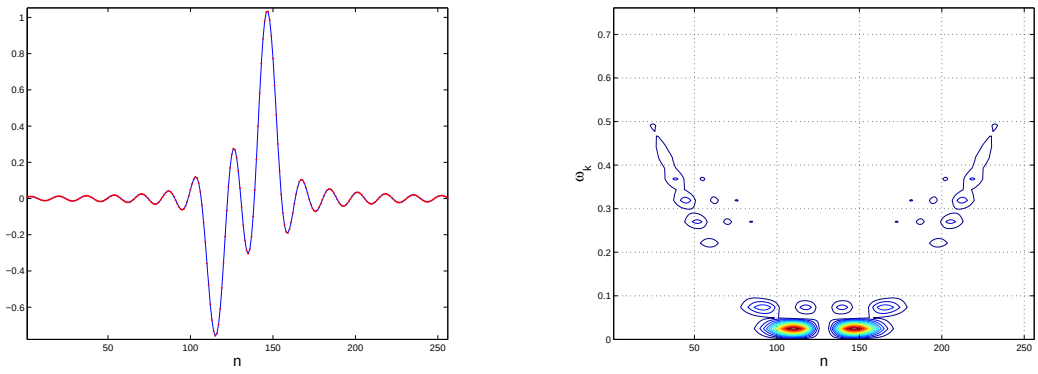

(a) (b)

Figure 24: An example of evolutionary Slepian spectrum: (a) $x_1(n)$, (b) $|X(n,\omega_k)|^2$.

5.3 SIMULATIONS

5.3.1 Slepian-based DET

To illustrate the baseband and bandpass Slepian representation and their Slepian-based DET, consider the test signals

$$\text{Baseband signal:} \quad x_1(t) = \text{sinc}(t-2.1) - 0.7\text{sinc}(t+1.7), 0 \le t \le 30$$

$$\text{Passband signal:} \quad x_2(t) = \text{sinc}^2(f_B t)\cos(2\pi f_C t + \tfrac{\pi}{3}), 0 \le t \le 1$$

where $f_C = 25.6$ Hz is a carrier frequency, and $f_B = 2$ Hz. Discrete signals $x_1(n)$ and $x_2(n)$, $0 \le n \le N-1, N = 256$, are obtained from the uniform sampling on the signal $x_1(t)$ and $x_2(t)$, respectively using a sampling period $T_s = 30/256$ and $T_s = 1/256$ sec. For the signal $x_1(n)$, the evolutionary Slepian spectrum $|X(n,\omega_k)|^2$ using the baseband DPSS shown in Fig. 23 is illustrated in Fig. 24. The evolutionary Slepian spectrum shows that the energy of the test signal $x_1(n)$ is highly concentrated in $n \in [100, 160]$ and ω_k is the normalized frequency i.e., $\omega_k/\pi \in [0, 1/2]$ rad. As shown in Fig. 24(b), the DET provides accurate representation for a nearly time-limited and band-limited signal in the time-frequency domain. The 256-point bandpass test signal $x_2(n)$ in Fig. 25(a) is to be

represented by the evolutionary Slepian spectrum. Its Fourier transform is shown in Fig. 25(a) where the signal energy is concentrated at normalized frequency 0.1. In many practical applications, the exact frequency band of the signal is known. Therefore, if we have enough knowledge about the spectrum characteristics of the signal, we can represent the signal with small number of DPSS. Figure 25(b) shows the evolutionary DPSS spectrum for $x_2(n)$ using baseband DPSS with $K = 64$ coefficients and normalized bandwidth of $W = 1/8$. The evolutionary DPSS spectrum using bandpass DPSS is also shown in Fig. 25(c) where $K = 4$, $W = 1/128$ and $W_c = 0.1$. Therefore, if we project the signal that has bandpass characteristics on the DET domain, the signal can be restored only by a small number of basis, i.e., bandpass DPSS with the same accuracy obtained from baseband DPSS.

5.3.2 Reconstruction of irregularly sampled signals

In this section, we perform three different simulations to illustrate the effectiveness of DET based POCS. We use the POCS methodology for reconstruction of nonuniformly sampled and band-limited signals.

- **Nonuniform jittering sampling with known distribution**: Irregularly-spaced samples $\{x(n_i)\}$ are obtained from the original signal $x(n)$ by $x(n_i) = x(\lceil n\frac{N}{L} + \tau \rfloor)$ where τ is the timing jitter with normal distribution $\mathcal{N}(0, \sigma^2)$ and $\lceil \rfloor$ denotes the nearest integer, and L is a decimation factor.

  Figure 26(a) shows the irregularly-spaced samples with 32-point($L = 8$) from the test signal $x_1(n)$. In this simulation, the parameters for the baseband DPSS are $W = 1/16$, and $K = 32$. As shown in Fig. 26(b), (c), and (d), the original signal can be recovered with very small error after 40 iterations. Figure 27 shows the relationship between the degree of irregularity($\tau \sim \mathcal{N}(0, \sigma^2)$) and the performance in terms of mean absolute error (MAE) and the speed of convergence. It is clear that the performance depends on the degree of irregularity. Figure 27 also suggests that, although the number of iterations should be increased according to the degree of irregularity, a nearly perfect reconstruction can be possible after 100 iterations. In case of nonstationary signals such as a chirp, the restored signal using bandpass DPSS based DET is shown in Fig. 28. The results clearly

indicate that the reconstruction of the non-uniformly sampled nonstationary signal can be possible with very small error. For a speech signal, the restored results using baseband and bandpass DPSS based DET are shown in Fig. 29. Its frequency components are also shown in Fig. 29(b) showing that the energy of the signal is concentrated in a normalized frequency band $0.02 < \omega < 0.1$. Note that the bandpass DPSS based DET projection converges faster than the baseband approach for a bandpass type signal. It is clear that the bandpass type signal can be restored only by a small number of components and the iteration, with the same MAE performance compared to baseband DPSS based DET, converges faster. Therefore, the DET based POCS algorithm provides a fast and accurate technique for recovering band-limited samples from the irregularly-spaced subsamples.

- **Nonuniform jittering sampling with unknown distribution**: In this simulation, we consider the extreme case of irregularly-spaced, i.e., randomly-spaced subsamples. Figure 30 shows examples of restored signal from the randomly-spaced subsamples for test signal $x_1(n)$ and the speech signal, given above. As shown in Fig. 30, for a time-limited signal such as $x_1(n)$, the restored performance strongly depends on the sampling distribution. For the speech signal, since its energy is well distributed in the time domain, the restored signal is not sensitive to the distribution of sampling points. Note that the MAE values of the restored speech signals under 5 different random sampling patterns lie between 0.2 and 0.3 after convergence. This result clearly indicates that for a signal with uniformly distributed energy in the time domain, the DET based POCS algorithm is capable of signal recovery from randomly-spaced subsamples. As pointed out in [89], if the gaps between missing samples due to randomly-spaced are large, iterative technique such as POCS is more efficient than non-iterative method.

- **Block or contiguous sample losses**: For the recovery of uniformly sampled signals with contiguous lost samples, the same projection methodology is applied in this simulation. A general assumption is that the lost data on the sampled signals compared to the total number of samples is small and that the available samples are representatives of the original signal [92]. Figure 31 shows examples of restored speech signal by bandpass DPSS ($K = 16$) based DET from the uniformly-spaced speech signal with continuous missing data. For larger values of missing samples, since the assumption does not hold

due to severe loss of information on the signal, the performance of signal recovery is degraded. However, the proposed method shows very promising results as shown in Fig. 31.

5.4 CONCLUSIONS

In this chapter, we have introduced a new discrete evolutionary Slepian transform capable of efficient representation of band-limited signals. For the evolutionary kernel window, baseband and bandpass DPSS are used for the representation of baseband and bandpass signals, respectively. The evolutionary Slepian spectrum provides an accurate representation of time and band limited signal in the time-frequency domain. For the reconstruction, the DET based POCS algorithm is applied in the area of signal recovery from nonuniformly spaced subsamples. For a signal that has bandpass characteristics, the signal can be represented by a small number of bandpass DPSS coefficients with the same accuracy obtained from baseband DPSS, and then restored by small number of projection iteration with the same MAE performance compared to baseband DPSS based DET.

The DET based POCS algorithm is shown to provide fast and accurate technique for recovering the band-limited samples from the irregularly-spaced subsamples. Although there are remaining issues that need further study, for instance the upper error bound by the number and distribution of missing samples, the proposed method shows very promising results, i.e., capable of signal recovery from randomly-spaced subsamples and continuous lost samples.

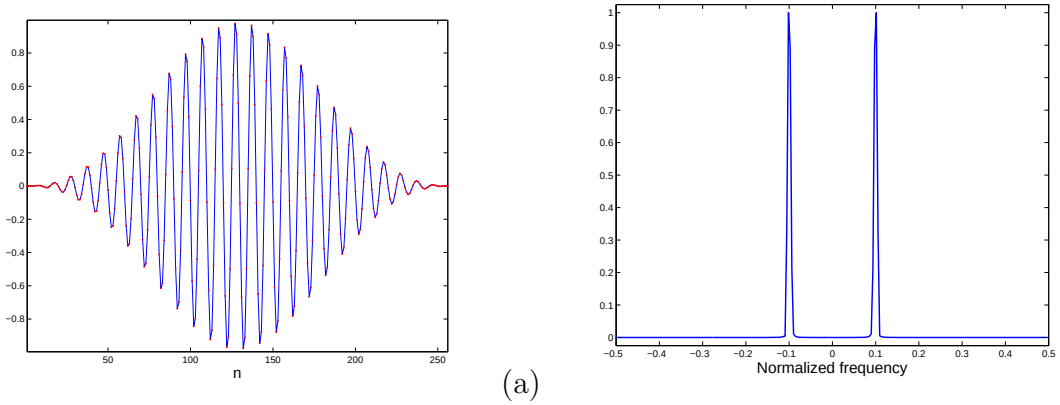

(a)

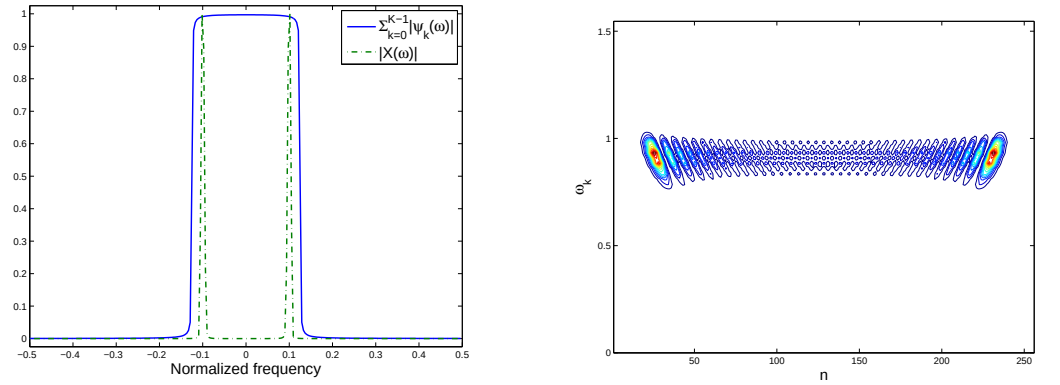

(b)

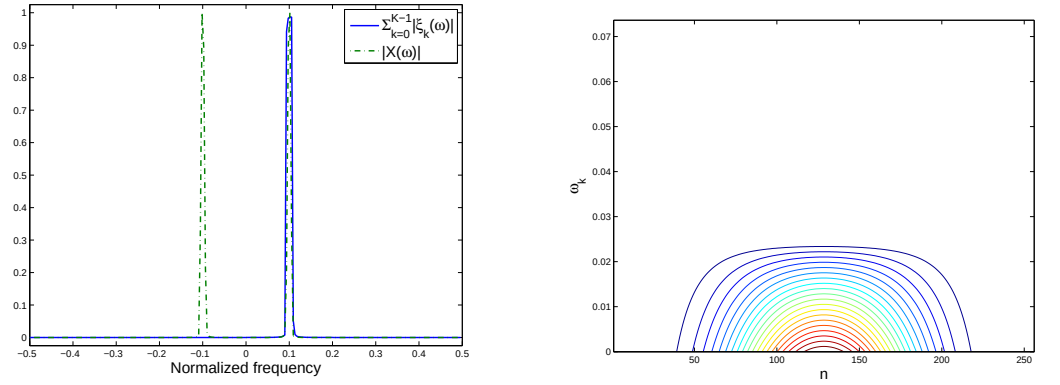

(c)

Figure 25: Comparison of evolutionary Slepian spectrum for passband test signal using baseband and bandpass DPSS: (a) $x_2(n)$ and its spectrum $|X(\omega)|$, (b) spectrum of baseband DPSS ($K = 64$) and corresponding $|X(n, \omega_k)|^2$, (c) spectrum of bandpass DPSS ($K = 4$) and corresponding $|G(n, \omega_k)|^2$.

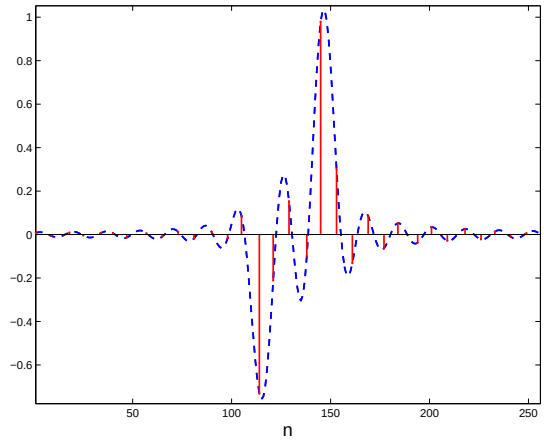

(a)

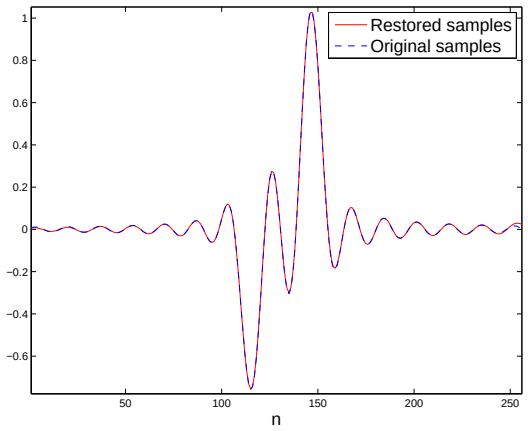

(b)

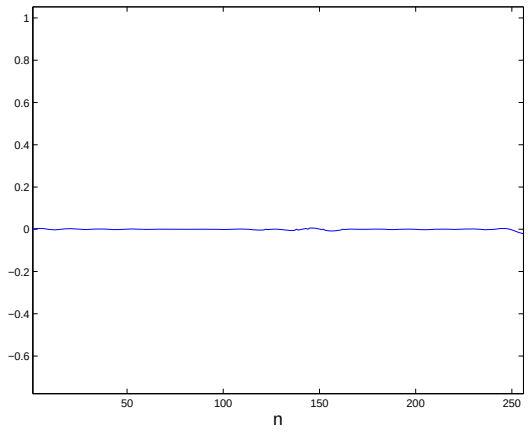

(c)

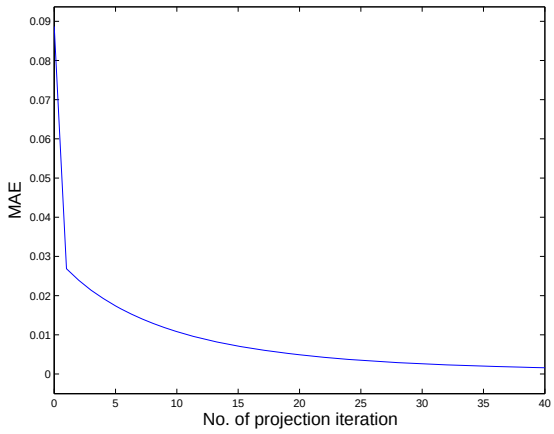

(d)

Figure 26: Restored results for the test signal $x_1(n)$: (a) irregularly-spaced subsamples ($L = 8$, $\tau \sim \mathcal{N}(0, 1)$), (b) restored signal, (c) error, (d) convergence behavior.

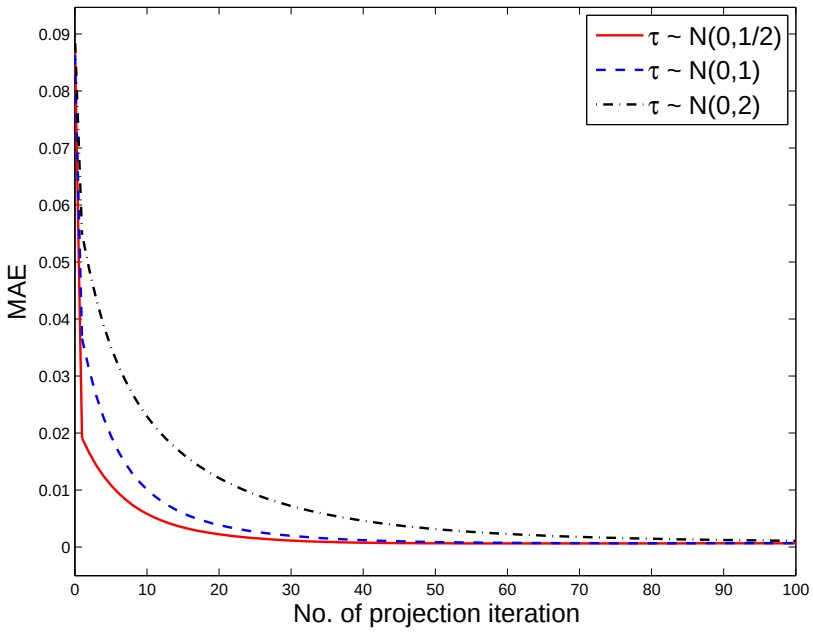

Figure 27: Convergence speed and MAE performance according to the degree of irregularity.

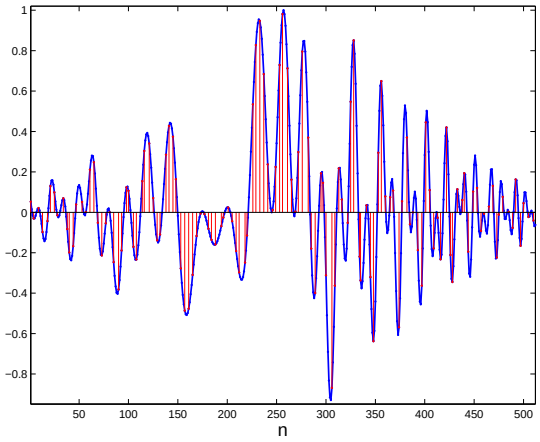

(a)

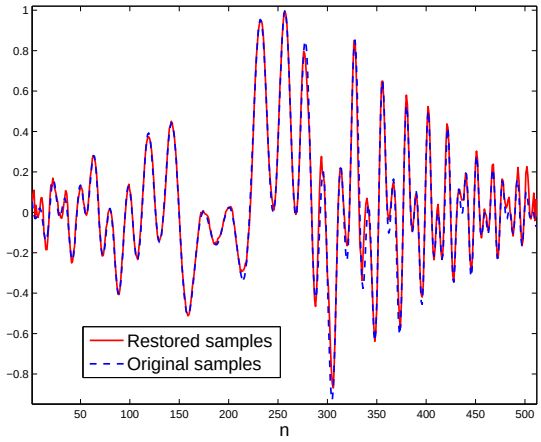

(b)

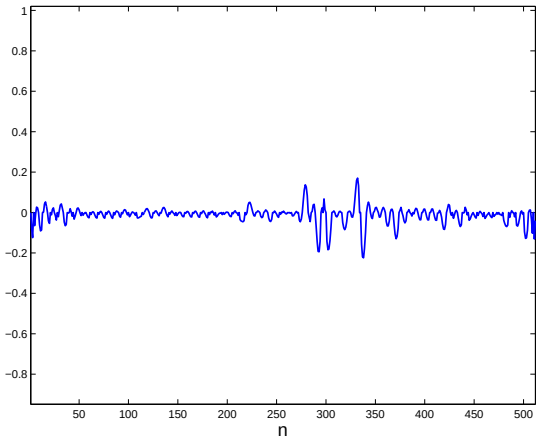

(c)

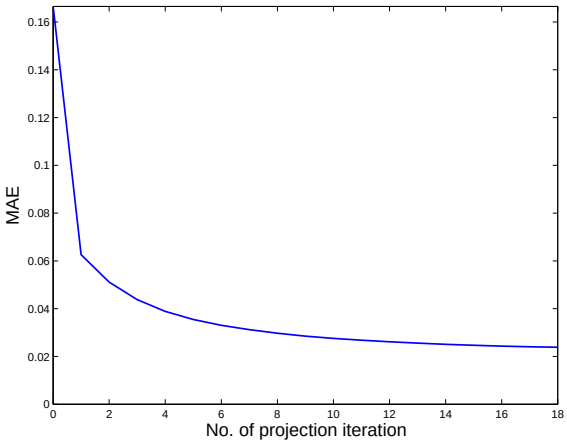

(d)

Figure 28: Restored results for the chirp signal ($N = 512$): (a) irregularly-spaced subsamples ($L = 4$, $\tau \sim \mathcal{N}(0, 1/2)$), (b) restored signal by bandpass DPSS ($K = 64, W_c = 1/16$) based DET, (c) error, (d) convergence behavior.

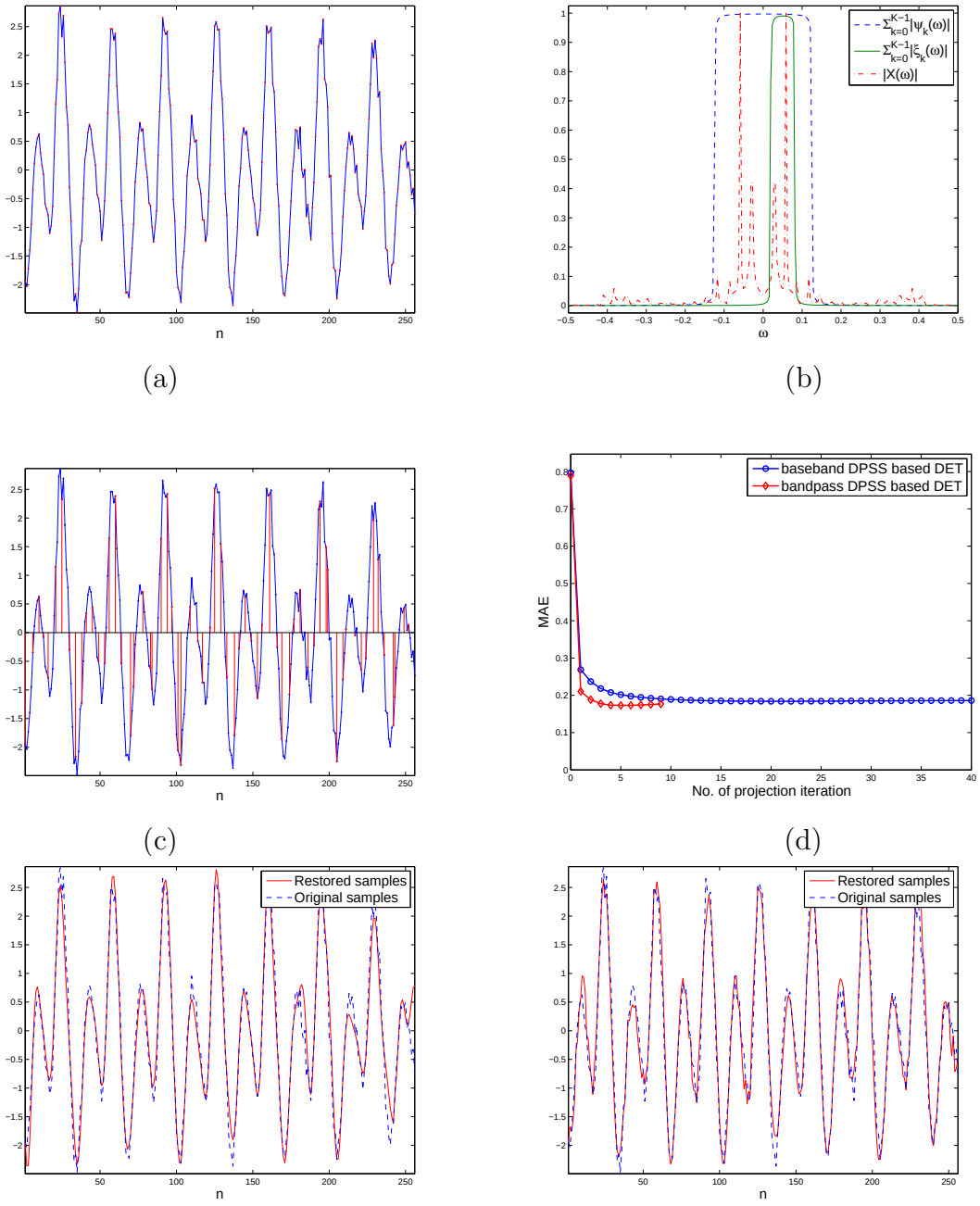

Figure 29: Restored results for the speech signal: (a) speech signal, (b) spectrum of speech, baseband and bandpass DPSS, (c) irregularly-spaced subsamples ($L = 4$, $\tau \sim \mathcal{N}(0, 1/2)$), (d) convergence behaviours, (e) restored signal by baseband DPSS ($K = 64$) based DET, (f) restored signal by bandpass DPSS ($K = 16, W_c = 0.05$) based DET.

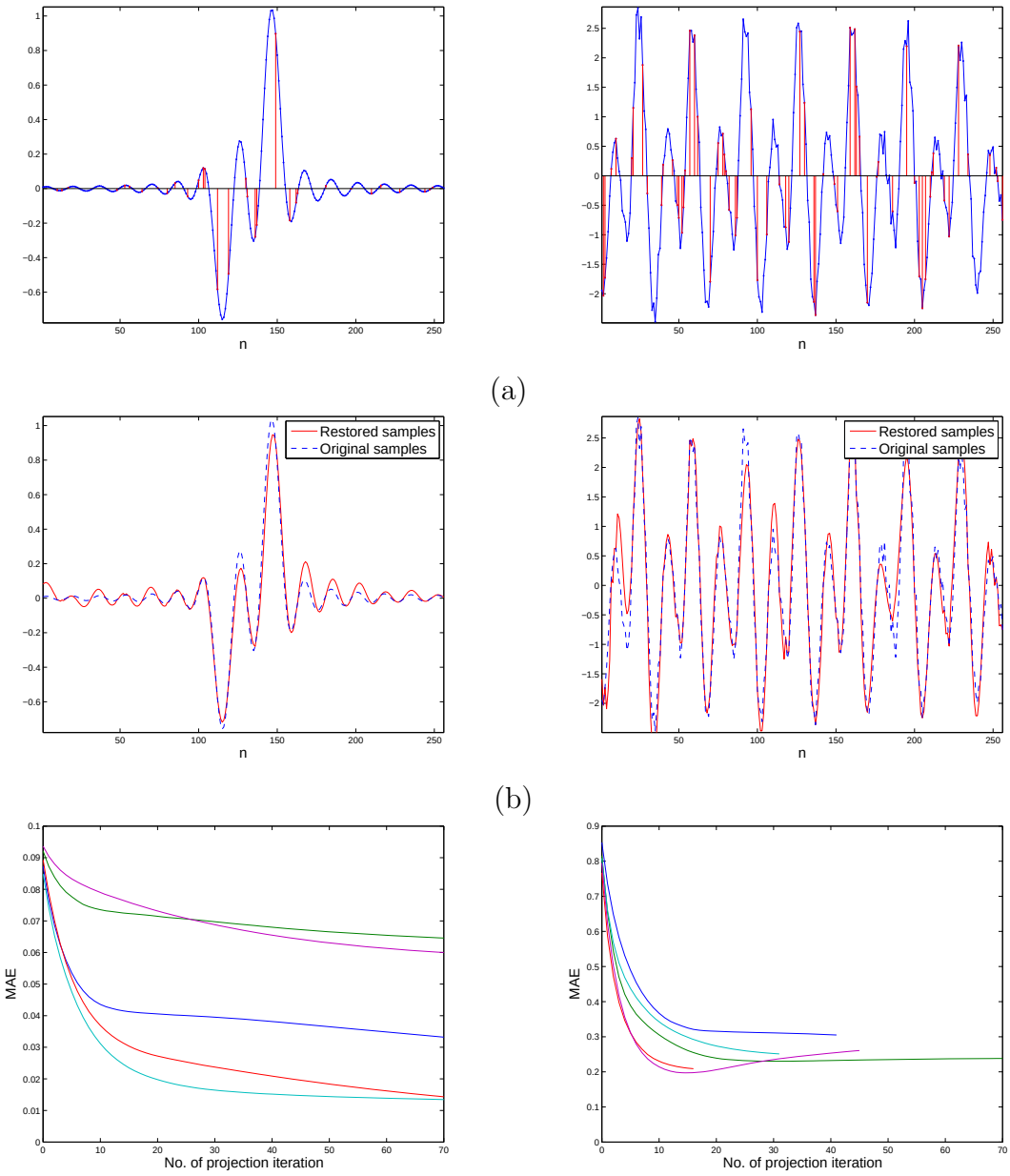

Figure 30: Restored results for randomly-spaced subsamples: (a) randomly-spaced subsampled test and speech signals, (b) restored test signal by baseband DPSS based DET ($L = 8, K = 32$) and restored speech signal by bandpass DPSS based DET ($L = 4, K = 16$), (c) convergence behaviors of 5 different random sampling patterns (left: test signal, right: speech signal).

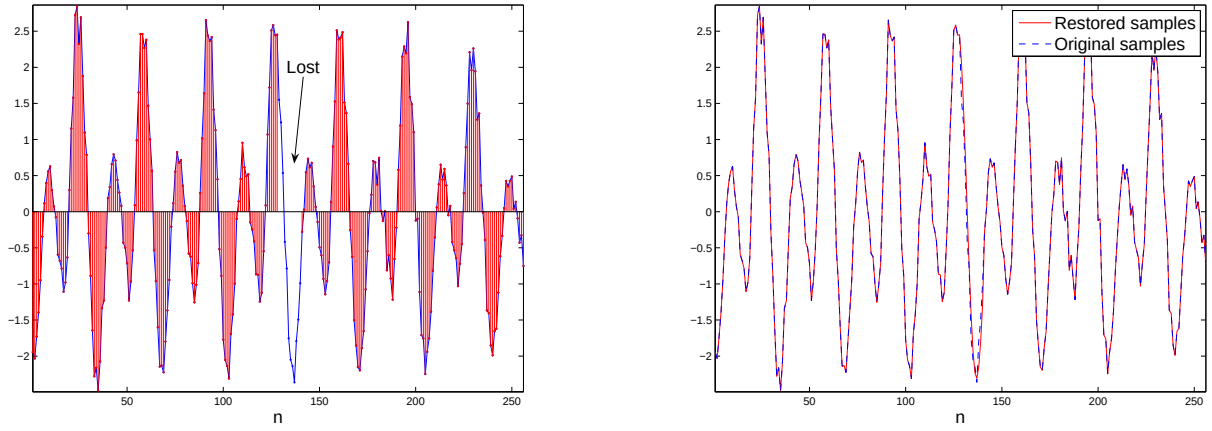

(a)

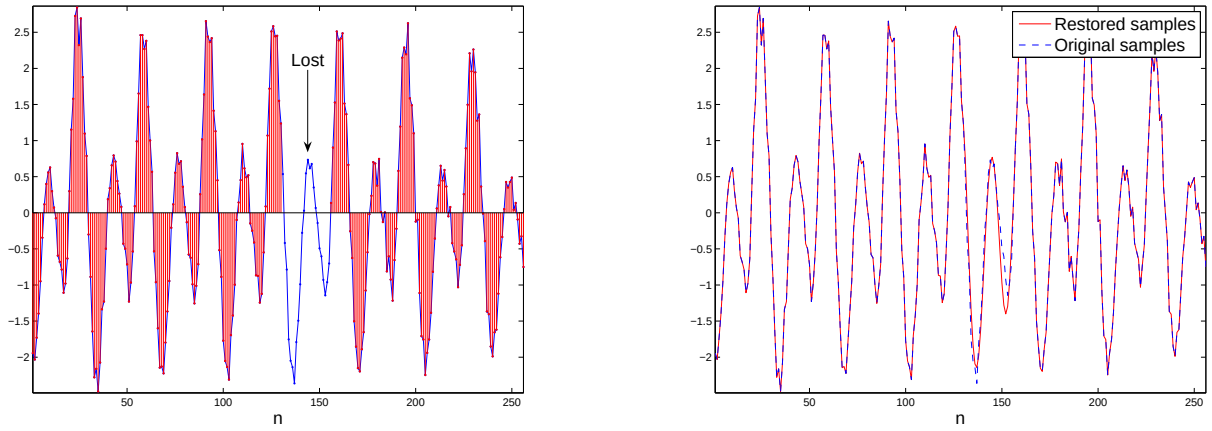

(b)

Figure 31: Restored results for continuous lost samples: (a) restored speech signal from 12 missing data after 10 iterations, (b) restored speech signal from 25 missing data after 70 iterations.

6.0 TIME ENCODING AND NONUNIFORM SAMPLING

In the previous chapter, we considered stochastic jitter sampling (SJS) and reconstruction. It has recently been shown that an Asynchronous Sigma Delta Modulator (ASDM), can be used to sample a signal in a non-uniform way [17, 16]. ASDMs can be used to convert an analog continuous-time input signal into a continuous time binary amplitude output signal [17]. Through this conversion, the information in the amplitude of the input signal is coded in the pulse width of the output signal. ASDMs have the same structure as sigma delta modulators (SDM) but without quantization. However, the description of an ASDM is more complex than that of SDMs, as the simplification of a linear loop that is excited by an extra uncorrelated noise source is not valid here. ASDMs are closed loop nonlinear systems. In particular, the interest is in nonlinear elements with binary output (single-bit quantizers, nonlinear amplifiers and binary switches) and especially quantizers with switches [17]. Due to the hysteresis the nonlinear function performed by such a quantizer depends on both the sign and the phase of the input signal and introduces additional degree of freedom in the system design.

The most attractive property of an ASDM is its conversion of amplitude information into time information without an external sampling (clock) signal such that no quantization noise is introduced into system. In comparison, an external clock is required in an SDM and the input of the quantizer at each clock moment has to be represented by a certain discrete value, thus introducing quantization noise. In addition, a high frequency clock increases electromagnetic interference on supply rails and corrupts the analog signal to be sampled [16]. In the ASDMs the signal transition times depend on the properties of the input signal of the quantizer such that the moment of the transition coincides exactly with the moment of crossing the threshold. This internal timing mechanism is described by the unforced periodic

oscillations denoted as limit cycles. Due to its fully analog nature, the ASDM has a specific application area where pure analog processing is required.

The ASDM can be used as a simple but high-precision and low-power alternative for the standard SDM and for those and other applications that do not functionally require digitization in time [17]. This concept of digitization in time leaded to a new idea in the signal processing which is called continuous time digital signal processing [4]. In [16], the authors define the reconstruction process from the output of the ASDM and derive various reconstruction methods. They call their method of sampling in general as Time Encoding and of signal reconstruction as Time Decoding. We derive a computationally efficient reconstruction algorithm based on an interpretation of Shannon's sampling theory using the ASDM time codes which we believe is a novel way of combining asynchronous operations with the synchronous ones of the Shannon's sampling theory by using PSWF. In the following section we will describe the operation of an ASDM and the corresponding time encoding and decoding as an alternative to uniform sampling and reconstruction and give a computationally efficient reconstruction algorithm.

6.1 ASDM FOR TIME-ENCODING

ASDMs have recently begun gaining more attention as the conventional analog to digital converters have significant limitations which can not be compensated efficiently in many emerging applications. ASDM are a new way of representing analog signals in terms of a discrete form without the need of a clock [5, 17, 16] and since ASDM have a very simple circuitry it can operate at a low current and supply voltage. The reconstruction of a bandlimited signal from the output of an ASDM is similar to the reconstruction of a bandlimited signal from nonuniform samples. In the irregular sampling both the sample values and the time instants of the samples are required to reconstruct the signal, thus the twice the amount of data to be transmitted. Compared to just the sample values in uniform sampling, irregular sampling is not preferable. However, when sampling with an ASDM, it is possible to reconstruct the bandlimited signal just from the zero crossings of the ASDM output which

is an asynchronous binary signal. The zero crossings of that signal give enough information to reconstruct the signal compared to the amplitude information in the conventional analog to digital converter systems. Due to elimination of the clock and the power consumption accompanying it, we investigate ASDMs as a way of data acquisition in neural implants. The ASDM is a nonlinear feedback system which can be implemented as a combination of an integrator and a non-inverting Schmitt trigger [17]. In the ASDM, amplitude information of a signal $x(t)$ is transformed into time information without the quantization error that exists in the synchronous sigma delta modulators. Assuming that the input $x(t)$ of the ASDM is band-limited, with a maximum frequency Ω_{max}, and bounded, $|x(t)| \leq c$, it can be seen from

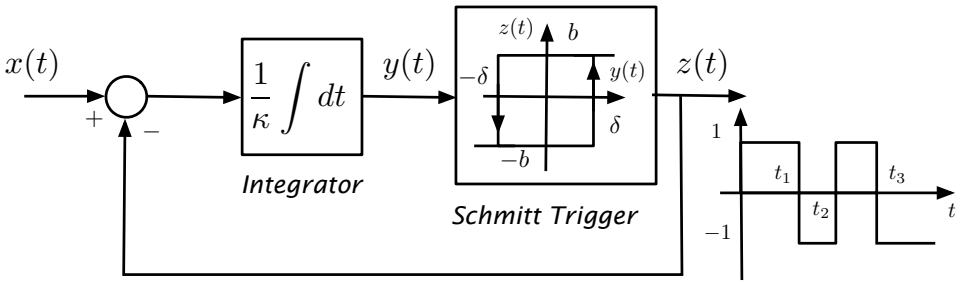

Figure 32: Asynchronous sigma delta modulator.

Fig. 32 that the output of the integrator, $y(t)$, is given by

$$y(t) = y(t_o) + \frac{1}{\kappa}\int_{t_o}^{t}[x(u) - z(u)]du.$$

for all $t > t_o$, where κ, δ, and b are strictly positive numbers and $x(t)$ is a Lebesgues measurable function [16]. Note that $y(t)$ is a continuously increasing (decreasing) function whenever the value of the feedback is positive (negative). Due to the operating characteristic of the Schmitt trigger, output $y(t)$ increases monotonically until it reaches the value δ if the feedback is b or decreases monotonically to $-\delta$ if the feedback is $-b$ for any arbitrary initial value of the integrator. After $y(t)$ reaches the value δ from below or $-\delta$ from above, the output of the Schmitt trigger $z(t)$ flips from $-b$ to b and from b to $-b$, respectively. Therefore, we can assume that for some initial condition at $t = t_o$, we have $(y(t_o), z(t_o)) = (-\delta, -b)$ and in a small neighborhood of $t > t_o$, the TEM is described by [16],

$$\delta = -\delta + \frac{1}{\kappa}\int_{t_o}^{t}[x(u) + b]du \tag{6.1}$$

and since $y(t)$ increases monotonically, the trigger switches to the state (b, δ) at the time $t = t_1 > t_o$ the equation

$$-\delta = \delta + \frac{1}{\kappa}\int_{t_1}^{t}[x(u) - b]du \tag{6.2}$$

is satisfied for some $t = t_2 > t_1$. Generalizing (6.1) and (6.2), for the strictly increasing sequence t_k, $k \in Z$ the following equation

$$\int_{t_k}^{t_{k+1}} x(u)du = (-1)^k[-b(t_{k+1} - t_k) + 2\kappa\delta] \tag{6.3}$$

uniquely describes the relationship between $z(t)$ and $x(t)$ for all $t \in R$ and $|y| \leq \delta$ [16]. For future use we call the right-hand side term of (6.3) as $v(k)$ such that

$$v(k) = (-1)^k[-b(t_{k+1} - t_k) + 2\kappa\delta]. \tag{6.4}$$

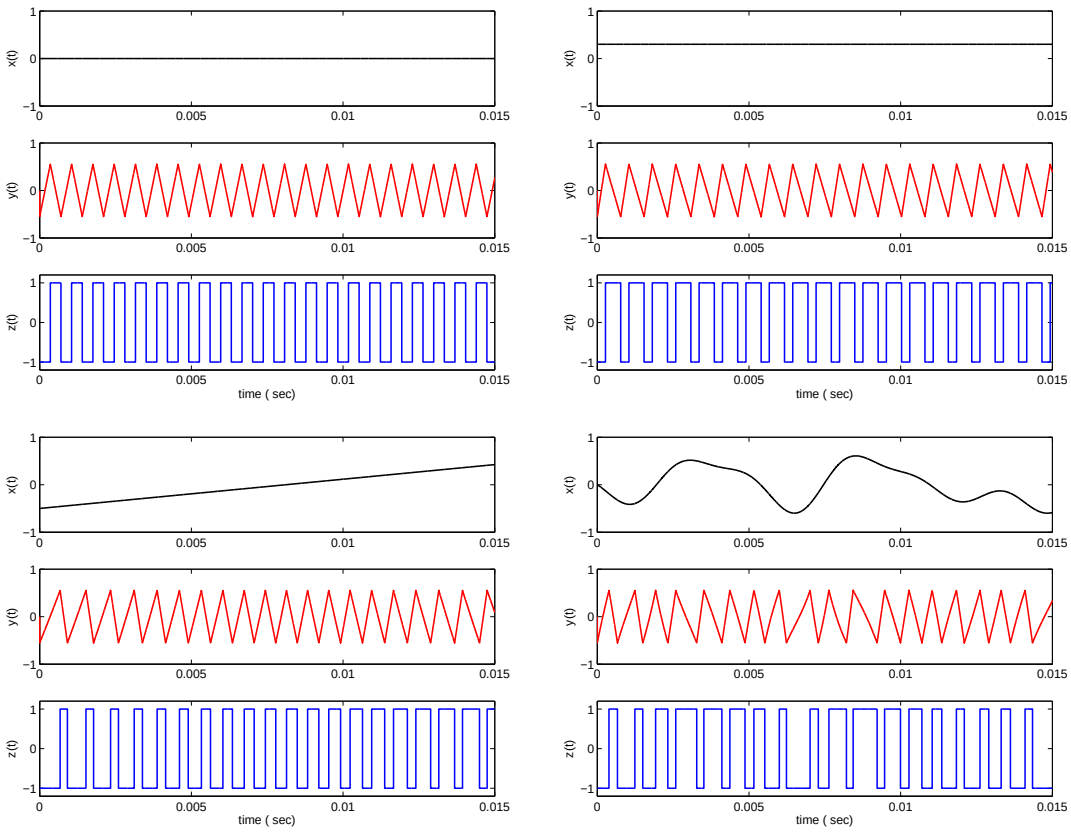

Figure 33: Examples of the processing of ASDM for different inputs $x(t)$.

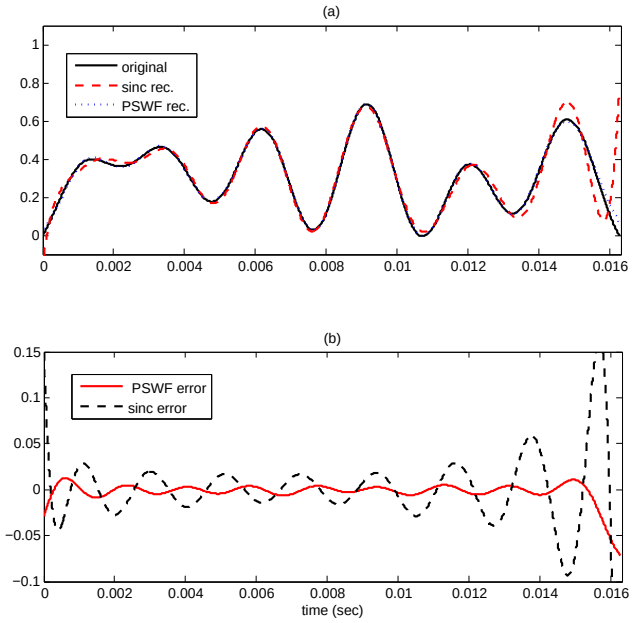

Figure 34: (a) reconstructed vs. original EEG, (b) reconstruction error.

The perfect reconstruction of $x(t)$ is possible provided that the nonuniform sequence $\{t_k\}$ satisfies the condition [17, 16] :

$$\max_k (t_{k+1} - t_k) \leq T_N \tag{6.5}$$

where $T_N = \pi/\Omega_{max}$ is the Nyquist sampling period. Indeed, the upper and lower bounds for trigger times can be found by applying the mean value theorem to the term on the left hand side of equation (6.3) such that we obtain

$$(-1)^k x(\zeta_k)(t_{k+1} - t_k) = -b(t_{k+1} - t_k) + 2\kappa\delta \tag{6.6}$$

where $\zeta_k \in [t_k, t_{k+1}]$ and since $x(t)$ is bounded, i.e., $|x(t)| \leq c$, solving for $t_{k+1} - t_k$, we obtain

$$\frac{2\kappa\delta}{b+c} \leq t_{k+1} - t_k \leq \frac{2\kappa\delta}{b-c}$$

providing a way to choose the parameters b, δ, and κ in terms of the Nyquist sampling rate $T_N \leq 2\kappa\delta/(b-c)$.

6.2 DPSS FOR ASDM RECONSTRUCTION ALGORITHM

The reconstruction of the band-limited signal $x(t)$ from the zero-crossings of $z(t)$ requires a finite length approximation of the sinc function $g(t)$, and an approximation of the integral in equation (6.3). Basically there are two ways of sinc representation:

- Using inverse Fourier transform of the rectangular function $G(\Omega)$, bandlimited to $[-\Omega_o, \Omega_o]$ as

$$g(t) = \frac{1}{2\pi}\int_{-\Omega_o}^{\Omega_o} e^{j\Omega t} d\Omega = \frac{\sin(\Omega_o t)}{\pi t} \tag{6.7}$$

- Approximation of $g(t)$ from line spectrum and by sampling $G(\Omega)$ to get $G_k(\Omega) = \delta(\Omega - k\Omega_o/N)$ as

$$\begin{aligned} g(t) \simeq \frac{1}{2\pi}\int_{-\Omega_o}^{\Omega_o}\sum_{k=-N}^{N}\delta(\Omega - k\Omega_o/N)e^{j\Omega t}d\Omega &= \frac{1}{2\pi}\sum_{k=-N}^{N}\int_{-\Omega_o}^{\Omega_o} e^{j\frac{\Omega_o}{N}kt}\delta(\Omega - k\Omega_o/N)d\Omega \\ &= \frac{1}{2\pi}\sum_{k=-N}^{N} e^{jk\frac{\Omega_o}{N}t} = \frac{1}{2\pi}\sum_{m=0}^{2N} e^{j\frac{\Omega_o}{N}(m-N)t} \\ &= \frac{e^{-j\Omega_o t}}{2\pi}\frac{1 - e^{j\Omega_o(2N+1)t/N}}{1 - e^{j\Omega_o t/N}} \\ &= \frac{1}{2\pi}\frac{\sin(\Omega_o t(2N+1)/2N)}{\sin(\Omega_o t/2N)} \end{aligned} \tag{6.8}$$

where $m = k+N$. Using the approximation from the line spectrum, a reconstruction formula from nonuniform samples is

$$\begin{aligned} x(t) &= \sum_k c_k g(t - s_k) \\ &\approx \sum_k c_k \frac{1}{2\pi}\sum_{m=-N}^{N} e^{j(t-s_k)m\Omega_o/N} \\ &= \sum_{m=-N}^{N}\frac{1}{2\pi}[\sum_k c_k e^{j\frac{\Omega_o}{N}s_k m}]e^{j\Omega_o/Ntm} \\ x(t) &\cong \sum_{m=-N}^{N} d(m)e^{\frac{j\Omega_o tm}{N}} \end{aligned} \tag{6.9}$$

here $s_k = t_k + t_{k+1}/2$. If one can solve the above equation for $d(m)$, the reconstruction can be done. We can replace (6.9)in (6.3) to solve for $d(m)$. In [16], the sinc function represented by $S(t)$ is approximated by complex exponentials as

$$S(t) \approx \sum_{m=-L}^{L} \alpha e^{jm\Omega_0 t} = \alpha \frac{\sin((L+0.5)\Omega_0 t)}{\sin(0.5\Omega_0 t)} \tag{6.10}$$

where L is an arbitrary large number not connected with the signal $x(t)$, and $\Omega_0 = \frac{\Omega_{max}}{L}$.

Assume that the input to the ASDM is approximated by a PSWF projection

$$x(t) \approx \hat{x}(t) = \sum_{n=0}^{M-1} \gamma_{M,n} \varphi_n(t)$$

where the value of M is chosen by making the frequency of the $\varphi_M(t)$ coincide with the frequency of $x(t)$. If we let $t = k\Delta_t$, such that $\Delta_t < \pi/\Omega_{max}$ the projection can be written

$$\hat{\mathbf{x}} = \mathbf{\Phi}\ \gamma_{\mathbf{M}} \tag{6.11}$$

The integral in (6.3), for $b = 1$, can be approximated by means of the trapezoidal rule as

$$\begin{aligned} \int_{t_k}^{t_{k+1}} x(t)dt \quad &\approx \quad 0.5x(t_k)\Delta_t + \sum_{i=1}^{N_k-1} x(t_k + i\Delta_t)\Delta_t \\ &\quad +0.5x(t_{k+1})\Delta_t \end{aligned}$$

where $N_k = (t_{k+1} - t_k)/\Delta_t$. Letting $v(k)$ in Eq. (6.4) be the entries of a vector $\mathbf{v}$ computed at each of the $\{t_k\}$ values by

$$v(k) \approx \mathbf{q_k}^{\mathbf{T}}\ \mathbf{\Phi}\ \gamma_{\mathbf{M}}$$

where the entries of the row vector $\mathbf{q_k}$ are given as

$$q_{k,j} = \begin{cases} 0.5\Delta_t & j = 0, \text{ and } j = N_k \\ \Delta_t & N_k + 1 \le j \le N_k - 1 \\ 0 & \text{otherwise} \end{cases}$$

Thus for the time sequence $\{t_k,\ k = 1, \cdots, K\}$ equation (6.3) can be written as

$$\mathbf{v} = \mathbf{Q}\ \mathbf{\Phi}\ \gamma_{\mathbf{M}} \tag{6.12}$$

where $\mathbf{Q}$ is the matrix composed of the vector $\mathbf{q_k}$ and the vector $\mathbf{v}$ is composed of (6.4). Computing

$$\gamma_{\mathbf{M}} = [\mathbf{Q}\ \mathbf{\Phi}]^{\dagger}\mathbf{v} \tag{6.13}$$

we can use it to find the projection $\hat{x}$ in (6.11) where † represents the pseudo-inverse operation. We will demonstrate the advantages of using PSWF reconstruction over the sinc based reconstruction method in some simulations after we propose a transmission method for the ASDM output signal.

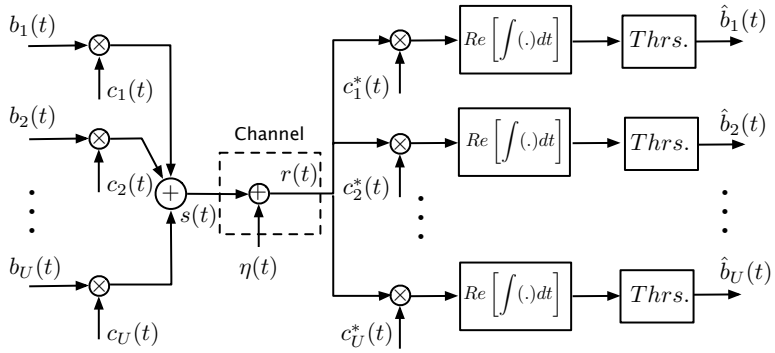

Figure 35: Chirp OFDM for uniform symbol period.

6.2.1 Chirp Modulation for ASDM Signals

We consider the transmission of binary signals $\{z_n(t)\}$, $n = 1, \cdots, N$ from an array of N ASDMs which can be used for data acquisition in a brain computer interface system (BCI). These signals need to be transmitted in the most efficient way from the BCI to an intermediate personal digital assistant (PDA) capable of transmitting the signal to a server where the signal analysis is performed. Each of the signals is a train of pulses with non-uniform zero-crossings. We explore the application of orthogonal frequency division multiplexing (OFDM) (see Fig. 35) using orthonormal chirp basis for the modulation of the N time-encoded signals.

6.2.2 Uniform symbol period

Chirp modulation has been applied successfully in OFDM [97]. In OFDM system the data is divided into several parallel data streams or channels, one for each sub-carrier. Each sub-carrier is modulated with a conventional modulation scheme at a low symbol rate, maintaining total data rates similar to conventional single-carrier modulation schemes in the same bandwidth. OFDM is robust against narrow-band co-channel interference, intersymbol interference (ISI) and fading caused by multipath propagation. Also it has high spectral efficiency as compared to conventional modulation schemes, spread spectrum, etc. OFDM has an efficient implementation using Fast Fourier Transform (FFT) and it has low sensitivity to time synchronization errors. In the case of the transmission of source symbols $+1$ or -1 with a uniform period T, if we have orthonormal chirps $c_k(t)$ for users $k = 1, \cdots, U$ the baseband transmitted signal for user k is given by $s_k(t) = b_k(t)c_k(t)$ where $b_k(t)$ is either 1 or -1 for $t_0 \leq t \leq t_0 + T$. Assuming perfect synchronization at the receiver and that the only channel effect is addition of Gaussian noise $\eta(t)$, the baseband received signal is

$$r(t) = \sum_{k=1}^{U} s_k(t) + \eta(t) \tag{6.14}$$

To recover the source symbols, multiplying the received signals by the conjugate of the chirps, $c_k^*(t)$ we obtain a decision variable for user k

$$\begin{aligned} y_k &= \int_{t_0}^{t_0+T} r(t)c_k^*(t)dt \\ &= \sum_{n=1}^{U} b_n(t) \int_{t_0}^{t_0+T} c_n(t)c_k^*(t)dt + \int_{t_0}^{t_0+T} \eta(t)c_k^*(t)dt \\ &= b_k(t) + \int_{t_0}^{t_0+T} \eta(t)c_k^*(t)dt \qquad t_0 \leq t \leq t_0 + T \end{aligned} \tag{6.15}$$

and the value of $b_k(t)$, which is either 1 or -1, is estimated by a thresholder. The orthonormality of the chirps mitigates the multiple access interference caused by other users different from the user we are interested in.

Consider a set of frequency modulated linear chirps with instantaneous frequencies

$$\phi_k(t) = \theta t + 2f_k \qquad k = 1, \cdots, U \tag{6.16}$$

where θ is a common chirp rate, and $f_k = \alpha_k/T$ is a multiple of the frequency corresponding to the symbol period T. The chirps are given by

$$c_k(t) \;=\; e^{j\pi\phi_k(t)t} = e^{j\pi\theta t^2} e^{j2\pi f_k t}$$

The orthonormality of the chirps $\{c_k(t)\}$ depends on the orthonormality of the $\{e^{j2\pi f_k t}\}$ terms. Indeed, the common chirp rate makes it so that

$$\begin{aligned} \frac{1}{T}\int_{t_0}^{t_0+T} c_k(t)c_n^*(t)dt &= \frac{1}{T}\int_{t_0}^{t_0+T} e^{j2\pi(f_k-f_n)t}dt \\ &= \begin{cases} 1 & k=n \\ 0 & k\neq n \end{cases} \end{aligned} \tag{6.17}$$

In [97] the orthonormal chirps are obtained from the properties of the kernel of the fractional Fourier transform, but such relation is unnecessary as shown above.

6.2.3 Nonuniform symbol period

Applying the chirp-modulated OFDM for the transmission of the time-encoded signals obtained from N ASDMs is complicated by the fact that the pulses corresponding to the symbols do not have a uniform period as before. Indeed the duty-cycle modulation that is being used to get $z(t)$ from $x(t)$ gives that the pulse width $\alpha_k(t)$ and the pulse period $\tau_k(t)$ of two consecutive pulses give a duty-cycle

$$\frac{\alpha_k(t)}{\tau_k(t)} = \frac{1+x_k(t)}{2}$$

for $x_k(t)$ in $[t_k, t_{k+2}]$. Thus only when $x(t) = 0$ we would have uniform pulse periods. In this case of nonuniform pulse duration, we will again consider chirps with a common chirp rate θ, but with frequencies $f_n = 1/\hat{T}$ where

$$\hat{T} = \min\{T_n(k)\}$$

and $T_n(k) = t_n(k+1) - t_n(k)$ are the time intervals from the signals $\{z_n(t),\, n = 1, \cdots, N\}$. The bandwidth allocated to the n^{th}-ASDM, $F_n = f_{n+1} - f_n$, is divided into M sub-bands with frequencies

$$f_n(m) = f_n + \frac{F_n}{M} m \qquad m = 0, \cdots, M-1 \tag{6.18}$$

Using these frequencies and the zero crossings $\{t_n(k)\}$ from $z_n(t)$ we create an array of chirps with instantaneous frequencies

$$\phi_{n,m}(t - t_n(m)) = \theta(t - t_n(m)) + 2f_n(m) \tag{6.19}$$

when $t \in [t_n(m), t_n(m+1)]$ and $-\infty$ otherwise (so that the chirp is zero outside $[t_n(k), t_n(k+1)]$). Thus the chirp

$$c_{nm}(t) = e^{j\pi\phi_{nm}(t)t} = e^{j\pi\theta t^2} e^{j2\pi f_n(m)t} \tag{6.20}$$

for $t_m \le t \le t_{m+1}$ and zero otherwise. Considering an analysis time segment $t_0 \le t \le t_0 + T_f$, where $T_f = \beta\hat{T}$ for a small integer β, the orthonormality of the chirps $c_{nm}(t)$ is kept by the common chirp rate and by the orthogonality of the complex exponentials with frequencies $\{f_n(m)\}$. Each consecutive pulse in $z_n(t)$ is multiplied by a chirp with an increasing frequency $f_n(m)$. Assuming again that the effect of the channel is only the addition of Gaussian noise, the received signal is now

$$\begin{aligned} r(t) &= \sum_{n=1}^{N} \sum_{m=0}^{M-1} s_{nm}(t) + \eta(t) \\ &= \sum_{n=1}^{N} \sum_{m=0}^{M-1} z_n(t) c_{nm}(t) + \eta(t) \end{aligned} \tag{6.21}$$

If we multiply this signal by $e^{-j\pi\theta t^2}$ the resulting signal is

$$\begin{aligned} y(t) &= r(t) e^{-j\pi\theta t^2} \\ &= \sum_{n=1}^{N} \sum_{m=0}^{M-1} z_n(t) e^{j2\pi f_n(m)t} + \eta(t) e^{-j\pi\theta t^2} \end{aligned} \tag{6.22}$$

and when we pass this signal through a band-pass filter of bandwidth F_n gives

$$\tilde{y}_n(t) = \sum_{m=0}^{M-1} z_n(t) e^{j2\pi f_n(m)t} + \tilde{\eta}(t) \tag{6.23}$$

which is a combination of sinusoids in the bandwidth assigned to channel n, and where $\tilde{\eta}(t)$ is the noise within that band-width.

If we express $z_n(t)$ for $t_0 \leq t \leq t_0 + T_f$ as a concatenation of rectangular pulses using the unit-step signal $u(t)$ and let $d_\ell = \pm 1$ for the subchannels being occupied and zero for those that are not, we get

$$z_n(t) = \sum_{\ell=0}^{M-1} d_\ell [u(t - t_n(\ell+1)) - u(t - t_n(\ell))] \tag{6.24}$$

The Fourier transform of $z_n(t)$ is then

$$Z_n(\omega) = \sum_{\ell=0}^{M-1} d_\ell \int_{t_n(\ell)}^{t_n(\ell+1)} e^{-j\omega t} dt \tag{6.25}$$

and then the Fourier transform of $\tilde{y}_n(t)$ is given by

$$\tilde{Y}_n(\omega) = \sum_{m=0}^{M-1} Z_n(\omega - 2\pi f_n(m)) + \tilde{\eta}(\omega)$$

If we filter $\tilde{Y}_n(\omega)$ of center frequency $f_n(m)$ and determine the value of this function at the frequencies $f_n(m)$, for $m \in [0, \cdots, M-1]$ we obtain

$$\begin{aligned} \hat{Y}_n(f_n(m)) &= Z_n(0) + \tilde{\eta}(2\pi f_n(m)) \\ &= d_m \left[t_n(m+1) - t_n(m) \right] \\ &\quad + \tilde{\eta}(2\pi f_n(m)) \end{aligned} \tag{6.26}$$

so that $|\hat{Y}_n(f_n(m))| \approx t_n(m+1) - t_n(m)$. We have obtained that for the m-subchannel in the n-channel with high signal to noise ratio the corresponding period is $T_n(m) = t_n(m+1) - t_n(m)$ and the corresponding value d_m.

6.3 SIMULATIONS

In the first set of simulations, to illustrate the duty-cycle modulation performed by the ASDM, we consider four different signals. When $x(t) = 0$, the output of the integrator is a symmetric triangular signal and the output $z(t)$ of the ASDM is a train of square pulses of uniform symbol duration. In any other case we obtain rectangular pulses with a duty cycle depending on the value of the amplitude of the input signal. Fig. 33 shows the cases when the input is zero, a positive constant, a ramp and an arbitrary signal. A characteristic of these cycles is that the average of the input signal $x(t)$ equals the average of the output signal $z(t)$ in each of the intervals $[t_k, t_{k+2}]$.

Later, we do a simulation to compare the sinc approximation based reconstruction to DPSS projection. Fig. 34, we compare the two kinds of reconstruction. To illustrate the transmission, we consider four outputs from ASDMs $\{z_n(t),\ n = 1, 2, 3, 4\}$ which are shown in Fig. 36, for a small interval. Our algorithm provides the duration of each of the symbols in seconds and also the value ± 1 which will provide us the data necessary to reconstruct the original signals in each of the channels. To illustrate the performance of the algorithm when noise is added by the channel, we did a Monte Carlo simulation with 500 trials for each signal to noise ratio (SNR) and make these vary from -10 to 10 dBs. The results show that our procedure is quite robust to additive noise. As a more general example where we consider a real situation which will create the following binary outputs $z(t)$ as in Fig. 37. In our simulations we used subdural EEG signals of an epilepsy patient. For 4-channels, ASDM sampling was applied giving time codes for each $z_u(t)$, $u = 1, \ldots, 4$. The parameters of the ASDM were chosen for a sampling period of 5 msec. The Fig. 38 illustrates the demodulation and reconstruction.

6.4 CONCLUSIONS

In this chapter we considered a reconstruction method based on PSWF for the time codes of an ASDM sampling system. ASDM is a low-power nonlinear feedback system which has

potential applications in biomedical implants which require low power consumption, low electromagnetic interference and small size. We also consider an efficient modulation system to be used together with the binary signals from ASDM output. In this case we chose orthogonal frequency division multiplexing (OFDM)which works efficiently. In OFDM system the data is divided into several parallel data streams or channels, one for each sub-carrier. Each sub-carrier is modulated with a conventional modulation scheme at a low symbol rate, maintaining total data rates similar to conventional single-carrier modulation schemes in the same bandwidth. OFDM is robust against narrow-band co-channel interference, intersymbol interference (ISI) and fading caused by multipath propagation. Also it has high spectral efficiency as compared to conventional modulation schemes, spread spectrum, etc. OFDM has an efficient implementation using Fast Fourier Transform (FFT) and it has low sensitivity to time synchronization errors. We modified an OFDM system to be used for a group of ASDM sensors which we believe is a promising way of data communication between bioimplants and personal digital assistants(PDA) for health monitoring applications.

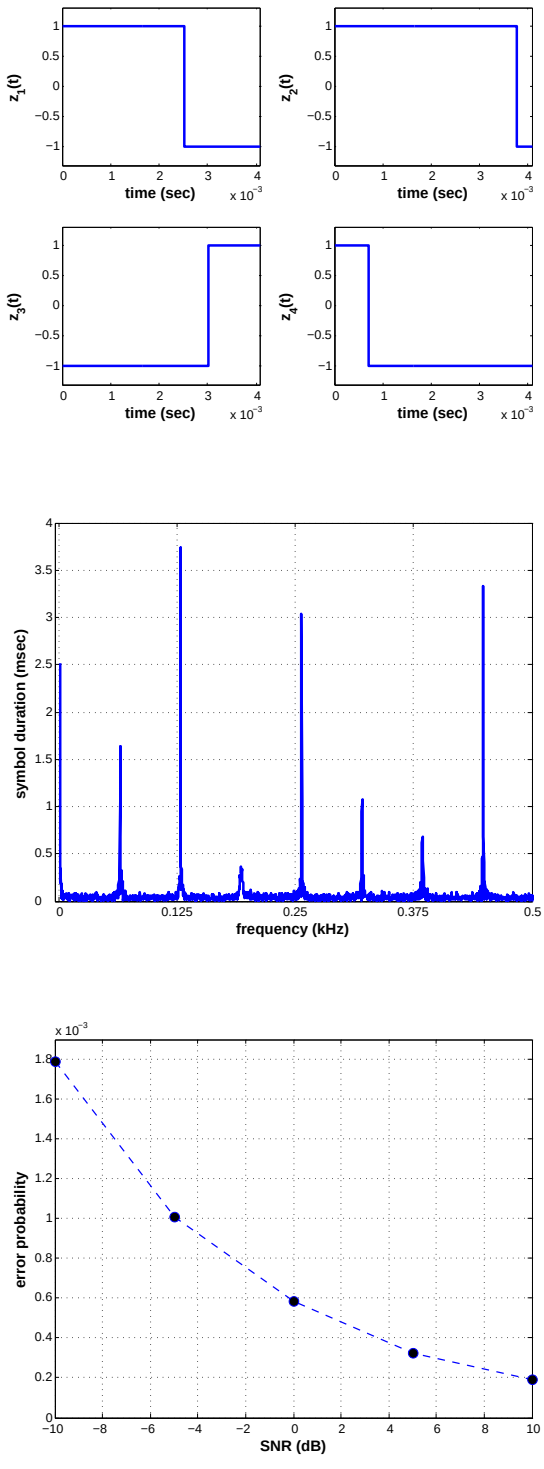

Figure 36: Transmission of four channel binary signals.

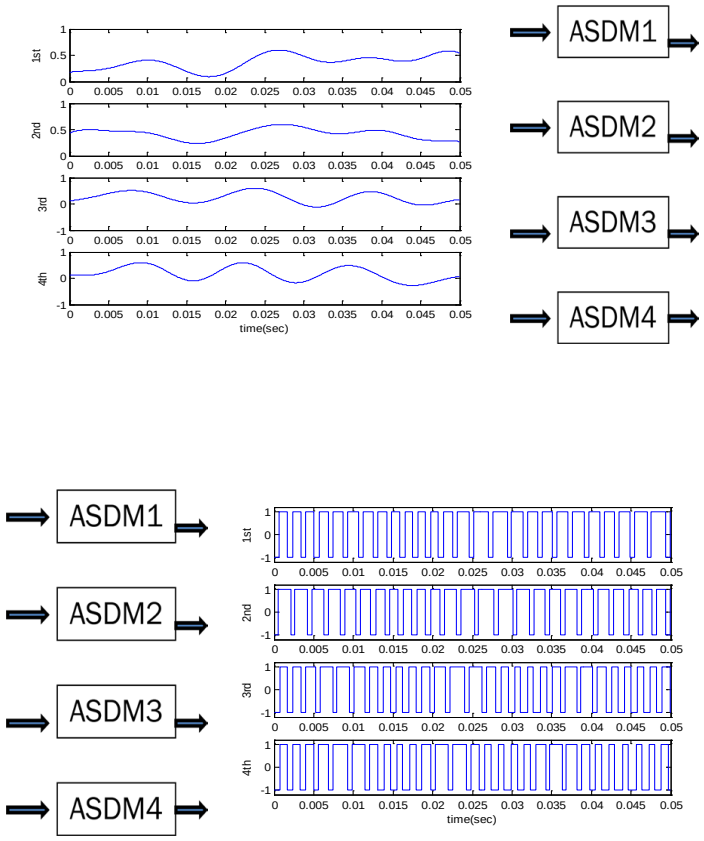

Figure 37: Top: 4 channel input for ASDM, Bottom: Output of ASDM for 4 channel.

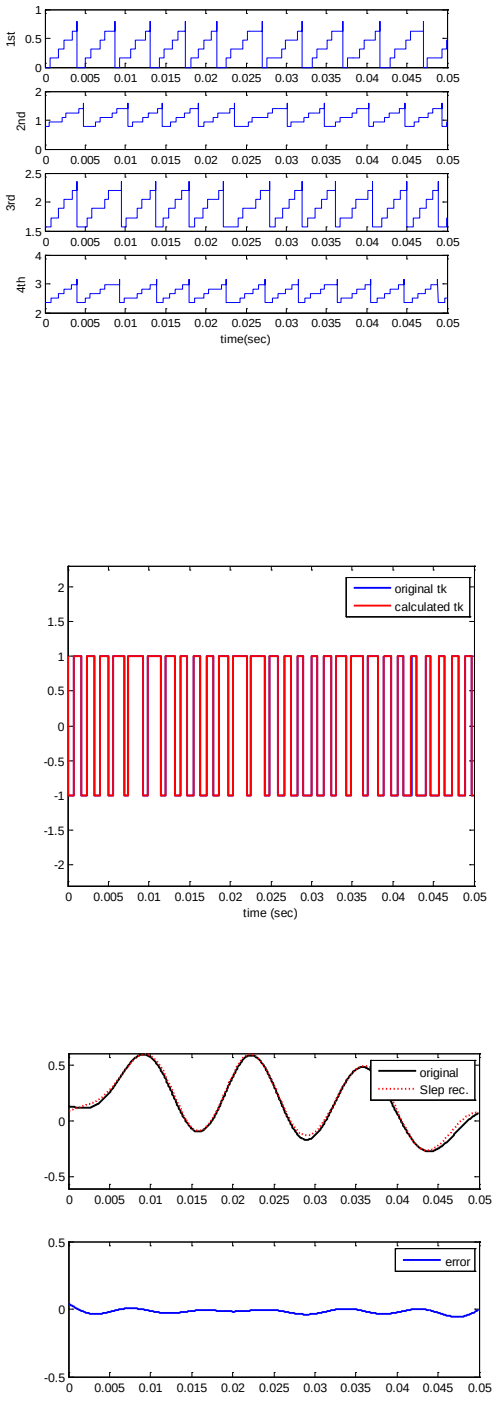

Figure 38: Top: Frequency assignment for four of the channels, Middle: Demodulation of one of the channels (4th channel), Bottom: reconstruction of the signal from demodulated codes.

7.0 FUTURE WORK

Our future goal is to establish a collaborative, multidisciplinary and integrative research to provide solutions for a variety of application domains: healthcare, environmental monitoring and communications. In order to realize this goal, we will focus on the following research areas:

- We will extend our research interests to include data acquisition technologies for the development of advanced sensors and actuators.
- We will carry out research on embedded systems and sensor networks since understanding of the current technologies is very important for successful implementation of the data acquisition algorithms. We intend to continue this research for asynchronous signal processing for low-complexity, real-time and energy-aware signal compression.
- In the stabilization of networked control systems, where the sampling intervals are time-varying, various form of nonuniform sampling methods can be used to increase performance. To the best of our knowledge, there is not enough research on this important problem, therefore we are motivated to do both theoretical and experimental work on this subject

BIBLIOGRAPHY

[1] F. Eng, *Nonuniform sampling in statistical signal processing*, PhD Thesis, Department of Electrical Engineering. Linköping University, Linköping, Sweden, 2007.

[2] T. Strohmer, "Numerical analysis of the nonuniform sampling problem," *Journal of Computational and Applied Mathematics*, vol. 112, pp. 297-316, 2000.

[3] N. Sayiner, "A Level-crossing sampling scheme for A/D conversion," *IEEE Transactions on Circuits and Systems II*, vol. 45, no. 4, pp. 335-339, April 1996.

[4] Y. Tsividis, "Digital signal processing in continuous time: A possibility for avoiding aliasing and reducing quantization error," *Procedings of IEEE International conference on Acoustics Speech and Signal Processing* (ICASSP), vol. II, pp. 589-593, Montreal , May 2004.

[5] M. Miskowicz, "Send-on-Delta Concept: an Event-Based Data Reporting Strategy," *Sensors* 2006, 6, 49-63. Sensors 2010, 10(3), 2242-2261; doi:10.3390/s100302242.

[6] E. J. Candes, "Compressive sampling," *in Proceedings of the International Congress of Mathematics*, vol. 3, Spain, pp. 1433-1452, 2006.

[7] D. Slepian and H. O. Pollak, "Prolate spheroidal wave functions, Fourier analysis and uncertainty," *Bell Systems Techical Journal*, vol. 40, pp. 43-64, 1961.

[8] K. M. Guan and A. C. Singer, "A level-crossing sampling scheme for non-bandlimited signals," *IEEE International Conference on Acoustics, Speech and Signal Procesing*, vol. 3, pp. 381-383, May 2006.

[9] H. Feichtinger, *Pseudo-inverse matrix methods for signal reconstrcution from partial data*, SPIE-Conference, Boston, Nov. 1991.

[10] J. Hogan, "Frame-based nonuniform sampling in Paley-Wiener spaces," *Journal of Applied Functional Analysis*, 2, 361-400, 2007.

[11] R. Suleesathira, L. F. Chaparro, and A. Akan, "Discrete evolutionary transform for time-frequency signal analysis," *Journal of Franklin Institute*, vol. 337, no.4, pp. 347-364, 2000.

[12] M. B. Priestley, *Non-linear and non-stationary time series analysis*, Academic Press, London, 1988.

[13] J. A. Tropp, M. B.Wakin, D. Baron, and R. G. Baraniuk, "Random filters for compressive sampling and reconstruction," *in Proceedings IEEE International Conference Acoustics, Speech and Signal Processing*, pp. III 872875, May 2006.

[14] L. G. Gubin, B. T. Polyak, and E. V. Raik, "The method of projections for finding the common point of convex sets," *USSR Computational Mathematics and Physics*, vol. 7, no. 6, pp. 1-24, 1967.

[15] L. M. Bregman, "Finding the common point of convex sets by the method of successive projections," *Dokl. Akad. Nauk. USSR*, vol. 162, no. 3, pp. 487-490, 1965.

[16] A. Lazar and L. Toth, "Perfect recovery and sensitivity analysis of time encoded bandlimited signal," *IEEE Transactions on Circuits and Systems*, pp. 2060-2073, Oct. 2004.

[17] E. Roza, "Analog-to-digital conversion via duty-cycle modulation," *IEEE Transactions on Circuits and Systems*, vol. 44, pp. 907-914, Nov. 1997.

[18] M. Unser, "Sampling-50 Years after Shannon," *Proceedings of IEEE*, vol. 88, no. 4, pp. 569-587, April 2000.

[19] R. G. Vaughan, N. L. Scott, D. R. White, "The theory of bandpass sampling," *IEEE Transactions on Circuits and Systems*, pp. 1973-1984, vol. 39, no. 9, Sept. 1991.

[20] C. Flammer, "Spheroidal Wave Functions," Stanford University Press, Stanford, CA, 1957. MR0089520 (19:689a).

[21] M. Kozin, V. Volkov, D. Svergun, "A compact algorithm for evaluating linear prolate functions," *IEEE Transactions on Signal Processing*, 45, 10751077, 1997.

[22] H. Xiao, *Prolate spheroidal wave functions, quadrature, interpolation, and asymptotic formulae*, Ph.D. Thesis, Yale University, 2001.

[23] F. Marvasti, *Nonuniform Sampling theory and Practice*, Kluwer Academic/Plnum Publishers, Newyork, 2001.

[24] G. Golub and D. O'Leary, "Some History of the Conjugate Gradient and Lanczos Methods," *In SIAM Review*, 31, 50-102, 1989.

[25] M. Greitans, "Enhanced signal processing in time and frequency domains in the case of non-uniform sampling," *International Conference on Sampling Theory and Application*, SampTA'03, May 26-29, 2003, Strobl, Salzburg, Austria.

[26] I. C. Moore, M. Cada, "Prolate spheroidal wave functions, an introduction to the Slepian series and its properties," *Applied Computational and Harmonic Analysis*, 16 (2004), no. 3, 208230. 33E10 (33E30 42C10)

[27] A. Aldroubi and K. Grchenig, "Nonuniform sampling and reconstruction in shift-invariant spaces," *In SIAM Review*, vol. 43(4):pp. 585–620, 2001.

[28] D. L. Donoho and P. B. Stark, "Uncertainty principles and signal recovery," *SIAM Journal on Applied Mathematics*, 49(3):90631, 1989.

[29] C. Grönwall, O. Steinvall, F. Gustafsson and T. Chevalier, "Influence of laser radar sensor parameters on range-measurement and shape-fitting uncertainties," *Optical Engineering*, volume 46(10), 2007.

[30] S. Roques and C. Thiebaut, "Spectral contents of astronomical unequally spaced time-series: contribution of time-frequency and time-scale analyses," *IEEE International Conference on Acoustics, Speech, and Signal Processing*, vol. 6, pp. 473476, Hong Kong, 2003.

[31] J. Elbornsson and F. Gustafsson, "Equalization of Time Errors in Time Interleaved ADC System –Part I: Theory," *Automatic Control Reports*, Linköping University, Department of Electrical Engineering, The Institute of Technology, Sweden.

[32] K. Grochenig, "Reconstruction algorithms in irregular sampling theory," *Computational Mathematics*, vol. 59, pp. 181194, 1992.

[33] G. Strang and T. Nguyen, *Wavelets and Filter Banks*, Wellesley-Cambridge Press, 2nd Edition, 1997.

[34] H. Landau, *Necessary density conditions for sampling and interpolation of certain entire functions*, Acta Mathematics, 1967.

[35] J.M. Varah, *A lower bound for the smallest singular value of a matrix*, Linear Algebra Application, 11 (1975), pp. 3-5.

[36] J. Benedetto, *Irregular sampling and frames," In Wavelets: A Tutorial in Theory and Practice*, Academic Press Inc., Modern Sampling Theory, Birkhäuser Verlag.

[37] R. J. Duffin and J. J. Eachus, "Some notes on an expansion theorem of Paley and Wiener," *Bulletin of American Mathematical Society*, pp. 850-855, 48, 1942.

[38] P. Vaidyanathan and V. Liu, "Efficient reconstruction of band-limited sequences from nonuniformly decimated versions by use of polyphase filter banks," *IEEE Transactions on Acoustics, Speech and Signal Processing*, vol. 38, pp. 1927-1936, Nov. 1990.

[39] H. Johansson and P. Löwenborg, "Reconstruction of nonuniformly sampled bandlimited signals by means of time-varying discrete-time FIR filters," *Hindawi Publishing Corporation EURASIP Journal on Applied Signal Processing*, Vol. 2006, Article ID 64185, Pages 118.

[40] J. Yen, "On nonuniform sampling of bandwidth-limited signals," *IRE Transactions on Circuit Theory*, vol. 3, no. 4, pp. 251-257, 1956.

[41] R. Frieden, *In Progress in optics*, Vol. IX, North-Holland, Amsterdam 1971, pp. 3–13.

[42] C. Vezyrtzi and Y. Tsividis, "Processing of signals using level-crossing sampling," *IEEE International Symposium on Circuits and Systems*, pp. 2293-2296, May 2009.

[43] J. L. Rojo-Alvarez, C. Figuera-Pozuelo, et al., "Nonuniform interpolation of noisy signals using support vector machines," *IEEE Transactions on Signal Processing*, vol. 55, no. 8, pp. 4116-4126, Aug. 2007.

[44] M. Greitans and R. Shavelis, "Speech sampling by level-crossing and its reconstruction using spline-based filtering ," *Proceedings of the 14th International Conference on Systems, Signals and Image Processing*, pp. 305-308, 2007.

[45] M. Greitans and R. Shavelis, "Signal-dependent techniques for non-stationary signal sampling and reconstruction," *17th European Signal Processing Conference*, pp. 2613-2617, Scotland, Aug. 2009.

[46] P. C. Hansen, "Rank-deficient and discrete ill posed problems: Numerical aspects of linear inversion," *SIAM, Mathematical Modeling and Computation.*

[47] G. Walters and X. Shen, "Sampling with prolate spheroidal wave functions," *Sampling Theory in Signal and Image Processing*, vol. 2, pp. 25-52, 2003.

[48] H. Choi and D. C. Munson, "Analysis and design of minimax-optimal interpolators," *IEEE Transactions on Signal Processing*, vol. 46, pp. 1571-1579, June 1998.

[49] W. Cheney, D. Kincaid, *Numerical Mathematics and Computing*, Broks/Cole, 763 pages, 2007.

[50] A. N. Tikhonov, "Solution of incorrectly formulated problems and the regularization method," *Soviet Math. Dokl.*, vol. 4, pp. 1035–1038, 1963.

[51] P. C. Hansen and D. P. Oleary, "The Use of the L-Curve in the Regularization of Discrete Ill-Posed Problems," *SIAM Journal on Scientific Computing* 14 (6), pp. 1487-1503.

[52] J. J. Ding and S. C. Pei, "Reducing sampling error by prolate spheroidal wave functions and fractional Fourier transform," *IEEE International Conference on Acoustics, Speech and Signal Processing*, vol. 4, pp. 217-220, Mar. 2005.

[53] S. Senay, L. F. Chaparro, and L. Durak, "Reconstruction of nonuniformly sampled time-limited signals using prolate spheroidal wave functions," *Signal Processing*, vol. 89, pp. 2585-2595, Dec. 2009.

[54] J. Oh, S. Senay, and L. F. Chaparro, "Signal recovery from nonuniformly-spaced samples using evolutionary Slepian transform based POCS," *EURASIP Journal of Advances in Signal Processing*, vol. 2010, pp. 1-12, 2010, DOI:10.1155/2010/367317.

[55] E. J. Candes and M. B. Walkin, "An introduction to compressive sampling [a sensing/sampling paradigm that goes against the common knowledge in data acquistion]," *IEEE Signal Processing Magazine*, vol. 25, no. 2, pp. 21-30, Mar. 2008.

[56] J. Tropp and A. C. Gilbert, "Signal recovery from partial information via orthogonal matching pursuit," *IEEE Transactions on Information Theory*, vol. 53, pp. 4655-4666, Dec. 2007.

[57] D. L. Donoho, I. Drori, Y. Tsaig, and J. L. Starck, "Sparse solution of underdetermined linear equations by stagewise orthogonal matching pursuit," Technical Report, 2006.

[58] S. Oraintara, W.C. Karl, D.A. Castanon, and T.Q. Nguyen, "A method for choosing the regularization parameter in generalized Tikhonov regularized linear inverse problems," *International Conference on Image Processing*, vol. 1, pp. 93-96, 2000.

[59] M. Arigovindan, M. Sulhing, P. Hunziker, and M. Unser, "Variational image reconstruction from arbitrarily spaced samples: a fast multiresolution spline," *IEEE Transactions on Image Processing*, vol. 14, no. 4, pp. 450-460, Apr. 2005.

[60] D. L. Donoho, "Compressed sensing," *IEEE Trans. Inform. Theory*, vol. 52, pp. 1289–1306, Apr. 2006.

[61] M. Vetterli, P. Marziliano and T. Blu, "Sampling signals with finite rate of innovation," *IEEE Transactions on Signal Processing*, Vol. 50, No. 6, pp. 1417-1428, 2002.

[62] S. Dharanipragada and K. S. Arun, "Bandlimited extrapolation using time-bandwidth dimension," *IEEE Transactions on Signal Processing*, Vol. 45, No. 12, pp. 2951–2966, Dec. 1997.

[63] J. A. Hogan, J. D. Lakey, *Time-frequency and time-scale methods: adaptive decompositions, uncertainty principles, and sampling*, Birkhäuser, 388 pages, 2005.

[64] R. G. Baraniuk, "Compressive sensing," in *IEEE Signal Processing Magazine*, pp. 118–121, Jul. 2007.

[65] E. J. Candes, J. Romberg, and T. Tao, "Robust uncertainty principles: exact signal reconstruction from highly incomplete frequency information," *IEEE Transactions on Information Theory*, vol. 52, pp. 489-509, Feb. 2006.

[66] L. Weiss and R. N. McDonough, "Prony's method, z-transforms, and Pade approximation," *SIAM Review* Vol.5, pp. 145-154, 1983.

[67] L. Colucio, A. Eisinberg, and G. Fedele, "A Prony-like method for nonuniform sampling,"*Signal Processing*, Vol. 87, No.10, pp. 2484-2490, Oct. 2007.

[68] E. J. Candes and J. Romberg, *Toolbox ℓ_1-MAGIC*, California Institute of Technology, Pasadena, CA ($http://www.acm.caltech.edu/l1magic$).

[69] L. Cohen, *Time-frequency Analysis: Theory and Applications*. Prentice-Hall, New York, 1995.

[70] L. Durak and O. Arıkan, "Short-time Fourier transform: two fundamental properties and an optimal implementation," *IEEE Transactions on Signal Processing*, Vol. 51, pp. 1231–1242, May 2003.

[71] V. Namias, "The fractional order Fourier transform and its application to quantum mechanics," *J. Inst. Math. Appl.*, Vol. 25, pp. 241–265, 1980.

[72] H. M. Ozaktas, Z. Zalevsky, and M. A. Kutay, *The Fractional Fourier Transform with Applications in Optics and Signal Processing*, John Wiley & Sons, New York, 2001.

[73] L. B. Almedia, "The fractional Fourier transform and time-frequency representations," *IEEE Transactions on Signal Processing*, Vol. 42, pp. 3084–3091, Nov. 1994.

[74] H. M. Ozaktas, O. Arıkan, M. A. Kutay, and G. Bozdagi, "Digital computation of the fractional Fourier transform," *IEEE Transactions on Signal Processing*, vol. 44, No. 9, pp. 2141–2150, Sep. 1996.

[75] A. W. Lohmann and B. H. Soffer, "Relationships between the Radon–Wigner and fractional Fourier transforms," *Journal of Optical Society of America*, vol. 11, pp. 1798–1801, 1994.

[76] S. Yeh, and H. Stark, "Iterative and one-step reconstruction from nonuniform samples by convex projections," *Journal of Optical Society of America*, vol. 7, no. 3, pp. 491-499, 1990.

[77] R. Stasinski and J. Konard, "POCS-based image reconstruction from irregularly-spaced samples," *Proceedings of IEEE International Conference on Image Processing*, vol. II, pp. 315-318, Sept. 2000.

[78] J. Park, D.-C. Park, R.J. Marks, and M.A. El-Sharkawi, "Block loss recovery in DCT image encoding using POCS," *Proceedings of IEEE International Symposium on Circuits and Systems*, vol. 5, pp. 245-248, Sept. 2002.

[79] T. Krauss, C. Moler and Eric Breitenberger, Copyright 1988–2004, The MathWorks, Inc.

[80] S. Senay, L.F. Chaparro, M. Sun, R. J. Sclabassi, "Time encoding and reconstruction of multichannel data by brain implants using asynchronous sigma delta modulators," *31st International. Conference of the IEEE Engineering in Medicine and Biology Society* (EMBC), Minneapolis, Minnesota, USA, Sept. 2009.

[81] H. Huang and A. Makur, "A new iterative reconstruction scheme for signal reconstruction," *IEEE Asia Pacific Conference on Circuits and Systems*, pp. 336-339, Dec. 2008.

[82] T. Ogawa and M. Haseyama, "Adaptive reconstruction method of missing texture based on projection onto convex sets," *IEEE International Conference on Acoustics, Speech and Signal Processing*, vol. 1, pp. I-697-I-700, April 2007.

[83] J. Chen, L. Zhang, J. Luo, and Y. Zhu, "MRI reconstruction from 2D partial k-space using POCS algorithm," *3rd International Conference on Bioinformatics and Biomedical Engineering*, pp. 1-4, June 2009.

[84] H. G. Feichtinger, W. Kozek and T. Strohmer, "Reconstruction of signals from irregular samples of its short-time Fourier transform," *Proceedings of SPIE*, San Diego, July 1995.

[85] H. E. Guven, H. M. Ozaktas, A. E. Cetin, and B. Barshan,"Signal recovery from partial fractional Fourier domain information and its applications," *IET Signal Processing*, vol. 2, no. 1, pp. 15-25, 2008.

[86] A. Serbes and L. Durak, "Optimum signal and image recovery by the method of alternating projections in fractional Fourier domains," *Communications in Nonlinear Science and Numerical Simulation*, vol. 15, pp. 675-689, Mar. 2010.

[87] M. Sun, and R. J. Sclabassi, "Precise determination of starting time of epileptic seizures using subdural EEG and Wavelet transforms," *Proceedings of IEEE-SP International Symposium on Time-Frequency and Time-Scale*, pp. 257-260, 1998.

[88] D. Slepian, "Prolate spheroidal wave functions, Fourier analysis and uncertainty. V: The discrete case," *Bell Systems Techical Journal*, vol. 57, pp. 1371-1430, 1978.

[89] P. J. S. G. Ferreira, "The stability of a procedure for the recovery of lost samples in band-limited signals," *Signal Processing*, vol. 40, pp. 195-205, Nov. 1994.

[90] E. Sejdic, M. Luccini, S. Primak, K. Baddour, and T. Willink, "Channel estimation using DPSS based frames," *IEEE International Conference on Acoustics, Speech and Signal Processing*, pp. 2849-2852, Mar. 2008.

[91] S. Senay, L. F. Chaparro, and A. Akan, "Chirp channel estimation and OFDM transmission using discrete prolate spheroidal sequences," *SPPRA*, vol. 64, pp. 281-286, Feb. 2008.

[92] P. Oliveria, "Interpolation of signals with missing data using PCA," *IEEE International Conference on Acoustics, Speech and Signal Processing*, vol. 3, May 2006.

[93] J. Mark and T. Todd, "A nonuniform sampling approach to data compression," *IEEE Transactions on Communications*, vol. 29, pp. 24-32, Jan. 1981.

[94] M. Hanke, *Conjugate Gradient Type Methods for Ill-Posed Problems*, Longman, Harlow, 1995.

[95] K. M. Guan, S,. Kozat, and A. C. Singer, "Adaptive reference levels in a level-crossing analog-to-digital converter," *EURASIP Journal on Advances in Signal Processing*, vol. 2008, Article ID 513706, 11 pages, doi:10.1155/2008/513706.

[96] A. I. Zayed, "A generalization of the prolate spheroidal wave functions," *Proceeding of American Mathematics Society*, vol. 135, no. 7, pp. 2193-2203, Jul. 2007.

[97] M. Martone, "A multicarrier system based on the Fractional Fourier Transform for time-frequency-selective channels," *IEEE Transactions on Communications*, pp. 1011-1020, Jun. 2001.

[98] K. Khare and N. George, "Sampling theory approach to prolate spheroidal wavefunctions," *Journal of Physics: Mathematical and General*, 2003.